Lehigh University
Lehigh Preserve

Theses and Dissertations

1970

Computer simulation of the thermal profiles developed during magnetite oxidation in a traveling grate pellet plant

Karl D. Libsch
Lehigh University

Follow this and additional works at: https://preserve.lehigh.edu/etd

 Part of the Metallurgy Commons

Recommended Citation
Libsch, Karl D., "Computer simulation of the thermal profiles developed during magnetite oxidation in a traveling grate pellet plant" (1970). *Theses and Dissertations*. 3802.
https://preserve.lehigh.edu/etd/3802

This Thesis is brought to you for free and open access by Lehigh Preserve. It has been accepted for inclusion in Theses and Dissertations by an authorized administrator of Lehigh Preserve. For more information, please contact preserve@lehigh.edu.

COMPUTER SIMULATION OF THE THERMAL PROFILES DEVELOPED DURING MAGNETITE OXIDATION IN A TRAVELING GRATE PELLET PLANT

by

Karl David Libsch

A THESIS

Presented to the Graduate Committee

Of Lehigh University

in Candidacy for the Degree of

Master of Science

in

Department of Metallurgy and Materials Science

Lehigh University

1969

This thesis is accepted and approved in partial fulfillment of the requirements for the degree of Master of Science.

January 12, 1970
(Date)

Stephen K. Farby
Professor in Charge

C. S. Cundall
Chairman of the Department

ACKNOWLEDGEMENTS

The author wishes to acknowledge the Dravo Corporation, Pittsburgh, Pennsylvania, for supplying the industrial test data and ore samples, and the Bethlehem Steel Corporation, Bethlehem, Pennsylvania, for valuable assistance in balling and sizing the concentrate. The author also wishes to thank the sponsors of the Chemical Metallurgy Program at Lehigh University during the period this work was performed for financial support; these included American Metal Climax, Bethlehem Steel Corporation, Carpenter Technology Corporation, and United States Steel Corporation.

TABLE OF CONTENTS

LIST OF TABLES

LIST OF FIGURES

Page

ABSTRACT

A mathematical model which describes heat and mass transfer in the packed bed of a traveling grate pelletizing machine has been written. This mathematical model enables the temperature profiles which develop in the packed bed of a traveling grate pelletizing machine while magnetite oxidation occurs to be simulated. The model was written by formulating differential heat and mass balances for a thin slice of the bed which travels through the pelletizing furnace. In order to use the mathematical model, kinetic data for magnetite oxidation of ore balls of the concentrate concerned must be known. These kinetics have been determined for ore balls of two ores.

The kinetics were determined while preheated air flowed past the ore balls at a high enough rate so that gas film diffusion was not rate limiting. The rates of oxidation were found by interrupting the oxidation and weighing the partially oxidized pellets. They were determined isothermally at 300, 400, 500, 600, 700, 800, 900, and 1000°C. The results were fit empirically to allow use in the mathematical model.

The mathematical model was programmed on a digital computer using a digital analogue simulator. The program together with the kinetic data have been used to simulate the thermal profiles developed during magnetite oxidation during industrial pot testing with ore balls of the two concentrates. The simulated thermal profiles developed at different levels in the bed compare well with those measured in industrial pot testing.

INTRODUCTION

The object of iron ore pelletizing is to take finely ground ore concentrate and produce firm hard balls about 3/8 inch in diameter. These pellets must be strong enough to survive the trip from the mine at which they are produced to a blast furnace. They must have sufficient strength and the correct chemical properties to serve as blast furnace burden material.

The pelletizing process consists of two parts. The first of these is the preparation of the finely ground ore particles into green balls. These balls are conveyed to the indurating (heat hardening) machine where they are fired to become hard pellets which can be transported and used as blast furnace burden. The firing process can be accomplished in several ways. Commercially, this is done using either a shaft furnace, a traveling grate, or a traveling grate and kiln combination. In all of these processes, the green pellets must be heated so that they can successfully undergo drying, any reactions occurring during firing, firing itself, and cooling without cracking or spalling. If it is required that the pellet have certain chemical properties, the pellet must be heated so that these are obtained. A large percentage of the ores pelletized are originally magnetite or largely magnetite ores. With magnetite ores, the complete oxidation of magnetite to hematite is important. If the oxidation to hematite is incomplete, the resulting pellet consists of a core of magnetite surrounded by a shell of hematite. This core-shell situation causes poor compression strengths, which may lead to breakup of the pellets

in shipping and handling. It is also well known that reduction kinetics favor the use of hematite in the blast furnace (1).

In order to produce a successful pellet each ore concentrate ball must be heated at the correct rate. In a traveling grate plant, heating is done by passing hot air through a packed bed of ore concentrate balls. By properly controlling the temperature and flow rate of the air entering the bed, each ore concentrate ball can be heated at the correct rate. The temperature and flow rate of air entering the bed varies as the process proceeds. The way in which the temperature and flow rate of air vary with time is usually referred to as the hood profile. The hood profile which will yield successful pellets and be the most economical is determined by heat hardening ore concentrate balls in a refractory pot. The desired air flow and temperature entering the bed for any given time is passed through the bed in the pot and the temperature-time profile at different depths in the bed is recorded. At the end of the test, the hardened pellets are checked to see whether successful pellets have been made. The hood profile and the recorded temperature-time profile at different depths in the bed can be used to scale up to plant performance. This procedure is used to design new traveling grate pellet plants. It is also used to determine what modifications in existing traveling grate plants should be made to make them more economical and/or produce a better pellet if, perhaps, the properties of the concentrate to be pelletized changes.

Each ore concentrate has different properties. Also, the first pot test does not necessarily produce successful pellets and the most

economical test pattern. For these reasons many pot tests must be run to arrive at the best pattern. Pot testing is expensive both in capital and operating cost. Because of the expense, it is not economical to systematically investigate the effect of numerous variables which are presently thought to have only a minor influence on the process. The purpose of the present investigation is to mathematically model the traveling grate pelletizing plant so that the temperature-time profiles for different depths in the bed which develop while magnetite oxidation is taking place can be simulated. Because oxidation of magnetite to form hematite is an exothermic reaction, the kinetics of oxidation in concentrate ore balls significantly affect the shape of the hood profile. In the traveling grate machine, the hotter air passes through the top of the packed bed. When the temperature of the ore balls at the top of the bed is high enough, oxidation begins. Since heat is liberated by the oxidation, a greater amount of heat is present lower in the bed than would be present if no oxidation had occurred in the packing above it. Hence, ore balls lower in the bed are brought up to a temperature where they can react more quickly. The magnitude of this effect depends on how quickly oxidation proceeds and to what extent it proceeds at lower temperatures.

A mathematical model of the traveling grate pelletizing machine should allow an estimate of the effect of the different factors which might influence the magnetite oxidation reaction and therefore influence the performance of the machine. In order to check on the validity of the simulation, it is necessary to know the kinetics of oxidation for a given ore ball and pot test results for balls of the same ore

concentrate. This investigation includes the experimental determination of the kinetics of oxidation of ore balls of two different magnetite concentrates.

LITERATURE SEARCH

In order to simulate the thermal profiles developed in the packed bed of a traveling grate pelletizing machine, two factors must be considered. These are the amount of heat produced by oxidation and the amount of heat transfer in the bed. The kinetics of oxidation of magnetite in ore concentrate balls determine the amount of heat produced by oxidation. Levenspiel (2) points out that reaction in spherical particles of unchanging size can be visualized as five steps occurring in succession. These are:

Step 1: Diffusion of the gaseous reactant from the surrounding gases to the surface of the sphere.

Step 2: Transport of the gaseous reactant from the surface of the sphere to the reacting interface.

Step 3: Chemical reaction of the gaseous reactant with the solid.

Step 4: Transport of the gaseous reaction products from the reacting interface to the surface of the sphere.

Step 5: Diffusion of the gaseous reaction products from the surface of the sphere to the surrounding gases.

When magnetite is oxidized to form hematite, no gaseous reaction products are formed; thus, steps 4 and 5 do not occur. Each of the first three steps, however, do occur, and any one could be rate limiting.

The kinetics of oxidation of magnetite to form hematite in ore concentrate balls have been studied with (3,4) and without (5,6)

heated air flowing past the balls. Without flow, it was found that the reaction rate is limited by diffusion of oxygen to the surface of the ball. The kinetic studies of both Zetterstrom and Edstrom were made using heated air flowing past the ore balls. In both cases most of the data was taken after determining the flow rate above which step 1 was not rate limiting. Zetterstrom (5) found this flow rate to be close to 0.23 SCFM for a two inch diameter retort. The flow used for a similar cross-sectional area in a traveling grate pelletizing machine is usually about an order of magnitude greater. For this reason data taken when step 1 is not rate limiting must be used to determine the kinetics of oxidation in a traveling grate pelletizing machine.

Zetterstrom (5) studied the kinetics of magnetite oxidation for ore balls of several Mesabi Range concentrates. The data were taken by weighing ore balls packed in a retort during oxidation. Isothermal tests were attempted, but the air leaving the ore ball column was from 25 to 125°C higher than that entering it. The effects of changes in temperature, composition of the oxidizing gas, and concentrate particle size were investigated. The results of the testwork were plotted to illustrate the effect of the variables on oxidation rate. No theoretical explanation of the results was attempted.

The kinetics of oxidation for ore balls of Malmberget A-10 concentrate were studied by Edstrom (6,7). Data were obtained by heating a single ore concentrate ball isothermally at 1230°C while air of the same temperature flowed past it. The amount of oxidation was determined by weighing the ore ball before and after oxidation and by

measuring the width of the hematite shell. Edstrom postulated that when step 1 was not rate limiting, the reaction rate was limited by the flow or diffusion of oxygen through the hematite shell to the reacting interface. He showed that, if step 2 was rate limiting, then the rate of reaction could be described by the parabolic rate law as applied to a sphere. Using his data he was able to show that this law was obeyed.

Heat transfer in a packed bed can occur by several mechanisms. These include heat transfer from the gas to the packing, radiation from one solid particle to another, and conduction from solid particle to solid particle. In comparison to the amount of heat transferred from the gas to the packing, that transferred by radiation and conduction between particles is usually small (8,9,10). In some cases, however, the amount of heat transferred between pellets does become appreciable. Since the bed of a traveling grate pelletizing machine is heated to 2450°F, the heat transferred by radiation between particles might become important. Several investigators have proposed ways to calculate the amount of heat transferred in this manner (11,12,13). In the present investigation, the Damkohler expression as corrected to non-black body conditions will be used to estimate the amount of heat transferred by radiation between particles (12,13).

Heat transfer by the gas stream to the packing is normally considered using a film heat-transfer coefficient at high flow. At stagnant or low flow, an axial thermal conductivity is used (14). The flow used in a traveling grate pelletizing machine is in the turbulent region. Thus, only the film heat-transfer coefficient is the coef-

ficient for the heat transferred between the packing and the flowing fluid through the thin gas film surrounding each packing particle. It is normally defined as: (15)

$$dq_c = h_{\ell oc} \cdot (aA_t dz) \cdot (T_s - T_A) \qquad (1)$$

where:

q_c = heat transferred to the flowing fluid,

A_t = cross-sectional area of bed,

a = solid particle surface area per unit bed volume,

T_s = surface temperature of particle,

T_A = bulk temperature of the flowing fluid,

z = axial distance, and

$h_{\ell oc}$ = heat-transfer coefficient representative of a cross-sectional area perpendicular to the z direction.

Experimentally the following correlation has been found for $h_{\ell oc}$:

$$j_h = 0.91\, \psi Re^{-0.51} \qquad (Re < 50) \qquad (2)$$

$$j_h = 0.61\, \psi Re^{-0.41} \qquad (Re > 50) \qquad (3)$$

where:

ψ = shape factor (1.0 for spheres), and

j_h = Colburn analogy and is defined by

$$j_h = \left(\frac{h_{\ell oc}}{Cp_b\ Go} \right) \left(\frac{\hat{Cp}\ \mu}{k} \right)_f^{2/3} \qquad (4)$$

The terms in Equation (4) are defined as follows:

$\hat{C}p_b$ = specific heat at constant pressure per unit mass for the fluid,

μ = viscosity of fluid,

k = thermal conductivity of fluid,

G_o = mass velocity of fluid just before entering the bed,

f = subscript denoting that these properties are evaluated at the average of the air and packing surface temperatures, and

Re = packed bed Reynolds number and is defined by

$$Re = \frac{G_o}{a\ \mu_f \psi} \tag{5}$$

Eqs. (2) and (3) are the result of the work of a number of investigators and are thought to represent the best correlation. However, summaries of experimentally determined j_h versus Re correlations available in the literature (16,17,18) show that the experimental results vary substantially. Only an estimate of the amount of heat transferred can therefore be made.

To simulate the thermal profile developed in the packed bed of a traveling grate machine while oxidation occurs, a system of differential equations describing the situation must be solved. Heat transfer in the bed and the heat produced by oxidation must be included in these differential equations. A traveling grate used for pelletizing usually is at least nine foot wide (19). Because of the large width, it seems reasonable to assume that the temperature distribution in

most of the packed bed is not affected by heat flow through the sides of the bed. The bed of a traveling grate pelletizing machine during oxidation can therefore be regarded as an adiabatic packed bed with heat generation in the packing. Most investigators have derived two partial differential equations in order to describe such a situation. These equations are the heat balances for the gas and for the solid. Terms which take the various heat transfer mechanisms into account and include the heat effects due to reaction are used in developing these equations. The result of the derivation is usually a set of partial differential equations which are impossible to solve. By eliminating terms which are insignificant for the particular case considered, solvable equations are obtained.

The general case for heat transfer in an adiabatic packed bed with heat generation in the packing has been considered by Elliott (9). Elliott has also solved variations of the general case which allow estimation of the error in assuming that some of the heat transfer mechanisms are insignificant. Amundson and coworkers (10,20) have also considered the general case using rather formidable mathematics. Solutions of particular cases making certain assumptions have been carried out by a number of workers. Elliott's paper (9) lists the more important of these. In most cases digital computers have been used to do the calculation once the solution to the differential equations had been found. In some cases finite difference methods used together with a digital computer have been used to find the solution.

Some direct applications to sintering and pelletizing are available in the literature (21,22). These include a mathematical model of a traveling grate pelletizing machine proposed by Beale, Appleby, Butterfield, and Young (23). The method used to model the machine did not use results of kinetic data for drying or magnetite oxidation. Rather an enthalpy-temperature diagram was constructed using the authors experience. This enthalpy-temperature diagram was used together with two extremely simple partial differential equations--one for the gas and one for the solids--in order to obtain the thermal profile. The model considered only the effect of heat transfer from the gas to the solid and heat given off or consumed by reaction. The model becomes cumbersome to work with if other terms are added.

EXPERIMENTAL DATA ON MAGNETITE ORE CONCENTRATES

The reaction kinetics of oxidation of magnetite to form hematite in ore concentrate balls differ for each concentrate. In order to simulate the thermal profiles developed in the bed of a traveling grate pelletizing machine during magnetite oxidation, these kinetics must be known. To be sure that the kinetics used in this investigation were the same as those used in the pot tests to be simulated, kinetic data were obtained using ore balls of two magnetite concentrates.

As pointed out in the Literature Search, heated air must flow past the ore balls while the kinetic data are obtained. The velocity of the air must be great enough so that diffusion of oxygen from the surrounding gases to the surface of the sphere does not become rate limiting. This complicates both the experimental equipment design and procedure. In this investigation the kinetic data were obtained isothermally. Semicontinuous weighing of the sample while oxidation was taking place was used to determine the amount of oxidation.

Equipment

The equipment used in this investigation was that required to:

(1) preheat a measured amount of oil- and water-free air or nitrogen to the desired test temperature,

(2) provide a reaction chamber in which the preheated gas would remain at a constant temperature and in which the sample could be oxidized, and

(3) allow the sample to be weighed while held suspended inside the reaction chamber.

Figure 1 illustrates schematically the way in which the equipment was set up to meet these requirements.

A compressor was used to supply air. Water and oil in the air were removed using a Beach Sta-Dri filter. Air pressure was maintained constant with the use of a pressure regulator. The air flow rate into the heater was measured by a Dwyer flowmeter with a range of 0-40 SCFH. The nitrogen used was commercial grade nitrogen supplied in cylinders by Air Products and Chemicals, Incorporated. It had a dewpoint of approximately -90°F and contained about 15 ppm of oxygen. Nitrogen from the cylinder was used directly without any further purification. The nitrogen flow rate was measured using a flowmeter attached to the pressure regulator on the cylinder. The nitrogen also passed through a Matheson flowmeter with a range of 0-2 SCFH which was located on the panel board. This flowmeter was used only to indicate whether or not nitrogen was flowing to the heater. Both the nitrogen and the air passed from the flowmeter on the panel board into the arms of a "Y" gas mixer. The "Y" was of brass construction and a flow regulating valve was included in each arm of the "Y". The "Y" was never used to mix the two gases. Rather, the valves were used to admit either nitrogen or air to the gas heater.

Figure 2 shows a drawing of the gas heater and reaction chamber assembly. All parts shown on Figure 2 were of Inconel 600 alloy. A tube bundle was used for the heater rather than a spiral winding because of the geometry of the available furnace. Air was transferred from one tube of the heater to the other by holes drilled in-

side the two end pieces. The tubes and the end pieces were made separately. Assembly was accomplished by screwing the tubes into one end piece. The other tube bundle end was then placed on top of the tubes and the tubes screwed part way out of the one tube bundle and into the other. After testing, it was found that the tube bundle was not air tight. Attempts were made to seal the tube bundle by oxidizing the entire assembly at elevated temperatures. This procedure helped, but did not give an air tight heater. For this reason, the flow of heated air into the reaction chamber was measured frequently during the testwork. The procedure used is included in the section on Operational Techniques.

As shown in Figure 2, the reaction chamber was machined into one of the tube bundle ends. A lid for the reaction chamber was machined from Lavite. This lid covered the top of the chamber and provided for entrance of the wire used to support the sample holder. It also filled the top 1 1/4 inches of the reaction chamber. Tests using this lid indicated that the air temperature within the chamber was constant to within 10°C.

The sample holder was a one inch diameter mullite tube, two inches long. Four holes were cut in the side of the tube to allow the sample holder to be connected to the suspending wire. Three holes were also cut near the bottom of the tube. Nickel wire was placed through these holes to form a triangular grid which was used to support a nickel screen. The ore balls used for the sample were held in the sample holder by the screen. The grid and screen combination was used to allow the sample to be easily put in or taken out of the sample holder.

The screen was woven on a loom made during this investigation. Mullite cement was used to seal the holes cut near the bottom of the sample holder after the wire was inserted.

Nickel wire was placed through the holes in the top of the sample holder to form a cross at the center of the tube. To this cross a wire connecting the sample holder to the balance was attached. The connecting wire was Nickel wire of approximately 0.010 inch diameter and was sheathed in thermocouple insulators to help keep it straight. Tests made using only the sample holder and screen at 800°C revealed that there was no measurable oxidation of the sample holder, screen, or connecting wire.

The furnace used was heated with silicon carbide rod heating elements. A Wheelco controller was used to control the furnace temperature. The furnace was mounted on wheels so that it could be moved to allow the sample holder to be easily put in or taken out. Figure 3 shows a cross-sectional view of the furnace with the heater, reaction chamber, and sample holder in place. Figure 4 shows a photograph of the experimental setup during a run.

Materials

Ore balls of two different magnetite ore concentrates were used in this investigation. Both were mined and beneficiated in the United States. For the purpose of this investigation, the two ore concentrates will be named Ore 1 and Ore 2. Seven analyses for the concentrates as used in making the concentrate ore balls are included in Table I.

The concentrate ore balls were made from the ore concentrates using an airplane tire procedure (24). The airplane tire and balling equipment were located at the Homer Research Laboratories of Bethlehem Steel Corporation. The procedure consisted of two steps; the first was to prepare seeds of the material, and the second was to combine these seeds with more concentrate to make balls. The following procedure was used to make the seeds:

(1) The dry iron ore concentrate was screened to obtain the -16 mesh material.

(2) The inside of the tire was cleaned and dried.

(3) With the tire rotated at about 10 rpm, material was added until a tear drop shape of material was formed in the tire. A fine mist of water was sprayed on the material to help develop this shape.

(4) When some of the seeds were larger than the others in the tire, the seeds were taken out of the tire and screened. The -6 mesh, +16 mesh fraction was returned to the tire. More material and water mist were added.

(5) Step (4) was repeated with the -6 mesh, +8 mesh and +6 mesh, -4 mesh fractions being returned to the tire. When the +6 mesh, -4 mesh fraction returned to the tire seemed large enough, it was removed from the tire and +4 mesh, -1/4 in. fraction kept as seeds.

The following procedure was used to make ore concentrate balls using the seeds:

(1) The following were weighed out for making approximately 2000 grams of balls:

(a) 80-90 grams seeds

(b) 2000 grams of -16 mesh concentrate

(c) the appropriate amount of bentonite for 2000 grams of the concentrate to be balled

(d) about 20 or 30 grams less than the appropriate amount of water for 2000 grams of the concentrate to be balled.

(2) The concentrate and bentonite were placed on a rubber mat and mixed by folding the corners of the mat.

(3) The mixed material was added to a muller. With the muller on, the water was added and mulling continued for about 40 seconds.

(4) The water bottle was weighed. The mulled material was fluffed in a fluffer and the tire switched on at 25 rpm.

(5) The seeds were added to the tire and the fluffed material added slowly. Enough water mist was added as required to keep the balls growing.

(6) Balling was stopped after 2 1/2 minutes had elapsed. The balls were screened and separated into different size fractions. The smallest size fraction was returned to the tire and more material and water mist added.

(7) When it appeared that the balls in the tire had grown to about the same size as the next larger fraction, the

next larger fraction was added to the tire. This process continued until all of the balls and material had been added to the tire. The balls were then left in the tire for 30 seconds and removed. The total time taken for balling was about four minutes.

(8) The water bottle was weighed so that the per cent water in the ore balls could be calculated.

The amounts of seed concentrate, bentonite, and water used in balling concentrates of Ore 1 and Ore 2 are included in Table I. No bentonite was used in preparing the seeds for either concentrate.

After being prepared, the ore concentrate balls were stored in canning jars. The balls used as samples for test runs were sized to insure reproducible test results. Sizing was done using an aluminum template drilled with holes from 1/4 to 5/8 inch in diameter. One hole was drilled for each 1/64 inch interval. Ore balls of +35/64, -9/16 inches diameter were used for tests with Ore 1. Ore balls of +17/32, -35/64 inches diameter were used for Ore 2. It was noted on sizing the balls that they seemed to be spherical within 1/64 of an inch diameter.

To make sure that the sized balls were completely dry before testing, they were dried in an oven at 110°C overnight. The initial Fe^{+2} content of the concentrate balls was determined using the wet analysis procedure outlined in the section on operational techniques. The initial Fe^{+2} content for the dried balls of Ore 1 was analyzed as 19.9 wt pct Fe^{+2} and for Ore 2 as 20.2 wt pct Fe^{+2}. These values are

about 1 wt pct Fe^{+2} lower than the normal analyses for Ore 1 and Ore 2. It is thought that the lower analyses resulted either from the long period during which the concentrates were stored before balling or more probably from drying the ore balls in the drying oven overnight.

Operational Techniques

The following procedures have been used in the experimental runs. Slight variations were made in the procedure developed for taking kinetic data in order to verify the technique. These are pointed out when they occurred in the section on verification of experimental technique.

A. Weight Versus Time Measurement

The following procedure was developed to take the weight versus time data during an experimental run:

(1) The sample holder and screen with and without the sample were weighed outside the furnace. The weights were recorded. Two ore balls were used for the sample.

(2) Both air and nitrogen flowmeters were adjusted so that the amount of air or nitrogen flowing into the reaction chamber was close to 18 SCFH. All air flow to the tube bundle was shut off. Nitrogen was passed through the heater for at least three minutes.

(3) Power to the furnace was shut off. The Lavite lid of the reaction chamber was removed and the

lower segment of the connecting wire was passed through it. The Lavite lid and sample holder were placed in the reaction chamber.

(4) Power to the furnace was turned on and the furnace was moved underneath the analytical balance.

(5) The two segments of the connecting wire were snapped together.

(6) The balance and/or furnace were moved until the connecting wire held the sample holder so that it was not constrained by touching the side of the reaction chamber. The lack of constraint was tested by trying to make an initial weight measurement as outlined in steps (7), (8), (9), and (10).

(7) An initial estimate of the weight of the sample was made and the balance set up for that weight.

(8) Nitrogen flow was shut off and the balance allowed to swing three times.

(9) Nitrogen flow was turned on and another estimate of the weight made.

(10) Steps (7), (8), and (9) were repeated until the correct weight was found. This weight was then recorded.

(11) Once the initial weight was determined, nitrogen flow was shut off and the air flow and time indicator turned on.

(12) After two minutes had elapsed, the air flow and times were turned off, nitrogen flow turned on, and a weight measurement made as outlined in steps (7), (8), (9), and (10).

(13) Steps (11) and (12) were repeated until measurements had been made for 0, 2, 4, 6, 8, 10, 12, and 14 minutes of air flow.

(14) After the 14 minute measurement, power to the furnace was shut off, the two segments of connecting wire unsnapped, and the sample holder removed from the reaction chamber.

Note that in no case was less than 10 minutes or more than 30 minutes allowed to elapse between putting the sample in the reaction chamber and taking the initial weight measurement. If more than 30 minutes was required for the initial weight measurement, the run was aborted.

B. Calculation of % Ox Using Weight Versus Time Measurements

In order to allow the results of each test to be compared and also to allow the data to be used in the computer model, the weight gain measurements were converted to % Ox. The percent of oxidation, which will hereafter be referred to as % Ox, is defined as 100 times the ratio of the weight gained during oxidation to the weight which would be gained by the sample if it was completely oxidized. The following procedure was used to convert weight measurements to % Ox:

(1) The weights of the sample holder and screen with

and without the sample measured outside the furnace were subtracted. The result was taken as the sample weight.

(2) The weight which would be gained by the sample if it were completely oxidized was found by multiplying the sample weight by the weight fraction of magnetite in the concentrate before oxidation and $\frac{8.00}{231.55}$.

(3) The weight gain for each weight measurement during a test was determined by subtracting the weight recorded from the initial weight measurement made inside the reaction chamber.

(4) The weight gain was divided by the weight which would be gained by the sample if it was completely oxidized. This result was multiplied by 100 to give % Ox.

C. Measurement of the Flow Rate Into the Reaction Chamber

The following procedure was developed to allow the measurement of the flow rate into the reaction chamber at elevated temperatures before and after any run:

(1) An approximately five foot long stainless steel tube of 0.25 inch diameter was attached to a flowmeter using rubber tubing.

(2) A one to two inch long piece of canvas reinforced rubber tubing with an inside diameter of 0.25 inches

was slipped over the end of the stainless steel tube.

(3) With the furnace at temperature and air flowing through the heater, the power was turned off, and the Lavite lid removed.

(4) The stainless steel tube was jammed down the hole from which heated air entered the reaction chamber.

(5) The highest reading on the flowmeter was taken as the gas flow entering the reaction chamber.

(6) The tube was taken out, cap replaced, and current turned on.

At higher temperatures caution must be used as the rubber ignites after a short time in contact with the reaction vessel.

D. Measurement of Air Temperature in the Reaction Chamber

The air temperature in the reaction chamber was measured using an uncalibrated Alumel-Chromel thermocouple with a bare bead. The air temperature was measured before each test made at a different temperature. The furnace temperature was within ± 2°C of the desired temperature.

E. Ferrous Ion Analysis

The analytical procedure used for determining the wt pct Fe^{+2} was similar to that used by the Homer Research Laboratories of Bethlehem Steel Corporation. Errors in the analysis will result from metallic iron being present in the sample, as well as by the presence of unoxidized vanadium and organic materials other than graphitic

carbon (25). The procedure is as follows:

(1) Two glass tubes with 90° bends were placed in a rubber stopper. One of the glass tubes was constructed so that only a short length of glass poked through the stopper; the other, so that about three inches of tubing were beneath it. The stopper and glass tubing were placed in a 250 or 300 ml Erlenmeyer flask. This procedure was repeated until a flask complete with stopper and glass tubing has been made for each sample to be analyzed. One additional flask was made up using a two hole rubber stopper and one of the long glass bends.

(2) The flasks were connected with rubber tubing to form a flask train. This was done by connecting each short glass bend to the long glass bend on the next flask. The flask having only the long glass bend was filled with enough deionized water to immerse the end of the glass tubing. It was connected to the end of the flask train to serve as a bubbler.

(3) A predetermined amount of dry sample was weighed into the flasks.

(4) With the use of rubber tubing, the first flask was connected to a regulator of a gas cylinder containing dry CO_2. CO_2 was bubbled through the flask train for at least 5 minutes.

(5) 30 ml of 1:1 HCl and 10 to 12 drops of 48% HF were added to each flask containing a 1/2 gram sample. For larger samples an additional 10 ml of 1:1 HCl was added for each additional 1/2 gram of sample.

(6) The flask train was heated on a hot plate with CO_2 passing through it, close to, but not at the boiling point, until all of the sample dissolved.

(7) For each 1/2 gram sample to be analyzed, a solution of 15 ml of 1:1 H_3PO_4 and 6 to 8 drops of p-diphenylamine sulfonic acid sodium salt solution ($C_6H_5NHC_6H_4$-4-SO_3Na) was prepared. For larger samples an additional 5 ml of 1:1 H_3PO_4 was used for each additional 1/2 gram of sample.

(8) One of the flasks was removed from the flask train. The phosphoric acid and indicator were added. It was titrated immediately using 0.1 N $K_2Cr_2O_7$ solution. The end point was purple. This procedure was repeated until all of the flasks in the flask train had been titrated.

F. Verification of Experimental Technique

The procedure and some of the equipment used for measuring the kinetics of magnetite oxidation of ore concentrate balls were developed during this investigation. For this reason tests were made to determine the error inherent in the equipment and procedure. Tests were made for the following purposes:

(1) to illustrate the reproducibility of the testwork,

(2) to determine the amount of error in determining % Ox versus time data using the procedure for taking weight versus time measurements and calculating % Ox from these measurements outlined in the section on operational techniques, and

(3) to confirm that the air flow rate used in the tests was high enough so that diffusion of oxygen from the air to the surface of the ball was not rate limiting.

All of the tests were conducted with ore balls of Ore 1 and were run at 800°C.

Three tests were run to illustrate the reproducibility of the testwork. In these tests the procedures used to take weight versus time measurements and to calculate % Ox were the same as outlined in the section on operational techniques with the exception that in each test a different number of ore balls were used. In test CO-1, only one ore ball was used, in test CO-2 two ore balls were used, and in test CO-3 three ore balls were used. A different number of balls was used for each test so that any effect of convection currents on the reproducibility of weighing would be shown. Table II lists the results of these tests. Figure 5 shows a plot of % Ox versus time for these three tests. The figure shows that the procedures give results for % Ox which are reproducible to within 1 to 2 pct.

Seven tests, CO-4 through CO-10, were run to determine the error in obtaining kinetic data. In these tests the procedures outlined in the section on operational techniques were followed with the

following two exceptions:

(1) Each test was made for either two, four, six, eight, ten, twelve, or fourteen minutes. No intermediate weighing was done during these tests.

(2) After oxidation the sample was cooled with nitrogen flowing past it.

One ore ball from each run was used to prepare a sample for wet analysis of the wt pct Fe^{+2}. The other ball was mounted and ground so that the width of the hematite shell could be measured. A photograph of the ground ball was enlarged, and the shell width was measured directly and with the use of a planimeter. The results of the weight measurements, wet analyses, and shell width measurements are listed in Table III, and are plotted together with the results of test CO-2 in Figure 6. Three facts apparent from Figure 6 are:

(1) The results of measuring the hematite shell width to determine % Ox do not agree well with the results of either weight measurements or wet analysis.

(2) The results of the chemical analyses and the results of the weight measurements agree to within 1 or 2% Ox.

(3) As shown by comparison of the results of test CO-2 and the results of these tests, some oxidation does occur while taking weight measurements during a run. This oxidation, however, causes usually only a 1 or 2% Ox and at most a 5% Ox error.

Four tests, CO-11 through CO-14, were made to confirm that the flow rate used was high enough so that diffusion of oxygen from

the surrounding air to the surface of the ball was not rate limiting. The procedures used were those outlined in the section in operational techniques except a different flow rate was used for each test. The results of the testwork are listed in Table IV. Figure 7 is a plot of the % Ox versus time curves obtained for these tests and test CO-2. If diffusion of oxygen from the air to the surface of the ore ball is rate limiting, the test results should change for each flow rate used. As Figure 7 shows, the results of the tests made at 15, 18 and 21 SCFH were the same within experimental error. A flow of 18 SCFH is, therefore, enough to insure that diffusion of oxygen from the air to the surface of the ore ball is not rate limiting.

Experimental Results

The results of the experimental testwork done to determine the kinetics of magnetite oxidation in ore balls of Ore 1 and Ore 2 are listed in Tables V and VI. Testwork was done at 100°C intervals from 300° to 1000°C. Testwork was attempted above 1000°C; however, it was found that at this temperature the aluminum braid used to carry current to the silicon carbide heating elements in the furnace melted. For this reason no runs were made at temperatures above 1000°C.

In all of the testwork, the procedures outlined in the section on operational techniques were used. The % Ox versus time curves which resulted for Ore 1 are plotted in Figure 8 and for Ore 2 in Figure 9.

As shown by Figures 8 and 9, the tests made using both Ore 1 and Ore 2 at 900 and 1000°C gave results above 100% Ox. The amount of error inherent in the experimental procedures and equipment (as dis-

cussed in the sections on verification of operational techniques and equipment) allow the results taken at 900°C using Ore 1 to be explained. The other high results cannot be dismissed so easily. There are two possible explanations. The first of these depends on the fact that magnetite has been reported to be nonstoichiometric at temperatures above 1075°C (7). The calculation of % Ox is based, in part, on the weight fraction of magnetite originally in the ore. This was determined in this investigation from the wt pct ferrous iron obtained for the original concentrates assuming magnetite was stoichiometric ($FeO \cdot Fe_2O_3$). The second possibility is that at higher temperatures, the hematite in the concentrate might rapidly revert to magnetite. This reversion could then take place while the sample was being heated in nitrogen prior to the initial weight measurement in the reaction chamber. For both cases, the original weight fraction of magnetite would be low and the % Ox values high.

The form of the % Ox versus time curves recorded for Ore 1 and Ore 2 resemble those of Zetterstrom (5) more closely than those of Edstrom (6,7). As pointed out in the literature search, Edstrom showed that his data obeyed the parabolic rate law as applied to a sphere.

If the parabolic rate law is obeyed, the following equation would be satisfied (6,7):

$$t_E = R^2/k_E \left[\frac{(1-\sqrt[3]{1-Ox})^2}{2} - \frac{(1-\sqrt[3]{1-Ox})^3}{3} \right] \quad (6)$$

where:

t_E = time from the start of oxidation,

R = radius of ore ball,

Ox = % Ox/100

k_E = constant for oxidation of a ball of a given concentrate at a given temperature.

The data taken in this investigation, and the data obtained by Zetterstrom on Babbitt ore concentrate, were analyzed to find k/R^2 for each data point. The scatter in the k/R^2 values found using data points taken from the same % Ox versus time curves was large. The shape of the curves, predicted by the parabolic law using the different k/R^2 values, differed by about 10% Ox.

It is believed that the parabolic rate law did not work for these data because some unreacted magnetite probably was present in the hematite shell surrounding the unreacted magnetite core. The fact that % Ox values as calculated by measuring the width of the hematite shell in runs CO-4 through CO-10 was much higher than that obtained by weight measurement or wet analyses supports this hypothesis.

Data were obtained on the kinetics of magnetite oxidation of ore balls of Ore 1 and Ore 2 not to explain the kinetics, but rather to test the mathematical model developed during this investigation. In order to allow the data to be used in the mathematical model, they were fit to the following expression:

$$\% \text{ Ox} = A\ B^{C^{TI}} + D \qquad (7)$$

where:

A, B, C, D = constants for a particle of ore oxidized at a given temperature, and

TI = a linear function of time.

This expression was used because it fit all of the % Ox versus time data to within 4% Ox. Other equations were tried, but none fit the data as well using as few coefficients. A computer program was used to find the values of the coefficients for each data set. The program listing, along with instructions for its use, is included in Appendix B. The values of the coefficients which best fit the data are listed in Table VII.

DEVELOPMENT OF THE MATHEMATICAL MODEL

Differential equations which mathematically express the physical situation in the packed bed of a traveling grate pelletizing machine were developed during this investigation. Using these differential equations, the thermal profiles developed at different depths in the bed while magnetite oxidation was taking place were simulated. The differential equations were derived using the shell balance method discussed in detail by Bird, Stewart, and Lightfoot (15). Each of the variables in the equations were evaluated so that only the air and solid temperatures were unknown. These differential equations were then solved on a digital computer using an analogue simulator.

Development of the Fundamental Differential Equations

Differential equations describing the packed bed of a traveling grate pelletizing machine were derived using an infinitely thin slice of the bed. The slice had the width and the depth of the traveling grate machine. During the heat hardening process, it moved from the beginning to the end of the machine. The slice was considered to consist of two distinct and separate parts--an air lump containing only the air in the slice, and a pellet lump containing only the pellets. A mass and an energy balance were used to develop differential equations for each lump. The balances were made for an element z deep in each lump. The differential equations resulting from these balances were simplified and combined to give one equation for each lump. Because these two equations succinctly describe heat and mass transfer

to and from each lump they have been referred to during this investigation as the fundamental differential equations. Figure 10 illustrates the slice used, how the slice was divided into the air lump and the pellet lump, and the differential elements used for the mass and energy balances. In the mass and energy balances, both air and pellet temperature were assumed to vary only with time and depth in the slice. Also, the temperature of the pellets was assumed not to vary within a pellet. The temperature measurements made by Ban (26) inside oxidizing ore balls seem to substantiate this assumption.

The mass balance done for the air lump element follows:

mass in at z in Δt	$[\Delta t \ SCF \ \rho_A]_z$
mass out at $z + \Delta z$ in Δt	$[\Delta t \ SCF \ \rho_A]_{z \ + \Delta z}$
mass out to pellet lump for oxidation in Δt	$k \ F \ A_p \ \Delta z \ \Delta t$
mass at time t	$[A_A \ \Delta z \ \rho_A \ (T,P)]_t$
mass at time $t + \Delta t$	$[A_A \ \Delta z \ \rho_A \ (T,P)]_{t + \Delta t}$

where:

SCF = standard cm^3/min of air flowing through the element;

ρ_A = density of air for 1 standard cubic centimeter, g/std cm^3;

k = rate of reaction in grams of Fe_2O_3 produced per unit time and area of the pellet lump, g Fe_2O_3/cm^3 pellet lump;

F = stoichiometric ratio of grams O_2 used per gram of Fe_2O_3 produced;

A_p = cross-sectional area of pellet lump, cm^2;

A_A = cross-sectional area of air lump, cm^2; and

$\rho_A \ (T,P)$ = density of the air at the temperature and pressure in the element, g/cm^3.

The mass balance yields Eq. (8):

$$[\Delta t\ SCF\ \rho_A]_{z+\Delta z} - [\Delta t\ SCF\ \rho_A]_z + [A_A\ \Delta z\ \rho_A(T,P)]_{t+\Delta t} - [A_A\ \Delta z\ \rho_A(T,P)]_t + k\ F\ A_p\ \Delta z\ \Delta t = 0 \quad (8)$$

Rearrangement of Eq. (8) gives:

$$\frac{[SCF\ \rho_A]_{z+\Delta z} - [SCF\ \rho_A]_z}{\Delta z} + \frac{[A_A\ \rho_A(T,P)]_{t+\Delta t} - [A_A\ \rho_A(T,P)]_t}{\Delta t} + k\ F\ A_p = 0 \quad (9)$$

On taking the limit as $\Delta z \to 0$ and as $\Delta t \to 0$, Eq. (9) becomes:

$$\frac{\partial\ (SCF\rho_A)}{\partial z} + \frac{\partial\ (A_A\rho_A\ (T,P))}{\partial\ t} + k\ F\ Ap = 0 \quad (10)$$

The thermal balance done for the air lump element follows:

thermal energy in at z in Δt	$[\Delta t\ SCF\ \rho_A\ \Delta\ \hat{H}_A\ ]_z$
thermal energy out at $z + \Delta z$ in Δt	$[\Delta t\ SCF\ \rho_A\ \Delta\ \hat{H}_A\ ]_{z+\Delta z}$
thermal energy out by air used for oxidation in Δt	$k\ F\ A_p\ \Delta z\ \Delta\hat{H}_A\ \Delta t$
thermal energy out at z to the pellet lump in Δt	$[\Delta t\ q_c]_z$
thermal energy out at $z + \Delta z$ to the pellet lump in Δt	$[\Delta t\ q_c]_{z+\Delta z}$
thermal energy at time t	$[A_A\ \rho_A(T,P)\ \Delta\hat{H}_A\ \Delta z]_t$
thermal energy at time $t + \Delta t$	$[A_A\ \rho_A(T,P)\ \Delta\hat{H}_A\ \Delta z]_{t+\Delta t}$

where:

T_A = air temperature in °K;

$\Delta\hat{H}_A$ = enthalpy of air, cal/gm air; and

q_c = heat transferred to the air lump from the pellet lump, cal/min.

The thermal balance yields the following expression:

$$[\Delta t\ SCF\ \rho_A\ \Delta\hat{H}_A]_{z+\Delta z} - [\Delta t\ SCF\ \rho_A\ \Delta\hat{H}_A]_z$$

$$+[A_A\ \rho_A(T,P)\ \Delta\hat{H}_A\ \Delta z]_{t+\Delta t} - [A_A\ \rho_A(T,P)\ \Delta\hat{H}_A\ \Delta z]_t \qquad (11)$$

$$-[(\Delta t\ q_c)_{z+\Delta z} - (\Delta t\ q_c)_z] + k\ F\ A_p\ \Delta z\ \Delta\hat{H}_A\ \Delta t = 0$$

Upon rearranging Eq. (11), we get

$$\frac{[SCF\ \rho_A\ \Delta\hat{H}_A]_{z+\Delta z} - [SCF\ \rho_A\ \Delta\hat{H}_A]_z}{\Delta z} +$$

$$\frac{[A_A\ \rho_A(T,P)\ \Delta\hat{H}_A]_{t+\Delta t} - [A_A\ \rho_A(T,P)\ \Delta\hat{H}_A]_t}{\Delta t} \qquad (12)$$

$$\frac{[q_c]_{z+\Delta z} - [q_c]_z}{\Delta z} + k\ F\ A_p\ \Delta\hat{H}_A = 0$$

On taking the limit as $\Delta t \to 0$ and $\Delta z \to 0$, Eq. (12) becomes:

$$\frac{\partial(SCF\ \rho_A\ \Delta\hat{H}_A)}{\partial z} + \frac{\partial(A_A\ \rho_A(T,P)\ \Delta\hat{H}_A)}{\partial t} \qquad (13)$$

$$-\frac{\partial q_c}{\partial z} + k\ F\ Ap\ \Delta\hat{H}_A = 0$$

In this model, it was assumed that the amount of oxygen taken from the air by oxidation is negligible when compared with the total air flow. Calculations were made which illustrate that the maximum amount of

oxygen withdrawn from the air is about 6 vol. pct. By making this assumption Eqs. (10) and (13) reduced to:

$$\frac{\partial (SCF\, \rho_A)}{\partial z} = - \frac{\partial (A_A\ \rho_A(T,P))}{\partial t} \tag{14}$$

and

$$\frac{\partial (SCF\ \rho_A\ \Delta\hat{H}_A)}{\partial z} + \frac{\partial (A_A\ \rho_A(T,P)\ \Delta\hat{H}_A)}{\partial t} - \frac{\partial q_c}{\partial z} = 0 \tag{15}$$

By using the product rule on Eq. (15), we get:

$$- \frac{\partial q_c}{\partial z} + \Delta\hat{H}_A \frac{\partial (SCF\, \rho_A)}{\partial z} + SCF\rho_A \frac{\partial(\Delta\hat{H}_A)}{\partial z} + \Delta\hat{H}_A \frac{\partial (A_A\ \rho_A(T,P))}{\partial t} + A_A\ \rho_A(T,P) \frac{\partial (\Delta\hat{H}_A)}{\partial t} = 0 \tag{16}$$

Eq. (14) was substituted into Eq. (16) to give:

$$- \frac{\partial q_c}{\partial z} + \Delta\hat{H}_A \frac{\partial (SCF\ \rho_A)}{\partial z} + SCF\ \rho_A \frac{\partial (\Delta\hat{H}_A)}{\partial z} - \Delta H_A \frac{\partial (SCF\ \rho_A)}{\partial z} + A_A\ \rho_A(T,P) \frac{\partial (\Delta\hat{H}_A)}{\partial t} \tag{17}$$

$$= - \frac{\partial q_c}{\partial z} + SCF\ \rho_A \frac{\partial (\Delta\hat{H}_A)}{\partial z} + A_A\ \rho_A(T,P) \frac{\partial (\Delta\hat{H}_A)}{\partial t} = 0$$

The last term in Eq. (17) was assumed negligible in this development. Calculations were made which showed that it was about two orders of magnitude smaller than the other two terms in the equation. These calculations are discussed in the section on Discussion of Results. Making this assumption Eq. (17) reduced to:

$$- \frac{\partial q_c}{\partial z} + SCF\ \rho_A \frac{\partial (\Delta\hat{H}_A)}{\partial z} = 0 \tag{18}$$

The mass balance done for the pellet lump element follows:

Mass in at z in Δt	0
Mass out at $z + \Delta z$ in Δt	0
Mass in by reaction in Δt	$\Delta z \, \Delta t \, k \, F \, A_p$
Mass at time t	$[\rho A_p \Delta z]_t$
Mass at time $t + \Delta t$	$[\rho A_p \Delta z]_{t + \Delta t}$

where

ρ = density of pellet lump, g/cm^3 = density of a pellet, g/cm^3

From the mass balance, it can be shown that:

$$[\rho A_p \Delta z]_{t + \Delta t} - [\rho A_p \Delta z]_t - \Delta z \, \Delta t \, k \, F \, A_p = 0 \qquad (19)$$

Rearrangement of Eq. (19) gives

$$\frac{[\rho A_p]_{t + \Delta t} - [\rho A_p]_t}{\Delta t} - k \, F \, A_p = 0 \qquad (20)$$

On taking the limit as $\Delta t \to 0$, Eq. (20) becomes:

$$\frac{\partial (\rho A_p)}{\partial t} - k \, F \, A_p = 0 \qquad (21)$$

The thermal balance done for the pellet lump element follows:

Thermal energy in by conduction from pellet to pellet at z in Δt	$[\Delta t \, q_k]_z$
Thermal energy out by conduction from pellet to pellet at $z + \Delta z$ in Δt	$[\Delta t \, q_k]_{z + \Delta z}$
Thermal energy in by radiation from pellet to pellet at z in Δt	$[\Delta t \, q_r]_z$
Thermal energy out by radiation from pellet to pellet at $z + \Delta z$ in Δt	$[\Delta t \, q_r]_{z + \Delta z}$

Thermal energy in from oxygen entering the pellet lump	$\Delta t\ k\ F\ A_p\ \Delta z\ \Delta\hat{H}_A$
*Thermal energy in from air lump at z in Δt	$[\Delta t\ q_c]_z$
Thermal energy in from air lump at $z + \Delta z$ in Δt	$[\Delta t\ q_c]_{z+\Delta z}$
Thermal energy in by reaction in Δt	$q_X\ A_p\ \Delta z\ \Delta t$
Thermal energy at time t	$[A_p\ \Delta z\ \rho\ \Delta\hat{H}_p]_t$
Thermal energy at time $t + \Delta t$	$[A_p\ \Delta z\ \rho\ \Delta\hat{H}_p]_{t+\Delta t}$

where: q_k = heat transferred by conduction from particle to particle, cal/min;

q_r = heat transferred by radiation from solid particle to solid particle, cal/min; and

q_X = heat generated by oxidation of magnetite, cal/min cm^3 of pellet lump; and

$\Delta\hat{H}_p$ = enthalpy of the pellets, cal/cm^3 pellet lump.

The thermal balance yields

$$[\Delta t\ q_k]_{z+\Delta z} - [\Delta t\ q_k]_z + [\Delta t\ q_r]_{z+\Delta z} - [\Delta t\ q_r]_z$$

$$- \Delta t\ k\ F\ A_p\ \Delta z\ \Delta\hat{H}_A + [\Delta t\ q_c]_{z+\Delta z} - [\Delta t\ q_c]_z \qquad (22)$$

$$+ q_X\ A_p\ \Delta z\ \Delta t + [A_p\ \Delta z \rho \Delta\hat{H}_p]_{t+\Delta t} - [A_p\ \Delta z \rho \Delta\hat{H}_p]_t = 0$$

---

*From Figure 10b it might appear that the heat transfer from the air lump to the pellet lump would occur along the boundary between the two. The air lump and pellet lump were divided into two separate sections to give a conceptual picture. In reality, hot air flows in through the top of the element and out through the bottom.

Eq. (23) is obtained by rearranging Eq. (22).

$$\frac{[q_k]_{z+\Delta z} - [q_k]_z}{\Delta z} + \frac{[q_r]_{z+\Delta z} [q_r]_z}{\Delta z} - k F A_p \Delta\hat{H}_A \qquad (23)$$

$$+\frac{[q_c]_{z+\Delta z} - [q_c]_z}{\Delta z} - q_X A_p + \frac{[A_p \rho \Delta\hat{H}_p]_{t+\Delta t} - [A_p \rho \Delta\hat{H}_p]_t}{\Delta t} = 0$$

On taking the limit as $\Delta z \to 0$ and $\Delta t \to 0$, Eq. (23) becomes:

$$\frac{\partial q_k}{\partial z} + \frac{\partial q_r}{\partial z} + \frac{\partial q_c}{\partial z} - k F A_p \Delta\hat{H}_A + q_X A_p \frac{\partial (A_p \rho \Delta\hat{H}_p)}{\partial t} = 0 \qquad (24)$$

The amount of heat transferred from pellet to pellet by conduction was assumed negligible. With this assumption and the assumption that the amount of air transferred to the pellet lump by oxidation was negligible, Eq. (25) reduces to:

$$\frac{\partial q_r}{\partial z} + \frac{\partial q_c}{\partial z} + A_p q_x + \rho A_p \frac{\partial (\Delta\hat{H}_p)}{\partial t} = 0 \qquad (25)$$

The area of the pellet lump and that of the air lump are related by ε, the fraction voids in the packed bed. For a unit volume of bed:

$$A_p/A_t = 1 - \varepsilon \qquad (26)$$

$$A_A/A_t = \varepsilon \qquad (27)$$

where ε = fractional void volume. Substitution of Eqs. (26) and (27) into Eqs. (18) and (25) gives

$$- \frac{\partial q_c}{\partial z} + SCF \rho A \frac{\partial (\Delta\hat{H}_A)}{\partial z} = 0 \qquad (28)$$

$$\frac{\partial q_r}{\partial z} + \frac{\partial q_c}{\partial z} - (1-\varepsilon) A_t q_X + \rho (1-\varepsilon) A_t \frac{\partial (\Delta\hat{H}_p)}{\partial t} = 0 \qquad (29)$$

These are the fundamental differential equations.

Evaluation of the Variables in the Fundamental Differential Equations

In Eqs. (28) and (29), ρ_A, ρ , $(1-\epsilon)$, and A_t are constant. Each of the other quantities in the equations depends upon either air temperature, solid temperature, time, or a combination of these. In order to solve Eqs. (28) and (29), it was necessary to evaluate each of these quantities so that the temperature of the air and pellets were the only unknowns in the equations.

A. Evaluation of $\frac{\partial \Delta\hat{H}_A}{\partial z}$

The partial derivative of $\Delta\hat{H}_A$ with respect to z is such that:

$$\frac{\partial \Delta\hat{H}_A}{\partial z} = \hat{C}_{pA} \frac{\partial T_A}{\partial z} \tag{30}$$

where $\hat{C}_{pA}$ = specific heat at constant pressure of air, cal/gm °K. In order to evaluate $\frac{\partial \Delta\hat{H}_A}{\partial z}$, $\hat{C}_{pA}$ must be calculated by multiplying the vol. pct. of argon, nitrogen, and oxygen by their respective heat capacities at constant pressure and adding the results. The C_p equations used were:

$$C_{pN_2} = 6.6 + 1.02 \times 10^{-3} T_A \quad \text{cal/gm mole °K} \tag{31}$$

$$C_{pO_2} = 7.16 + 1.00 \times 10^{-3} T_A - 0.40 \times 10^{5} T_A^{-2} \text{cal/gm mole °K} \tag{32}$$

$$C_{pAr} = 5/2\ R = 4.96 \quad \text{cal/gm mole °K} \tag{33}$$

where:

C_{pN_2} = heat capacity at constant pressure of nitrogen, cal/gm mole °K;

C_{pO_2} = heat capacity at constant pressure of oxygen, cal/gm mole °K; and

C_{pAr} = heat capacity at constant pressure of argon, cal/gm mole °K.

Eqs. (31) and (32) were determined by the U. S. Bureau of Mines (27). Eq. (33) was derived by assuming argon to be an ideal monatomic gas (28). The composition of air was assumed to be 21 vol. pct. O_2, 78 vol. pct. N_2, and 1 vol. pct. Ar. The result of the calculations was:

$$C_{pA} = 6.7046 + 1.005 \times 10^{-3} T_A - 0.084 \times 10^{5} T_A^{-2} \qquad (34)$$

where C_{pA} = heat capacity at constant pressure of air, cal/gm mole °K. $\hat{C}_{pA}$ was found by dividing the right-hand side of Eq. (34) by 28.97, the molecular weight of air. The result was:

$$\hat{C}_{pA} = 0.2314 + 0.03469 \times 10^{-3} T_A - 0.0029 \times 10^{5} T_A^{-2} \qquad (35)$$

Therefore:

$$\frac{\partial \Delta \hat{H}_A}{\partial z} = (0.2314 + 0.03469 \times 10^{-3} T_A - 0.0029 \times 10^{5} T_A^{-2}) \frac{dT_A}{dz} \qquad (36)$$

B. Evaluation of $\frac{\partial \Delta \hat{H}_p}{\partial t}$

The partial derivation of $\Delta \hat{H}_p$ with respect to t is such that:

$$\frac{\partial \Delta \hat{H}_p}{\partial t} = \hat{C}_{pp} \frac{\partial T}{\partial t} \qquad (37)$$

where $\hat{C}_{p_p}$ = specific heat at constant pressure of the pellets, cal/gm °K.

In order to evaluate $\frac{\partial \Delta \hat{H}_p}{\partial t}$, $\hat{C}_{p_p}$ must be evaluated. $\hat{C}_{p_p}$ varies with time since the amounts of hematite and magnetite in a pellet vary with time. $\hat{C}_{p_p}$ was calculated using:

$$\hat{C}_{p_p} \times \frac{g \text{ pellet}}{cm^3} = \hat{C}_{pFe_3O_4} \times \frac{g \text{ } Fe_3O_4}{cm^3} + \hat{C}_{pFe_2O_3} \times \frac{g \text{ } Fe_2O_3}{cm^3} \qquad (38)$$

where $\hat{C}_{pFe_3O_4}$ = specific heat at constant pressure of magnetite, cal/gm °K, and

$\hat{C}_{pFe_3O_3}$ = specific heat at constant pressure of hematite, cal/gm °K.

Eqs. (31) and (32) were determined by the U. S. Bureau of Mines (27). Eq. (33) was derived by assuming argon to be an ideal monatomic gas (28). The composition of air was assumed to be 21 vol. pct. O_2, 78 vol. pct. N_2, and 1 vol. pct. Ar. The result of the calculations was:

$$C_{pA} = 6.7046 + 1.005 \times 10^{-3} T_A - 0.084 \times 10^{5} T_A^{-2} \qquad (34)$$

where C_{pA} = heat capacity at constant pressure of air, cal/gm mole °K. $\hat{C}_{pA}$ was found by dividing the right-hand side of Eq. (34) by 28.97, the molecular weight of air. The result was:

$$\hat{C}_{pA} = 0.2314 + 0.03469 \times 10^{-3} T_A - 0.0029 \times 10^{5} T_A^{-2} \qquad (35)$$

Therefore:

$$\frac{\partial \Delta \hat{H}_A}{\partial z} = (0.2314 + 0.03469 \times 10^{-3} T_A - 0.0029 \times 10^{5} T_A^{-2}) \frac{dT_A}{dz} \qquad (36)$$

B. Evaluation of $\frac{\partial \Delta \hat{H}_p}{\partial t}$

The partial derivation of $\Delta \hat{H}_p$ with respect to t is such that:

$$\frac{\partial \Delta \hat{H}_p}{\partial t} = \hat{C}_{pp} \frac{\partial T}{\partial t} \qquad (37)$$

where $\hat{C}_{p_p}$ = specific heat at constant pressure of the pellets, cal/gm °K.

In order to evaluate $\frac{\partial \Delta \hat{H}_p}{\partial t}$, $\hat{C}_{p_p}$ must be evaluated. $\hat{C}_{p_p}$ varies with time since the amounts of hematite and magnetite in a pellet vary with time. $\hat{C}_{p_p}$ was calculated using:

$$\hat{C}_{p_p} \times \frac{\text{g pellet}}{\text{cm}^3} = \hat{C}_{pFe_3O_4} \times \frac{\text{g } Fe_3O_4}{\text{cm}^3} + \hat{C}_{pFe_2O_3} \times \frac{\text{g } Fe_2O_3}{\text{cm}^3} \qquad (38)$$

where $C_{pFe_3O_4}$ = specific heat at constant pressure of magnetite, cal/gm °K, and

$\hat{C}_{pFe_3O_3}$ = specific heat at constant pressure of hematite, cal/gm °K.

It was assumed that the density of magnetite and hematite in an ore concentrate ball were close enough so that the density of the pellet did not vary with time. With this assumption, Eq. (38) becomes:

$$\hat{C}_{p_p} = \hat{C}_{pFe_3O_4} \times \frac{g\ Fe_3O_4/cm^3}{\rho} + \hat{C}_{pFe_2O_3} \times \frac{g\ Fe_2O_3/cm^3}{\rho} \qquad (39)$$

In order to find how g Fe_3O_4/cm^3 and g Fe_2O_3/cm^3 varied with time, it was necessary to use kinetic data. In this model, a k value was calculated from the kinetic data which was dependent on time and temperature.

It was assumed that the oxidation kinetics were affected only by time and temperature and that the amount of oxygen taken up by oxidation did not change the partial pressure of oxygen enough to affect oxidation kinetics. This assumption is discussed in the section on Discussion of Results. The k was such that:

$$\left[\frac{g\ Fe_2O_3}{cm^3}\right]_{t>o} = \int_o^t k(t,T)dt \qquad (40)$$

where: $\left[\frac{g\ Fe_2O_3}{cm^3}\right]_{t>o}$ = gm of hematite per cm^3 produced since time zero;

$k(t,T)$ = instantaneous rate of reaction, $\frac{g\ Fe_2O_3}{cm^3\ min}$.

The chemical equation for magnetite oxidation is:

$$4\ Fe_3O_4 + O_2 = 6\ Fe_2O_3 \qquad (41)$$

By using Eqs. (40) and (41), it can be shown that

$$\frac{gm\ moles\ Fe_3O_4}{cm^3} = \left[\frac{gm\ moles\ Fe_3O_4}{cm^3}\right]_{t=o} - 0.667 \left[\frac{gm\ moles\ Fe_2O_3}{cm^3}\right]_{t>o}$$

$$= \frac{C_{Fe_3O_4(t=0)}}{231.55} - \frac{0.667}{159.70} \int_o^t k(t,T)dt \qquad (42)$$

where $C_{Fe_3O_4(t=0)}$ = original concentration of magnetite in a pellet, g Fe_3O_4/cm^3.

Dividing both sides of Eq. (42) by the molecular weight of Fe_3O_4 gives:

$$\frac{g\ Fe_3O_4}{cm^3} = C_{Fe_3O_4(t=0)} - (0.667)\ \frac{(231.55)}{(159.70)} \int_o^t k(t,T)\ dt \qquad (43)$$

Substitution of Eq. (43) into Eq. (39) yields Eq. (44)

$$\hat{C}_{p_p} = \frac{C_{pFe_3O_4}}{\rho} \left(\frac{C_{Fe_3O_4(t=0)}}{231.55} - \frac{(0.667)}{159.70} \int_o^t k(t,T)\ dt \right)$$

$$+ \frac{C_{pFe_2O_3}}{\rho\ 159.70} \left(\int_o^t k(t,T)\ dt + C_{Fe_2O_3(t=0)} \right) \qquad (44)$$

where:

$C_{Fe_2O_3(t=0)}$ = original concentration of hematite in a pellet, g Fe_2O_3/cm^3;

$C_{pFe_3O_4}$ = heat capacity at constant pressure of magnetite, cal/g mole °K; and

$C_{pFe_2O_3}$ = heat capacity at constant pressure of hematite, cal/ g mole °K.

Eqs. (45) and (46) both of which were determined by the U. S. Bureau of Mines (27) are listed below:

$$C_{pFe_2O_3} = 31.71 + 1.76 \times 10^{-3}\ T \qquad (45)$$

$$C_{pFe_3O_4} = 48.0 \qquad (46)$$

These were substituted in Eq. (44) to give:

$$\hat{C}_{p_p} = \left[\frac{48.0}{\rho} \left(\frac{C_{Fe_3O_4(t=0)}}{231.55} - \frac{0.667}{159.70} \int_o^t k(t,T)\ dt \right) \right.$$

$$\left. + \left(\frac{31.71 + 1.76 \times 10^{-3}\ T}{159.70\rho} \right) \left(C_{Fe_2O_3(t=0)} + \int_o^t k(t,T)\ dt \right) \right] \qquad (47)$$

therefore,

$$\frac{\partial \hat{\Delta H}_p}{\partial t} = \left[\frac{48.0}{\rho} \left(\frac{C_{Fe_3O_4}(t=0)}{231.55} - \frac{0.667}{159.70} \int_0^t k(t,T)\, dt \right) + \left(\frac{31.71 + 1.76 \times 10^{-3}T}{159.70\, \rho} \right) \left(C_{Fe_2O_3}(t=0) + \int_0^t k(t,T)\, dt \right) \right] \frac{\partial T}{\partial t} \quad (48)$$

C. Evaluation of $\partial q_c / \partial z$

The amount of heat transferred from the pellet lump to the gas lump, q_c, was evaluated from Eqs. (1), (3), (4), and (5). The viscosity of air, μ, varies with temperature and is included in Eqs. (4) and (5). This viscosity was evaluated from a formula recommended in National Bureau of Standards Circular #564 (29):

$$\eta = \frac{145.8\ T_A^{3/2}}{T_A + 110.4} \times 10^{-7} \quad (49)$$

where η = viscosity in poise. Eq. (49), after being put into units of gm/cm min, becomes:

$$\mu = \frac{(8.65 \times 10^{-4})\ T_A^{3/2}}{(T_A + 110.4)} \quad (50)$$

where μ = viscosity, gm/cm min.

Substituting Eq. (50) into Eq. (5) gives:

$$Re = \frac{G_o\ (T_f + 110.4)}{a\ (8.65)\ (10^{-4})\ T_f^{3/2}} \quad (51)$$

where T_f = arithmetic average of T_A and T_S, in °K. Putting Eqs. (51) and (4) into Eq. (3) and transposing gives:

$$h_{\ell oc} = \frac{0.61 \left(\frac{G_o\ (T_f + 110.4)}{\psi\, a\ (8.65)\ (10^{-4})\ T_f^{3/2}} \right)^{\psi} \hat{C}_{pA}\, G_o}{\left(\frac{\hat{C}_p \mu}{k} \right)^{2/3}} \quad (52)$$

It was assumed that the Prandtl number, $\left(\frac{\hat{C}_{p\mu}}{k}\right)^{2/3}$, did not vary with temperature. A value of 0.827 was used for this dimensionless number. Also, since pellets are approximately spheres, it was assumed that $\psi = 1$. With the use of these assumptions, Eq. (52) reduces to:

$$h_{\ell oc} = \frac{\hat{C}_{pA}\, G_o}{0.827}\,(0.61)\left(\frac{G_o\,(T_f + 110.4)}{a\,(8.65)\,(10^{-4})\,T_f^{3/2}}\right)^{-0.41} \tag{53}$$

$$= (0.0407)\, G_o^{0.59}\, a^{0.041}\, \hat{C}_{pA} \left(\frac{T_f + 110.4}{T_f^{3/2}}\right)^{-0.41}$$

Substituting Eq. (53) into Eq. (1) and rearranging terms:

$$\frac{\partial q_c}{\partial z} = (0.0407)\, G_o^{0.59}\, a^{0.41}\, \hat{C}_{pA} \left(\frac{T_f + 110.4}{T_f^{3/2}}\right)^{-0.41} a\, A_t (T-T_A) \tag{54}$$

Note that T, pellet temperature, in this equation and all further equations is equivalent to T_S. Substitution of Eq. (35) and the definition of T_f into Eq. (52) gives

$$\frac{\partial q_c}{\partial z} = (0.0407)\, G_o^{0.59}\, A_t a^{1.41} \left[\frac{\left(\frac{T + T_A}{2}\right) + 110.4}{\left(\frac{T + T_A}{2}\right)^{3/2}}\right]^{-0.41} (T-T_A). \tag{55}$$

$$(0.2314 + 0.03469 \times 10^{-3} T_A - 0.0029 \times 10^{5} T_A^{-2})$$

D. Evaluation of q_x

The amount of heat produced by oxidation at a given instant in time, q_x, is such that:

$$q_x = k(t,T)\, \hat{\Delta H} \tag{56}$$

where:

$k(t,T) = \frac{g\ Fe_2O_3}{cm^3\ of\ pellet\text{-}min.}$ produced at the given time and temperature, and

$\Delta\hat{H}$ = heat required to produce one gram of Fe_2O_3 from magnetite.

was calculated using thermodynamic data taken from Kubaschewaski and Evans (30). The data used are shown below:

Compound	$\Delta H^{\circ}_{298°K}$	C_p, cal/gm mole-°K	Range (°K)
αFe_3O_4	-266,900 cal	$21.88 + 48.2 \times 10^{-3}T$	298 - 900
βFe_3O_4		48.00	900 - 1800
O_2	0	$7.16 + 1.00 \times 10^{-3}T - 0.40 \times 10^{5}T^{-2}$	298 - 3000
αFe_2O_3	-196,300 cal	$23.49 + 18.6 \times 10^{-3}T - 3.55 \times 10^{5}T^{-2}$	298 - 950
βFe_2O_3		36.0	950 - 1050
γFe_2O_3		$31.70 + 1.76 \times 10^{-3}T$	1050 - 1750

The results of the calculation were:

$$\Delta\hat{H} = -110.2 - 0.01058T + 0.005 \times 10^{-3}T^2 - \frac{0.000416 \times 10^5}{T} \qquad (57)$$

Hence,

$$q_x = k(t,T)\left[-110.2 - 0.01058T + 0.00500 \times 10^{-3}T^2 \frac{-0.000416 \times 10^5}{T}\right] \qquad (58)$$

E. Evaluation of q_r

The amount of heat transferred by radiation from pellet to pellet, q_r, was calculated using the Damkohler expression which follows (9):

$$\frac{\partial q_r}{\partial z} = \frac{\partial}{\partial z}\left\{\left[\frac{4\varepsilon}{4-\varepsilon} D_p \sigma T^3\right] \frac{\partial T}{\partial z}\right\} \qquad (59)$$

where:

ε = emissivity of pellets, dimensionless

= 0.8 (see Ref. (31));

D_p = average particle diameter, cm; and

σ = Stefan-Boltzmann constant.

F. Evaluation of k(t,T)

The instantaneous rate of oxidation of magnetite to form hematite in concentrate ore balls, k(t,T), was evaluated from the % Ox versus time curves determined experimentally. As discussed in the section on Experimental Data, these data were fit to the form:

$$\%Ox = AB^{C^{TI}} + D \tag{7}$$

By differentiating this expression, one obtains:

$$\frac{d(\%Ox)}{dt} = AB^{C^{TI}} \; C^{TI} \; \ell n\,(B) \; \ell n\,(C) \; \frac{d(TI)}{dt} \tag{60}$$

From the definition of %Ox, it was shown that:

$$\frac{g\ Fe_2O_3}{cm^3\ pellet} = (0.010345)\ (\%Ox)\ \rho\ (wt\ \%\ Fe_3O_4(t=0)) \tag{61}$$

where wt % $Fe_3O_4(t=0)$ = weight percent magnetite of the pellets before firing. By differentiating both sides of Eq. (61), it is seen that

$$\frac{\partial \left(\frac{g\ Fe_2O_3}{cm^3\ pellet}\right)}{\partial t} = 0.010345\ \rho\ (wt\%\ Fe\ O\ (t=0))\ \frac{\partial\ 0x\%}{\partial\ t} \tag{62}$$

Since k(t,T) is equal to the left-hand side of Eq. (62):

$$k(t,T) = 0.010345\ \rho\ (wt\%\ Fe_3O_4(t=0))\ \frac{\partial\ \%Ox}{\partial\ t} \tag{63}$$

In order to solve for k(t,T) using Eq. (63), it was necessary to calculate the values of A, B, C, and D for any temperature between 300°C and 1000°C. The method used to do this is discussed in the section on

Method of Solution of the Differential Equations.

G. Evaluation of G_o and SCF

The mass flow rate per unit cross-sectional area, G_o, and volume flow rate per unit cross-sectional area, SCF, vary with time during the heat hardening process. The way in which these variations were taken into account are also discussed in the section on Method of Solution of the Differential Equations.

Final Form of the Differential Equations

In developing the final form of the differential equations, Eqs. (36), (48), (55), and (59) were substituted into Eqs. (28) and (29); this gave the following two expressions:

$$-(0.0407)\ G_o^{0.59}\ A_t a^{1.41}\left[\frac{\left(\frac{T+T_A}{2}\right)+110.4}{\left(\frac{T+T_A}{2}\right)^{3/2}}\right]^{-0.41}(T-T_A)\ (0.2314$$

$$+\ 0.03469 \times 10^{-3}\ T_A - 0.0029 \times 10^{5}\ T_A^{-2})$$

$$+\ SCF\ \rho_A\ (0.2314 + 0.03469 \times 10^{-3} T_A - 0.0029 \times 10^{5} T_A^{-2}\ \frac{\partial T_A}{\partial z} = 0 \quad (64)$$

and

$$\frac{\partial}{\partial z}\left\{\left[\frac{4\varepsilon}{4-\varepsilon}\ D_p\ \sigma\ T^3\right]\ \frac{\partial T}{\partial z}\right\} + (0.0407)\ G_o^{0.59}\ A_t a^{1.41}$$

$$\left[\frac{\left(\frac{T+T_A}{2}\right)+110.4}{\left(\frac{T+T_A}{2}\right)^{3/2}}\right]^{-0.41}(T-T_A)\ (0.2314 + 0.03469 \times 10^{-3}\ T_A - 0.0029$$

$$\times 10^{5}\ T_A^{-2}) + (1-\varepsilon)\ A_t(-110.2-0.01058T+0.005 \times 10^{-3}\ T^{+2}$$

$$- \frac{0.00416 \times 10^5}{T}\Big) k(t,T) + \rho\,(1-\varepsilon)\,A_t \Bigg[\frac{48.0}{\rho}\Bigg(\frac{C_{Fe_3O_4}(t=0)}{\partial\, 231.55} - \frac{0.667}{159.70}\int_o^t k(t,T)\,dt\Bigg) + \Bigg(\frac{31.71 + 1.76 \times 10^{-3}T}{159.60\,\rho}\Bigg)\Bigg(C_{Fe_2O_3}(t=0) + \int_o^t k(t,T)\,dt\Bigg)\Bigg] \frac{\partial T}{\partial t} = 0 \tag{65}$$

The final form of the differential equations is obtained by simplifying Eqs. (64) and (65); these are as follows:

$$-(0.0407)\,G_o^{0.59}\,A_t a^{1.41}\left[\frac{\left(\frac{T+T_A}{2}\right)+110.4}{\left(\frac{T+T_A}{2}\right)^{3/2}}\right]^{-0.41}(T-T_A) + SCF\,\rho\,A\,\frac{\partial T_A}{\partial z} = 0 \tag{66}$$

and

$$\frac{\partial}{\partial z}\left\{\left[\frac{4\varepsilon}{4-\varepsilon}\,\frac{D_p}{A_t}\,\sigma\,T^3\right]\frac{\partial T}{\partial z}\right\} + (0.0407)\,G_o^{0.59}\,a^{1.41}\left[\frac{\left(\frac{T+T_A}{2}\right)+110.4}{\left(\frac{T+T_A}{2}\right)^{3/2}}\right]^{-0.41}(T-T_A)(0.2314+0.03469\times10^{-3}T_A - 0.0029 \times 10^5\,T_A^{-2})$$

$$+ (1-\varepsilon)\,(-110.2 - 0.01058\,T + 0.005 \times 10^{-3}\,T^2 - \frac{0.00416 \times 10^5}{T})\,k(t,T)$$

$$+ (1-\varepsilon)\Bigg[48.0\left(\frac{C_{Fe_3O_4}(t=0)}{231.55} - \frac{0.667}{159.70}\int_o^t k(t,T)\,dt\right) + \left(\frac{31.71 + 1.76 \times 10^{-3}T}{159.70}\right)\left(C_{Fe_2O_3}(t=0) + \int_o^t k(t,T)\,dt\right)\Bigg]\frac{\partial T}{\partial t} = 0 \tag{67}$$

METHOD OF SOLUTION OF THE DIFFERENTIAL EQUATIONS

The final forms of the differential equations, Eqs. (66) and (67), describe the heat and mass transfer which take place in a thin slice of the bed while magnetite oxidation occurs. These equations must be solved in order to simulate the thermal profiles developed in the bed during oxidation. To solve the equations, the slice was divided into 10 cells as shown in Figure 11. The air lump equation, Eq. (66), was solved analytically for each cell. This solution, together with the pellet lump equation (Eq. (67)) and the calculated value for the air temperature at the upper boundary of the cell were solved using an analogue simulator program on a digital computer. The results of the program were plots of the air and solids temperature versus time at different levels in the bed.

The air lump equation, Eq. (66), does not seem tractable. In order to make analytical solution possible, the term

$$\left[\frac{\left(\frac{T + T_A}{2}\right) + 110.4}{\left(\frac{T + T_A}{2}\right)^{3/2}}\right]^{-0.41}$$

was assumed constant with respect to z. Table VIII lists the results of calculations for this term using different values. From the table, it is clear that, as long as each cell is small enough so that the air temperature does not vary by more than 300°C within the element, this assumption is reasonable. In order to simplify the equation, it was also assumed that:

$$\left[\left(\frac{\left(\frac{T + T_A}{2}\right) + 110.4}{\left(\frac{T + T_A}{2}\right)^{3/2}}\right)^{-0.41}\right]_{\Delta z/2} = \left(\frac{T_n + 110.4}{T_n{}^{3/2}}\right)^{-0.41} \quad (70)$$

where:

$$\left[\left(\frac{\left(\frac{T + T_A}{2}\right) + 110.4}{\left(\frac{T + T_A}{2}\right)^{3/2}}\right)^{-0.41}\right]_{\Delta z/2} = \left(\frac{\left(\frac{T + T_A}{2}\right) + 110.4}{\left(\frac{T + T_A}{2}\right)^{3/2}}\right)^{-0.41}$$

evaluated in the center of the cell being considered; and T_n = pellet temperature for the cell being considered. This assumption also seems reasonable as long as the air and pellet temperatures do not vary by more than 300°C. By making these assumptions, substituting $SCF = \frac{G_o A}{\rho A}$, and solving for $\partial T_A / \partial t$, Eq. (66) becomes:

$$\frac{\partial T_A}{\partial z} = \frac{(0.0407)\ a^{1.41}}{G_o{}^{0.41}} \left(\frac{T_n + 110.4}{T_n{}^{3/2}}\right)^{-0.41} (T - T_A) \quad (71)$$

$$= K\ (T - T_A)$$

where: $$K = \frac{(0.0407)\ a^{1.41}}{G_o{}^{0.41}} \left(\frac{T_n + 110.4}{T_n{}^{3/2}}\right)^{-0.41}$$

Equation (71) was integrated as follows:

$$\frac{\partial T_A}{(T-T_A)} = K\, \partial z \quad (72)$$

$$\frac{\partial (T-T_A)}{(T-T_A)} = -K\, \partial z \quad (73)$$

$$\ell n\ (T-T_A) = -Kz + C \tag{74}$$

With the use of the following boundary conditions (see Figure 11):

$$z = 0,\ T = T_n,\ T_A = T_{A_o}$$

$$z = \Delta z/2,\ T = T_n,\ T_A = T_{A_n}$$

Eq. (74) becomes:

$$\ell n\ \frac{(T_n - T_{A_n})}{(T_n - T_{A_o})} = -K\ \frac{\Delta z}{2} \tag{75}$$

The solution of Eq. (75) for T_{A_n} gives:

$$T_{A_n} = T_n - (T_n - T_{A_o})\ e^{-K\cdot\Delta z/2} \tag{76}$$

Eq. (76) was used in the analogue simulator for all of the cells.

T_{A_o} for the first element was the temperature of the air entering the bed for the time being simulated. For the other elements T_{A_o} was calculated using Eq. (74) and the boundary conditions:

$$z = \Delta z/2,\ T = T_{n-1},\ T_A = T_{A_{n-1}}$$

$$z = \Delta z,\ T = T_{n-1},\ T_A = T_{A_o}$$

where z = as defined for the cell immediately above the cell for which T_{A_o} is required;

T_{n-1} = pellet temperature for the cell immediately aboye that for which T_{A_o} is required; and

$T_{A_{n-1}}$ = air temperature at the center of the cell immediately above that for which T_{A_o} is required.

The result was:

$$T_{A_o} = T_{n-1} - (T_{n-1} - T_{A_{n-1}})\ e^{-K\ \frac{\Delta z}{2}} \tag{77}$$

The pellet lump equation was solved for $\frac{\partial T}{\partial t}$ in order to allow it to be used in the analogue simulator program, It was further assumed that

$$(0.2314 + 0.03469 \times 10^{-3}T_A - 0.0029 \times 10^{5}T_A^{-2}) = (0.2314 + 0.03469 \times 10^{-3}T) \tag{78}$$

It can be shown that this is a reasonable assumption if the pellet and air temperatures do not differ by more than 300°C. Making this assumption and solving for $\frac{\partial T}{\partial t}$, one gets:

$$\frac{\partial T}{\partial t} = \left\{ \frac{1}{A_t} \frac{\partial}{\partial} \left\{ \left[\frac{4\varepsilon}{4-\varepsilon} D_p \sigma T^3 \right] \frac{\partial}{\partial} \frac{T}{z} \right\} \right.$$

$$+ \left\{ 0.0407 \, G_o^{0.59} \, a^{1.41} \left(\frac{T_n + 110.4}{T_n^{3/2}} \right)^{-0.41} (0.2314+0.03469 \times 10^{-3}T) \right\}$$

$$\left. + \left\{ (1-\varepsilon) \, k(t,T) \, (-110.2-0.01058T + 0.005 \times 10^{-3}T^2 \frac{-0.00416\times10^{5}}{T} \right\} \right\}$$

$$/\!/ \left\{ -(1-\varepsilon) \left\{ 48.0 \left[\frac{C_{Fe_3O_4}(t=0)}{231.55} - \frac{0.667}{159.70} \int_0^t k(t,T) \, dt \right] \right.\right.$$

$$\left.\left. + \frac{(31.71 + 1.76 \times 10^{-3}T)}{159.70} \left[C_{Fe_2O_3}(t=0) + \int_0^t k(t,T) \, dt \right] \right\} \right. \tag{79}$$

The digital analogue simulator program used to solve Eqs. (76), (77), and (79) was LEANS (32). A copy of the program and a user's manual are available, on request, from Dr. W. E. Schiesser, Department of Chemical Engineering, Lehigh University. The program is written so that subroutines written in FORTRAN IV can be used with the program. Twenty-five subroutines were used to solve the equations, simplify the block diagram, and allow the temperature of the air and solids to be plotted at the end of the program. The Calcomp plotter and subroutine

package was used to plot the results. The plotter allowed the results of the simulation to be plotted so that virtually continuous plots were obtained. Information on the Calcomp plotter and subroutine package is available from the Lehigh University Computer Center. An analogue block diagram showing the way in which the simulator was used to simulate the thermal profiles is included as Appendix C of this thesis. A listing of the program and subroutines used, along with the names of the input variables which must be supplied to the program, are included in Appendix D. The program was run on a CDC 6400 computer. An approximately 100 K memory core was required to run the program with the plotting capability. Each computer run cost from $10 to $15.

The subroutines are self-explanatory except for those which calculated k (t,T), $T_{A_{in}}$, and G_o. The subroutine used to calculate k (t,T) received the temperature and amount of magnetite oxidized at a given simulation time. Using this temperature, it was possible to search the tables listing A, B, C, and D until the two temperatures which were closest to the given temperature and for which values of the coefficients were known were found. The value of the coefficients for the temperature received by the subroutine was found by linear interpolation using these known values. From the calculated values of these coefficients and the amount of magnetite oxidized up to the present simulator time, the time at which the pellets would have been oxidizing if the oxidation had been isothermal was calculated. This value, along with the current values of the coefficients, was then substituted into Eq. (63) to find k (t,T).

$T_{A_{in}}$ is varied during the heat hardening process. This is done, as discussed in the Introduction, to permit the most economic, yet successful, heat hardening process. The data used to test this model gave the time during each run at which the temperature changed. From this information a table of the temperature entering the bed for each second during the test was constructed. The table was included in the subroutine which calculated the current value of $T_{A_{in}}$. The simulator time for which the value of $T_{A_{in}}$ was required was received by the subroutine from the main program and the corresponding value of $T_{A_{in}}$ found by searching the table.

The air flow rate through the pellet bed is measured only once a minute during a pot test. For the purposes of this model, it was assumed that the flow rate was the same as each second of the minute as the measured flow rate. With this assumption, a table giving the flow rate through the bed for each second during testing was constructed. G_o for a given simulator time was obtained from this table in the same way in which $T_{A_{in}}$ was found.

RESULTS

The mathematical model was checked by simulating the temperature-time profiles developed during magnetite oxidation for pot tests made industrially and comparing the measured and simulated profiles. The simulations were performed by using the same flow rate and temperature of air entering the bed versus time profiles as for the pot tests. Three pot tests were simulated for Ore 1, and three for Ore 2. In all cases the simulation was started when the pot test seemed to indicate that the ore ball drying was complete and ended when cooling commenced. Data on ball size, hood profile, and initial temperature for each cell were determined from pot test records.

The results of the simulation in the top, middle, and bottom of the bed were compared with pot measurements of the thermal profile at approximately the same location. Figures 12 through 29 compare the simulated and measured results. The exact location of the simulated profile and the measured profile for each run are included on each figure. Data used for each test for both simulation and comparison is included in Appendix E.

In all of the simulations, the radiation term was calculated, but was not used in finding the solids temperatures.

DISCUSSION OF RESULTS

Several assumptions were made in the development of the mathematical model with which the thermal profiles were simulated. The more important of these assumptions were:

(1) There is no temperature gradient within the pellets.

(2) The Prandtl number for air to the two-thirds power does not vary with temperature.

(3) The amount of heat transferred from pellet to pellet by conduction is negligible.

(4) The term $A_A \quad \rho_A \ (T,P) \ \frac{\partial \ \hat{\Delta H}_A}{\partial \ t}$ in Eq. (17) is negligible when compared with the other terms in the equation.

(5) The term $\left[\frac{\left(\frac{(T + T_A)}{2} \right) + 110.4}{\left(\frac{(T + T_A)}{2} \right)^{3/2}} \right]^{-0.41}$

is constant with respect to z and is equal to

$$\left(\frac{T + 110.4}{T^{3/2}} \right)^{-0.41}$$

(6) The Δz used was small enough so that an accurate estimate of the thermal profiles was obtained.

(7) The amount of oxygen taken from the air flowing past the pellets by oxidation is negligible when compared to the total flow rate.

(8) The amount of oxygen taken from the air flowing past the pellets by oxidation does not cause enough change in the partial pressure of oxygen to significantly affect oxidation kinetics.

Of these assumptions, numbers (4), (5), (6), (7), and (8) can be checked only by using the results of the simulation. The terms in Eq. (17) can be evaluated using data from any of the test runs. Looking at the results of Test 1-1, $T-T_A$ seems to be about 20°C as a minimum, $\frac{\partial T}{\partial t}$ = 10°C/cm as a minimum, and $\frac{\partial T}{\partial t}$ = 2000°C/min as a maximum. For these and the data presented for Test 1-1 in Appendix E, it is found that:

$$\frac{\partial q_c}{\partial z} = 69.3 \text{ cal/min cm}$$

$$SCF\ \rho_A \frac{\partial (\hat{\Delta H}_A)}{\partial z} = 24.1 \text{ cal/min cm}$$

$$A_A\ \rho_A\ (T,P) \frac{\partial (\hat{C}_{pA}\ T_A)}{\partial t} = 0.244 \text{ cal/min cm.}$$

From this calculation it is clear that the assumption that the term $A_A \rho_A\ (T,P) \frac{\partial (\hat{C}_{pA}\ T_A)}{\partial t}$ is negligible is valid.

As discussed in the Section on Method of Solution and illustrated in Table VIII, the assumption that the term

$$\left[\frac{\left(\frac{T + T_A}{2}\right) + 110.4}{\left(\frac{T + T_A}{2}\right)^{3/2}}\right]^{-0.41}$$

is constant with z and equal to $\left(\frac{T + 110.4}{T^{3/2}}\right)^{-0.41}$ is reasonable as long as the air and pellet temperatures do not vary by more than 300°C.

None of the eighteen thermal profiles simulated show this great a difference between air and pellet temperature. The usual difference exhibited by the profiles is between 50° and 100°C. This assumption is, therefore, also valid.

The assumption that enough cells had been used was checked by comparing the simulated temperatures obtained for identical positions in the bed when the normal z and half the normal z value were used. The results of both simulations near the middle of the simulation time agreed to within 40°F. It was decided that this small amount of variation showed that enough nodes had been used to obtain a good estimate of the thermal profile and that the addition of more nodes was uneconomical.

The results given by the computer program included the amount of magnetite which had been oxidized to hematite from the beginning of the simulation to the current simulator time. These values were used to evaluate the validity of assumptions (7) and (8). From the values the amount of oxygen taken from the air flowing past the pellets by oxidation for each minute of Test 1-1 and the partial pressure of oxygen at the bottom of the green pellet bed were calculated. Table IX shows the results of the calculations. The results indicate that the assumption that the amount of oxygen taken from the air flowing past the pellets by oxidation is negligible when compared to the total flow rate is reasonable. At most the flow rate leaving the bottom of the bed is about 6% lower than that entering the top. The results listed in Table IX also indicate that the partial pressure of oxygen in the air leaving the bottom of the bed is in some cases significantly lower than

that at the top of the bed. It was impossible to evaluate the extent to which this difference affects oxidation kinetics in ore concentrate balls since neither experimental data using different partial pressures of oxygen or a mechanism describing the oxidation kinetics for ore balls of the two concentrates used were available. From the partial pressures of oxygen listed in Table IX, it is apparent that the assumption that the amount of oxygen taken from the air flowing past the pellets does not cause enough change in the partial pressure of oxygen to significantly affect oxidation kinetics is the weakest assumption made in developing the mathematical model.

The results of the simulations done for pot tests 1-1, 1-2, 1-3, 2-1, and 2-2 all give an acceptable estimate of actual pot test performance. The results of the simulation of test 2-3 are not this good. When compared with the measured pot test profiles, the calculated results show the following characteristics:

(1) The calculated results compare excellently with pot test measurements for Figs. 12, 15, 18, 21, 24, and 27 in which both the simulated and measured results were made close to the top of the bed.

(2) Near the end of the simulation the calculated results for the middle and bottom of the bed are usually lower than the measured values.

(3) The calculated results obtained in the middle and bottom of the bed for all of the pot tests are higher than the measured values from the beginning to near the middle of the simulations.

The first two observations can be explained since data on the oxidation kinetics of balled magnetite ore concentrates could not be taken above 1000°C. The printed results of the computer program showed that the top few cells in the bed usually had completed oxidation when their temperatures rose above 1000°C. This was not true for nodes lower in the bed. The program assumed that the oxidation kinetics were the same as at 1000°C when this temperature was exceeded. A faster rate of oxidation would liberate heat quicker and would cause the thermal profiles to be closer to those measured. It is thought that oxidation is probably faster above 1000°C and that it was for this reason that the calculated results were lower than those measured near the end of the simulation.

There are two possible explanations for the third observation. The first explanation is that the ore balls may not have been completely dry when the simulation was started. Incomplete drying could cause a difference between the simulated and measured results in two ways. The first of these is that some heat which would otherwise be used to raise the temperature of the balls would be required for drying. The second is that, if drying and magnetite oxidation occurred simultaneously, the oxidation kinetics might be affected by the need for water vapor to be transported through the hematite shell. Both of these effects would result in the calculated profiles being higher than those measured. It is thought that the disagreement between the simulated and measured results for Test 2-3 can be explained in this manner. It was noted on the pot test records that the balls used for Test 2-3 were extremely wet.

The second possible explanation is that the measured thermal profiles may have been influenced by partial pressures of oxygen lower than 0.21 atm. being present during oxidation. This could have occurred because of oxygen consumed by oxidation above the depth for which the profile was measured. The mathematical model assumed that all oxidation occurred in air with a partial pressure of oxygen of 0.21 atm. A lower partial pressure should cause a slower reaction rate. For this reason, if lower partial pressures of oxygen were present in the bed during oxidation, the simulated profiles would be higher than those measured.

The agreement between the mathematical model and measured results is actually quite good considering that published correlations were used to formulate the final differential equations and no adjustment of any kind was made to the data used for the computer runs. It is the opinion of the author that this model is good enough to allow systematic evaluation of the effects of changes in variables affecting oxidation kinetics on the traveling grate process.

CONCLUSIONS

The following statements can be concluded from the results of this study:

(1) Measurements of weight gain during oxidation can be used to find the kinetics of magnetite oxidation for ore concentrate balls.

(2) The parabolic rate law as applied to a sphere does not necessarily apply to oxidation of magnetite ore concentrate balls.

(3) Using the model developed in this study, a systematic evaluation of the effects of changes affecting the kinetics of oxidation of magnetite in balled ore concentrates on the traveling grate pelletizing process should be possible.

(4) In order to obtain a more exact agreement between the mathematical model and measured results, data on the oxidation of balled magnetite ore concentrates at temperatures above 1000°C and using different oxygen partial pressures should be obtained.

APPENDIX A

NOMENCLATURE

NOMENCLATURE

a	=	solid particle surface area per unit bed volume
A	=	coefficient used in the expression which fit the kinetic data
A_A	=	cross-sectional area of air lump
A_p	=	cross-sectional area of pellet lump
A_t	=	cross-sectional area of bed
B	=	coefficient used in the expression which fit the kinetic data
C	=	coefficient used in the expression which fit the kinetic data
$C_{Fe_2O_3(t=0)}$	=	original concentration of hematite in a pellet, g Fe_2O_3/cm^3
$C_{Fe_3O_4(t=0)}$	=	original concentration of magnetite in a pellet, g Fe_3O_4/cm^3
C_{pA}	=	heat capacity of air at constant pressure, cal/gm mole °K
C_{pAr}	=	heat capacity at constant pressure of argon, cal/gm mole °K
$\hat{C}_{pb}$	=	specific heat at constant pressure per unit mass for the fluid, cal/gm °K
$C_{pFe_2O_3}$	=	heat capacity at constant pressure of hematite, cal/g mole °K
$\hat{C}_{pFe_2O_3}$	=	specific heat at constant pressure of hematite, cal/g °K

$C_{PFe_3O_4}$ = heat capacity at constant pressure of magnetite, cal/g mole °K

$\hat{C}_pFe_3O_4$ = specific heat at constant pressure of magnetite, cal/g °K

C_{pN_2} = heat capacity at constant pressure of nitrogen, cal/gm mole °K

C_{pO_2} = heat capacity at constant pressure of oxygen, cal/gm mole °K

$\hat{C}_{p_p}$ = specific heat at constant pressure of the pellets, cal/g °K

D = coefficient used in the expression which fit the kinetic data

D_p = average particle diameter

f = subscript denoting that these properties are evaluated at the average of the air and packing surface temperatures

F = stoichiometric ratio of grams O_2 used per gram of Fe_2O_3 produced

$\frac{gFe_2O_3}{cm^3}_{t>0}$ = grams of hematite per cm^3 produced since time zero

G_o = mass velocity of fluid just before entering the bed

$\Delta\hat{H}$ = heat required to produce one gram of Fe_2O_3 from magnetite

$\hat{\Delta H}_A$ = enthalpy of air, cal/gm

$\hat{\Delta H}_p$ = enthalpy of the pellets, cal/cm^3 pellet lump

$h_{\ell oc}$ = local heat transfer coefficient for a cross-sectional area in a packed bed

jh = Colburn analogy

k = thermal conductivity of fluid

k_E = constant for oxidation of a ball of magnetite concentrate at a given temperature as used in the parabolic rate law

k_o = rate of reaction in grams of Fe_2O_3 produced per unit time and area of the pellet lump

$$K = \frac{(0.0407)\ a^{1.41}}{G_o^{0.41}} \left(\frac{T_n + 110.4}{T_n^{3/2}} \right)^{-0.41}$$

k(k,T) } instantaneous rate of reaction, g Fe_2O_3/cm^3 min

ox = ox%/100

ox% = 100 times the ratio of weight gained during oxidation to the weight which would be gained by the sample if it was completely oxidized

q_c = heat transferred by the flowing fluid to the packing by convection

q_k = heat transferred by conduction from particle to particle, cal/min

q_r = heat transferred by radiation from solid particle to solid particle, cal/min

q_x = heat generated by oxidation of magnetite, cal/min cm^3 of pellet lump

R = radius of ore ball

Re = packed bed Reynolds number

= $G_o/a\ \mu_f$

SCF = standard cm^3/min of air flowing through the bed

t = time

t_E = time from the start of oxidation

T = pellet temperature in °K

T_A = air temperature in °K

T_{An-1} = air temperature at the center of the cell immediately above that for which T_{A_o} is required

T_{A_o} = temperature at the boundary between the cell under consideration and the cell immediately above it

TI = variable which has a linear relationship with sample number and is a function of time--used in the equation which fit the kinetic data

T_s = surface temperature of particle

T_n = pellet temperature for the cell being considered

T_{n-1} = pellet temperature for the cell immediately above the cell for which T_{A_o} is required

wt% Fe_3O_4 = weight percent magnetite of the pellets before firing

z = axial distance

$\triangle z$ = increment in axial distance

Greek Symbols:

ε = emissivity of pellets

ψ = shape factor

μ = viscosity of fluid

η = viscosity, poise

ρ = density of pellet

ρ_A = density of air for 1 standard cubic centimeter

$\rho_A(T,P)$ = density of the air at the temperature and pressure concerned

σ = Stefan-Boltzmann constant

APPENDIX B

COMPUTER PROGRAM USED TO CURVE FIT THE KINETIC DATA

The kinetic data obtained experimentally were fit empirically in order to allow its use in the mathematical model. The expression,

$$\% \text{ Ox} = AB^{C^{TI}} + D \qquad (7)$$

where A, B, C, and D = coefficients for a given data set

TI = variable which is a linear function of the sample number and a function of the time at which the sample was taken,

was found to fit the data adequately.

The coefficients A, B, C, and D for each isothermal set of data points were obtained using a computer program. A listing of this program is part of this appendix. In the listing the input variables are:

Q = number of data points/3 (must be an integer)

J = number of data points

FX = last D value to be used in the program

ANDIC = indicator to allow for more than one set of data

D = D value (s) to be tried

X(I) = time, minutes

Y(I) = % ox

T(I) = variable which is a linear function of the data point number and is also a function of time

The program listing follows:

```
$$$$$$$$$$$$$$$$$$$$$$$$$$$$$$$$$$$$$$$$$$$$$$$$$$$$$$$$$$$$$$$$$$$$$$$$$$$$$$$$$$$$

                DIMENSION X(30),Y(30),T(30),S1(10),S2(10),S3(10),YCALC(30),ERROR
               1(30),YM(30),YZ(30)
000003      103 READ 99,Q,J,FX,ANDIC
000017       99 FORMAT(F10.2,I10,2F10.2)
000017          M=J/3
000022          N=2*M
000023          L=M+1
000025          K=N+1
000027          DO 5 I=1,J
000030          READ 1,X(I),Y(I),T(I)
000041        1 FORMAT(3F10.5)
000041          Y(I)=Y(I)*0.01
000043        5 CONTINUE
000046       66 READ 71,D
000054       71 FORMAT(F10.7)
000054          SUM=0.0
000055          SAM=0.0
000055          SOM=0.0
000057          DO 7 I=1,M
000060          S1(I)=ALOG10(Y(I)-D)
000066        7 SUM=SUM+S1(I)
000072          DO 8 I=L,N
000074          S2(I)=ALOG10(Y(I)-D)
000102        8 SAM=SAM+S2(I)
000106          DO 9 I=K,J
000110          S3(I)=ALOG10(Y(I)-D)
000116        9 SOM=SOM+S3(I)
000122          P1=SUM
000123          P2=SAM
000125          P3=SOM
000126          C=((P2-P3)/(P1-P2))**(1./Q)
000137          B=10.**(((P1-P2)*(1.-C))/(1.-C**Q)**2)
000154          A=10.**((1./Q)*P1-((1./Q)*(P1-P2))/(1.-C**Q))
000173          AVERAG=0.0
000174          DO 17 I=1,J
000176          YM(I)=C**T(I)
000202          YZ(I)=B**YM(I)
000207          YCALC(I)=A*YZ(I) + D
000213          ERROR(I)=Y(I)-YCALC(I)
000215       17 AVERAG=AVERAG+ABS(ERROR(I))
000222          FP=J
000223          AV=AVERAG/FP
000225          PRINT 88
000230       88 FORMAT(10X,1HA,19X,1HB,18X,1HC,22X,1HD,13X,13HAVERAGE ERROR//)
000230          PRINT 89,A,B,C,D,AV
000246       89 FORMAT(5X,F10.5,10X,F10.9,10X,F10.6,10X,F11.5,10X,F10.4///)
000246          PRINT 100
000252      100 FORMAT(10X,4HX(I),11X,4HY(I),11X,4HT(I), 7X,8HYCALC(I), 8X,8HERROR
               1(I)//)
000252          DO 77 I=1,J
000254       77 PRINT 75,X(I),Y(I),T(I),YCALC(I),ERROR(I)
000274       75 FORMAT(5X,F10.2,5X,F10.5,5X,F10.4,5X,F10.5,5X,F10.4//)
000274          IF(D-FX)66,68,66
000276       68 CONTINUE
000276          IF(ANDIC) 103,103,102
000300      102 CONTINUE
000300          END
```

APPENDIX C

ANALOGUE BLOCK DIAGRAM USED FOR SOLUTION OF THE DIFFERENTIAL EQUATIONS

The following block diagram illustrates the method used to solve the differential equations describing the packed bed of a traveling grate pelletizing machine. The diagram illustrates the solution of Equations (66) and (67).

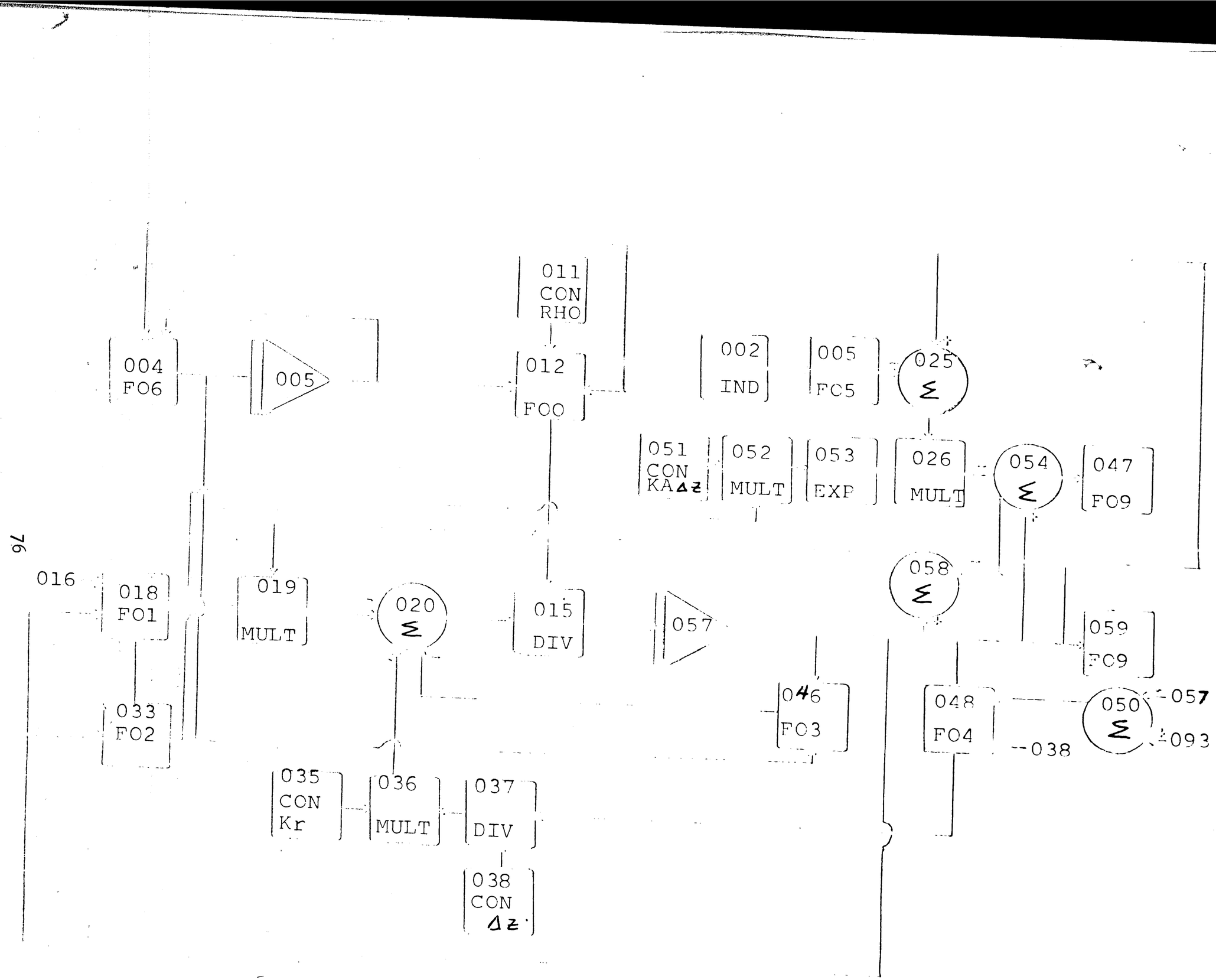
004
FO6
005
011
CON
RHO
012
FOO
002
IND
005
FC5
025
Σ
051
CON
KA Δz
052
MULT
053
EXP
026
MULT
054
Σ
047
FO9
016
018
FO1
019
MULT
020
Σ
015
DIV
057
058
Σ
059
FO9
033
FO2
046
FO3
048
FO4
050
Σ
057
093
038
035
CON
Kr
036
MULT
037
DIV
038
CON
Δz
76

BLOCK #1

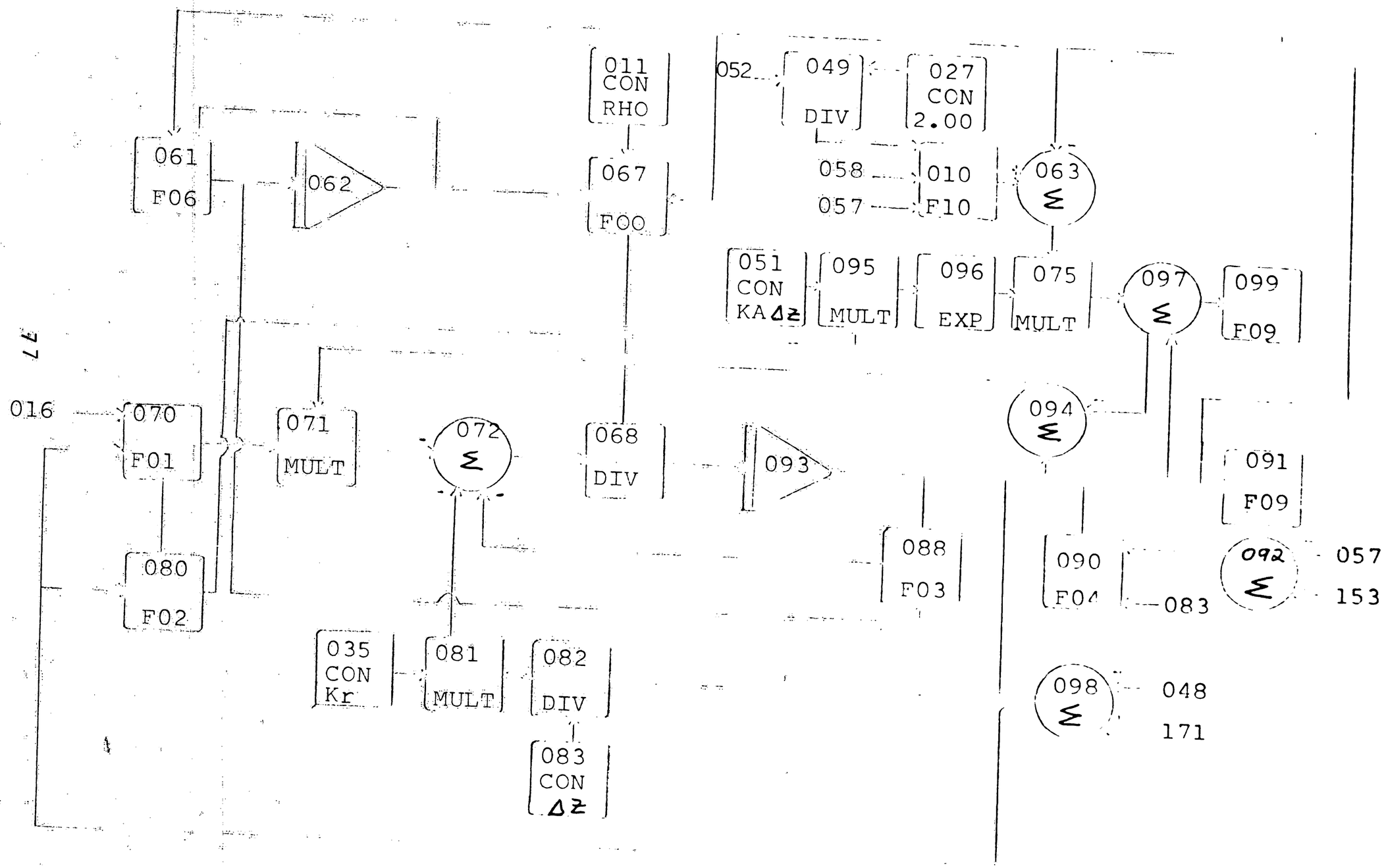
011
CON
RHO
052
049
DIV
027
CON
2.00
058
057
010
F10
063
061
F06
062
067
F00
051
CON
KA Δz
095
MULT
096
EXP
075
MULT
097
099
F09
094
091
F09
090
F04
092
057
153
083
088
F03
016
070
F01
071
MULT
072
068
DIV
093
080
F02
035
CON
Kr
081
MULT
082
DIV
083
CON
Δz
098
048
171

BLOCK #2

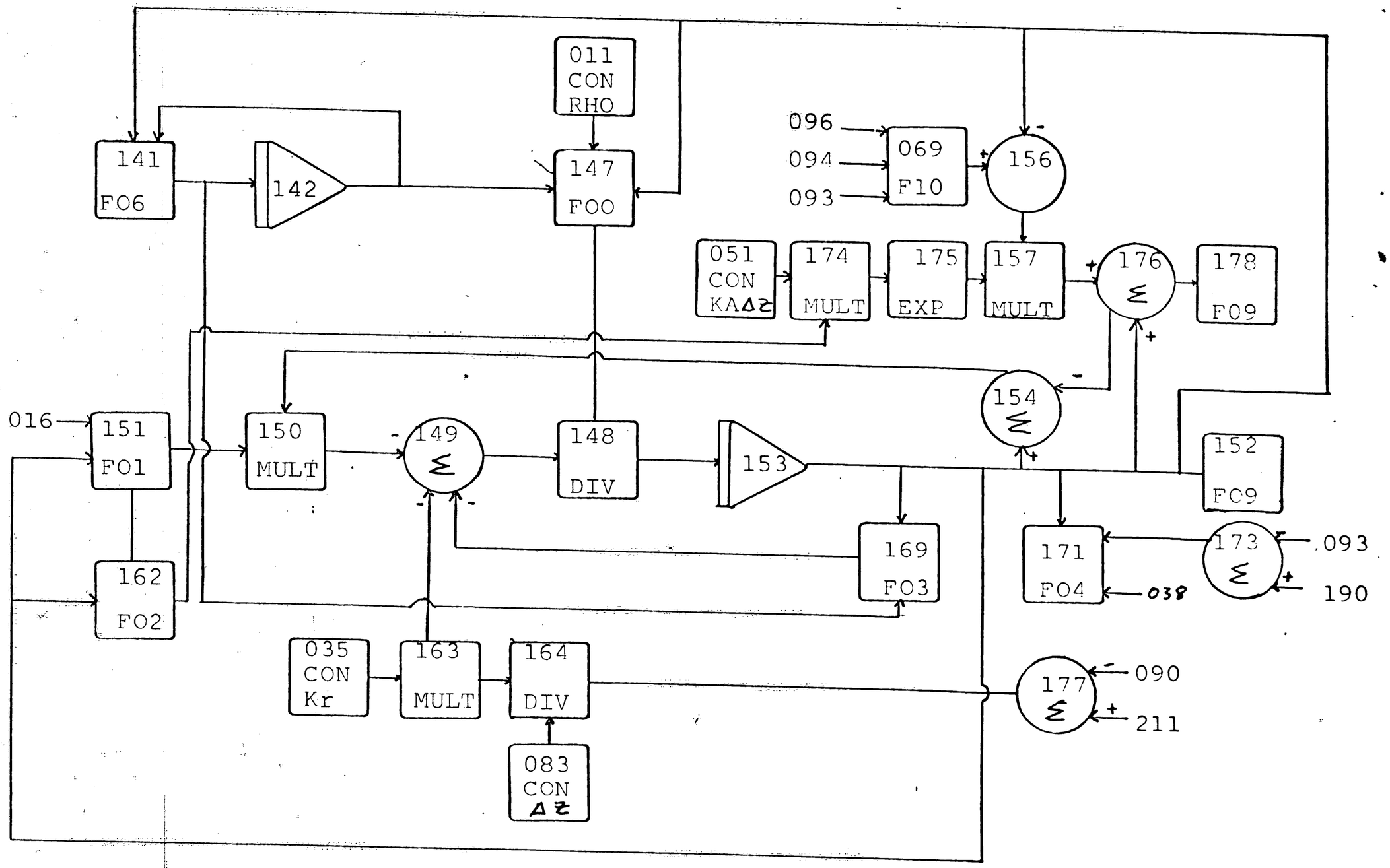
011
CON
RHO
141
FO6
142
147
FOO
096
094
093
069
F10
156
051
CON
KAΔ2
174
MULT
175
EXP
157
MULT
176
Σ
178
F09
154
Σ
016
151
FO1
150
MULT
149
Σ
148
DIV
153
152
FC9
162
FO2
169
FO3
171
FO4
173
Σ
093
038
190
035
CON
Kr
163
MULT
164
DIV
083
CON
Δz
177
Σ
090
211

BLOCK #3

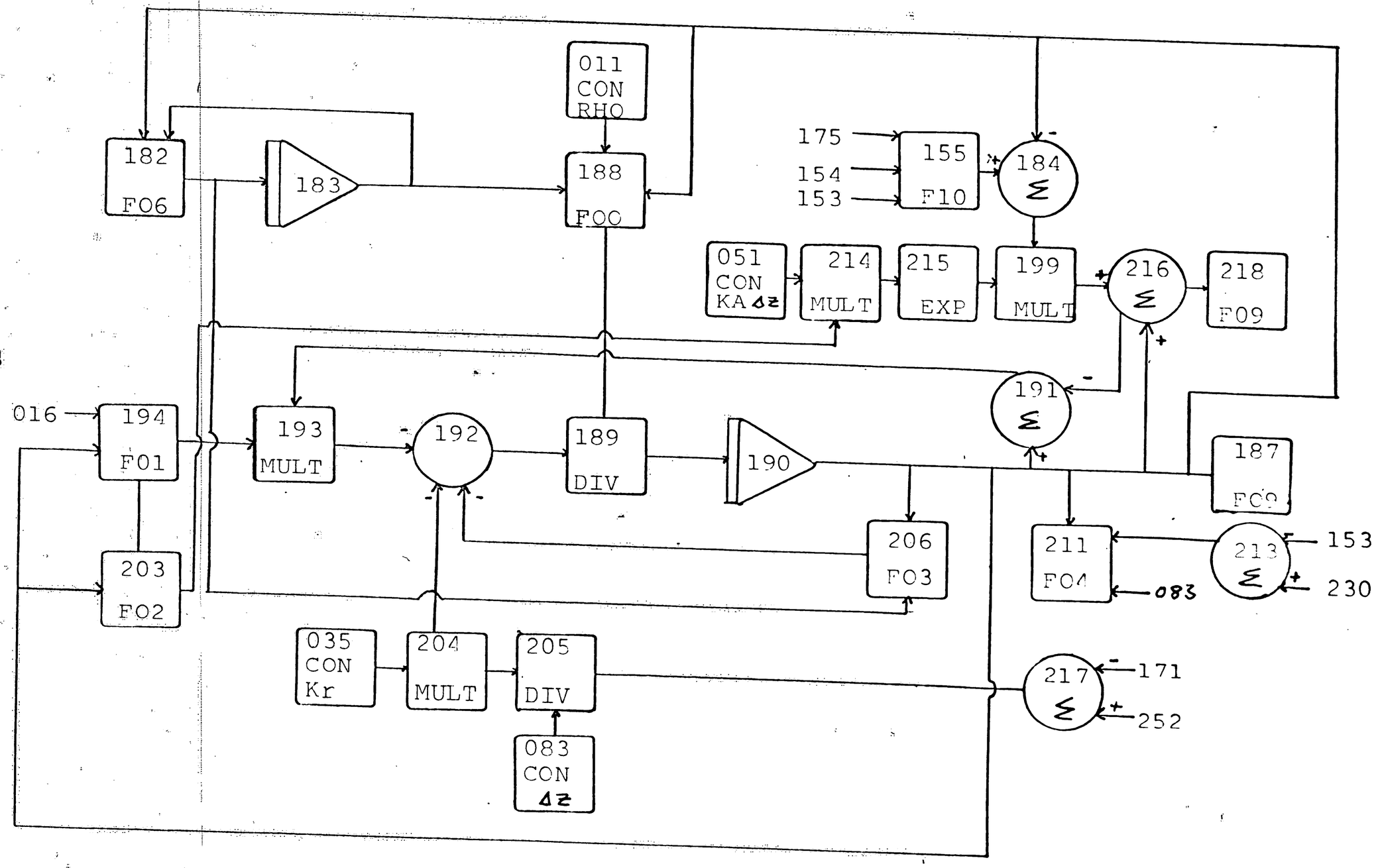
011
CON
RHO
182
F06
183
188
F00
175
154
153
155
F10
184
051
CON
KA Δz
214
MULT
215
EXP
199
MULT
216
218
F09
191
016
194
F01
193
MULT
192
189
DIV
190
187
F08
206
F03
203
F02
211
F04
213
153
083
230
035
CON
Kr
204
MULT
205
DIV
083
CON
Δz
217
171
252

BLOCK #4

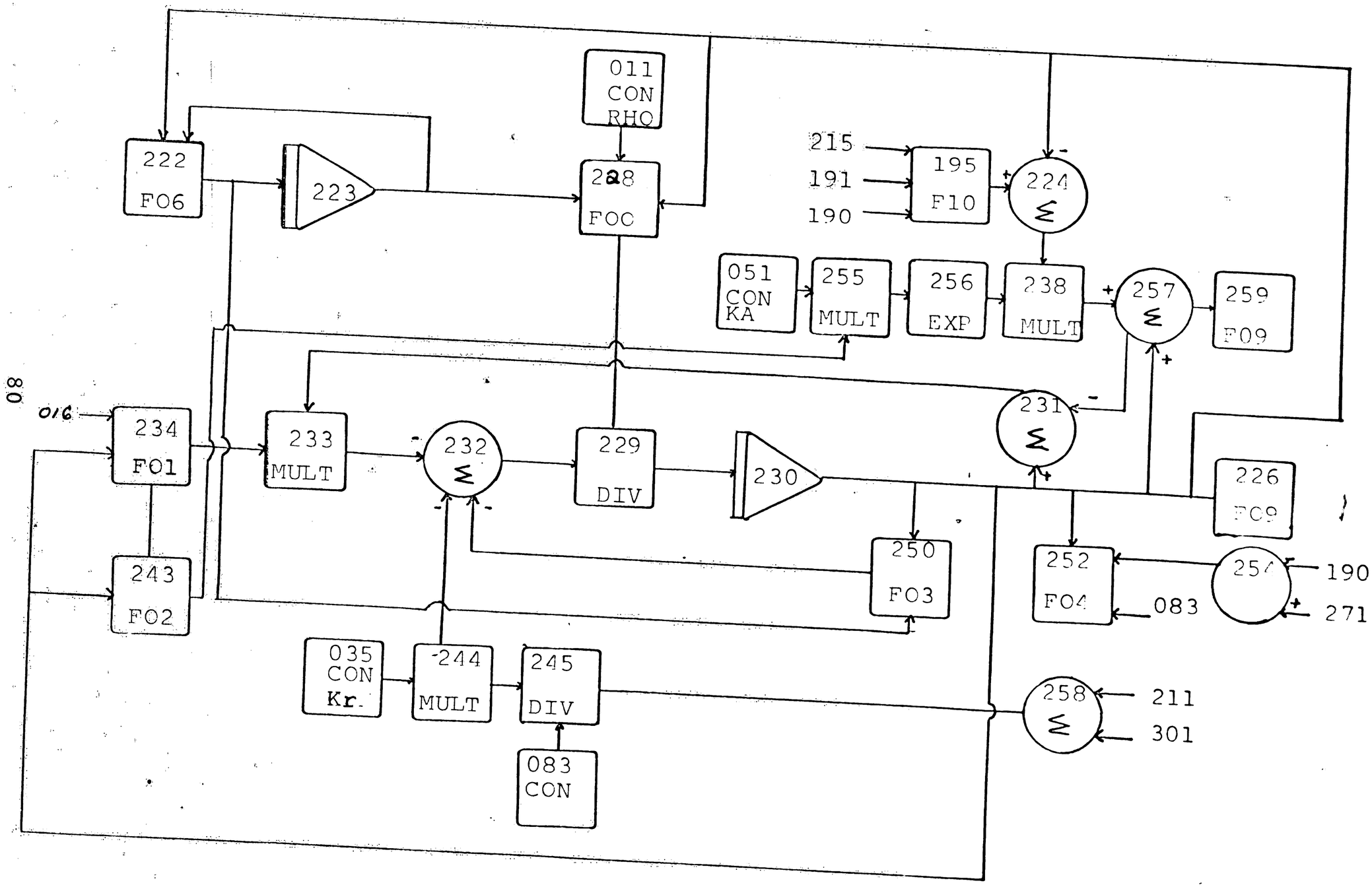
011
CON
RHO
222
F06
223
228
F0C
215
191
190
195
F10
224
Σ
051
CON
KA
255
MULT
256
EXP
238
MULT
257
Σ
259
F09
231
Σ
226
F08
016
234
F01
233
MULT
232
Σ
229
DIV
230
250
F03
252
F04
254
190
083
271
243
F02
035
CON
Kr.
244
MULT
245
DIV
083
CON
258
Σ
211
301
08

BLOCK #5

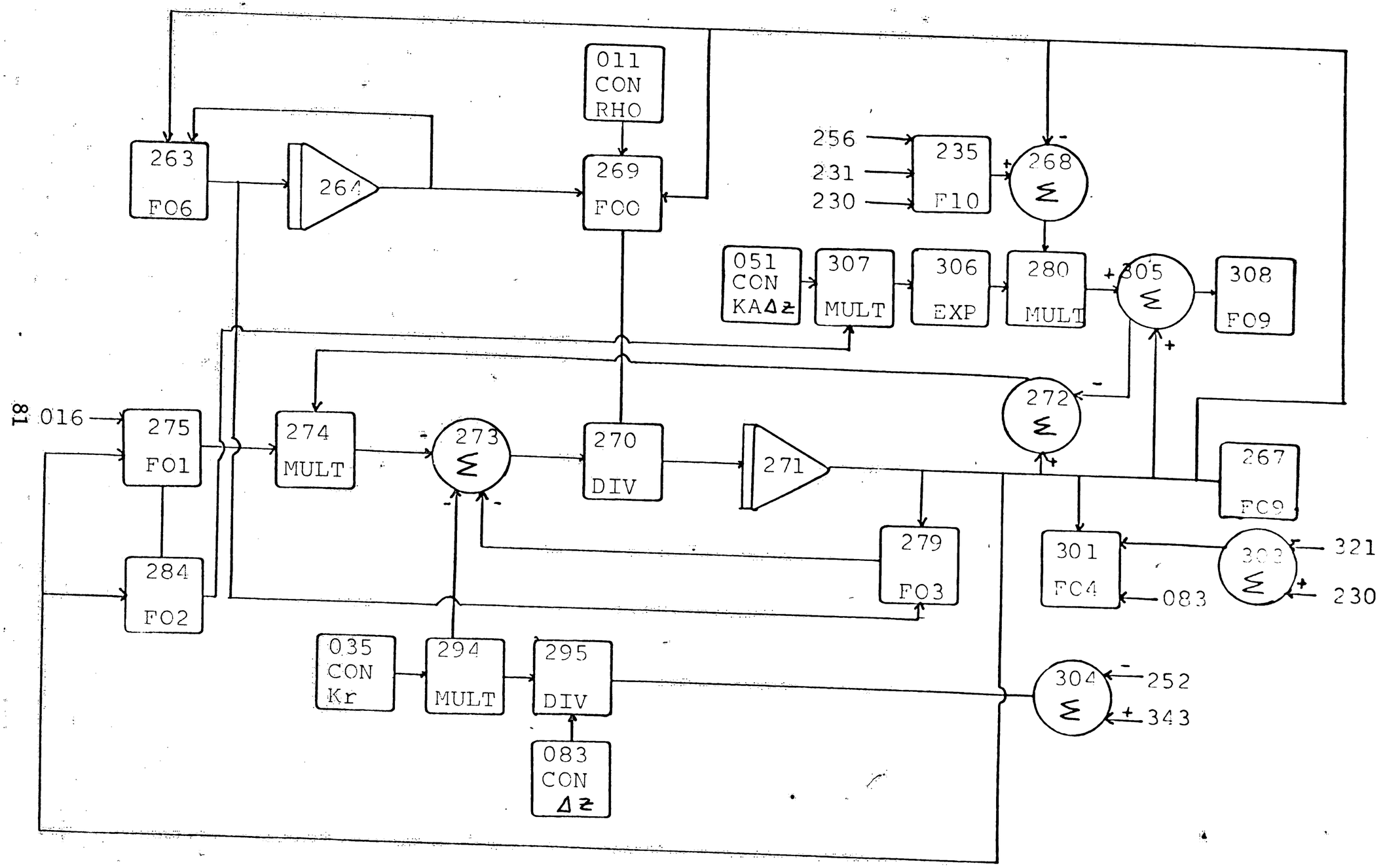
011
CON
RHO
263
F06
264
269
F00
256
231
230
235
F10
268
051
CON
KAΔz
307
MULT
306
EXP
280
MULT
305
308
F09
272
267
F09
81
016
275
F01
274
MULT
273
270
DIV
271
279
F03
284
F02
301
FC4
083
321
230
035
CON
Kr
294
MULT
295
DIV
083
CON
Δz
304
252
343

BLOCK #6

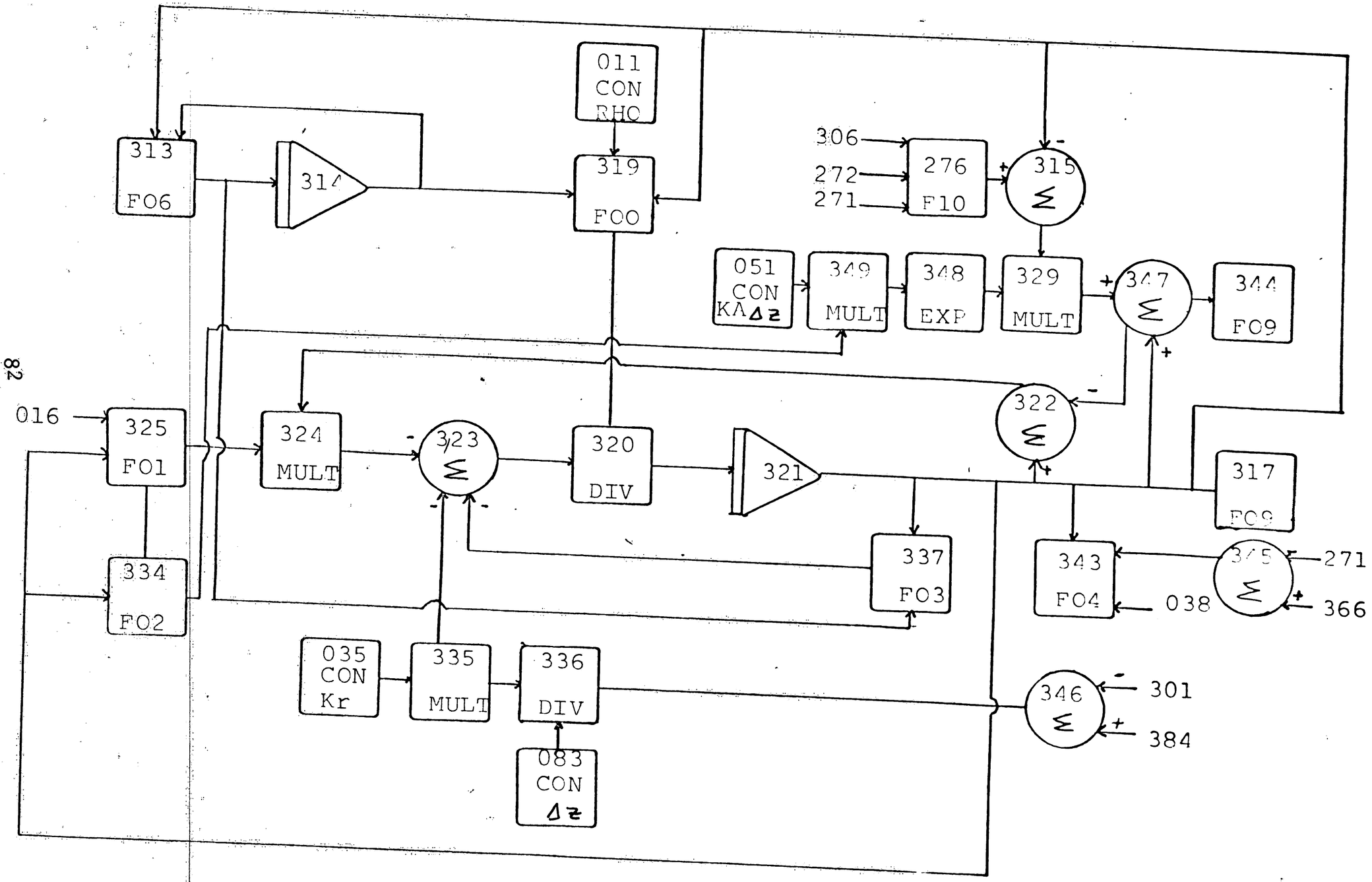
011
CON
RHO
313
FO6
314
319
FOO
306
272
271
276
F10
315
Σ
051
CON
KA Δz
349
MULT
348
EXP
329
MULT
347
Σ
344
FO9
322
Σ
016
325
FO1
324
MULT
323
Σ
320
DIV
321
317
FO8
334
FO2
337
FO3
343
FO4
345
Σ
271
038
366
035
CON
Kr
335
MULT
336
DIV
083
CON
Δz
346
Σ
301
384

BLOCK #4

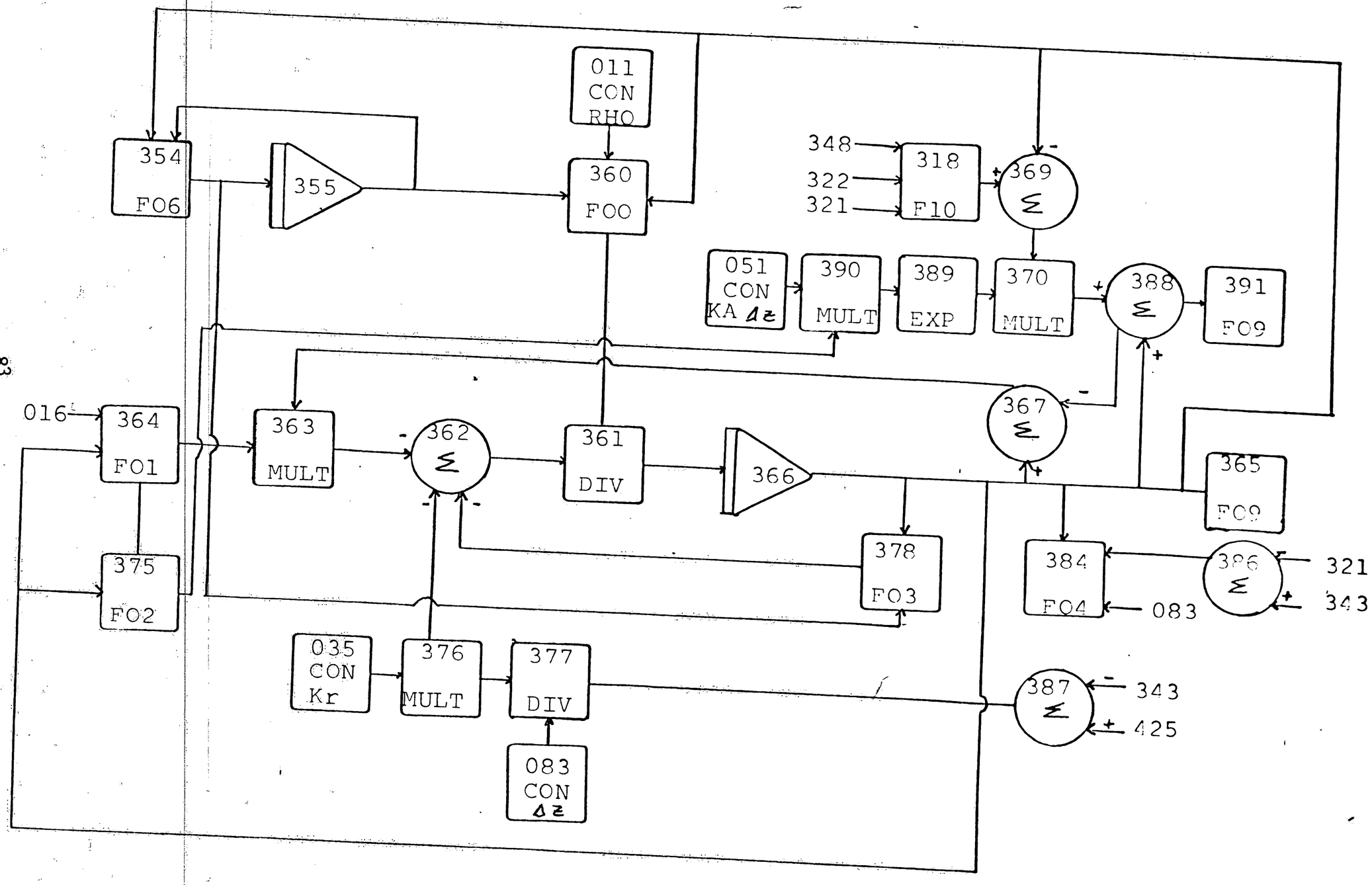
011
CON
RHO
354
FO6
355
360
FOO
348
322
321
318
F10
369
Σ
051
CON
KA Δz
390
MULT
389
EXP
370
MULT
388
Σ
391
FO9
016
364
FO1
363
MULT
362
Σ
361
DIV
366
367
Σ
365
FO9
375
FO2
378
FO3
384
FO4
386
Σ
321
343
083
035
CON
Kr
376
MULT
377
DIV
083
CON
Δz
387
Σ
343
425

BLOCK #8

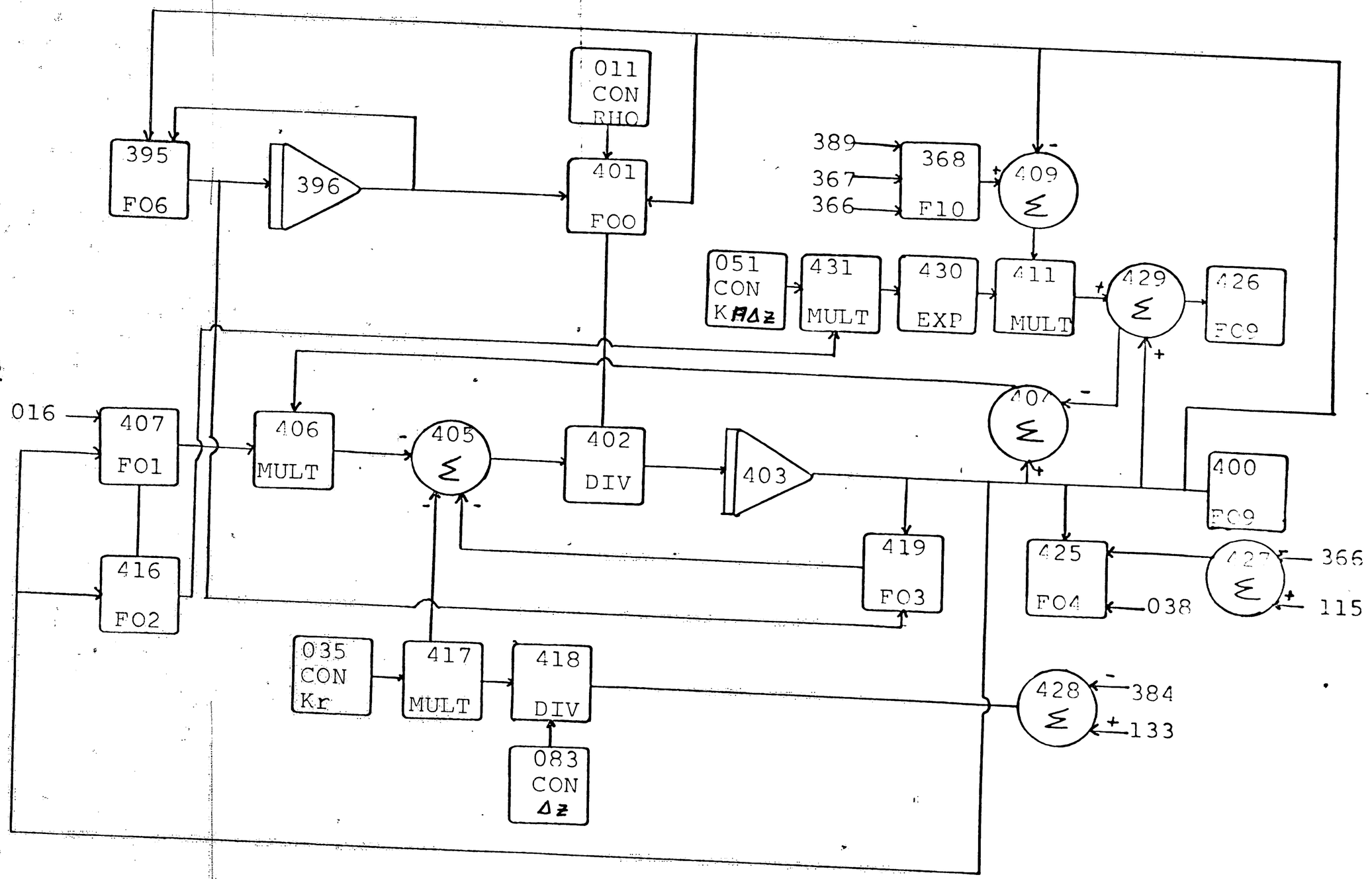
011
CON
RHO
395
F06
396
401
F00
389
367
366
368
F10
409
Σ
051
CON
K ΔZ
431
MULT
430
EXP
411
MULT
429
Σ
426
FC9
016
407
F01
406
MULT
405
Σ
402
DIV
403
407
Σ
400
FC9
416
F02
419
F03
425
F04
038
427
Σ
366
115
035
CON
Kr
417
MULT
418
DIV
083
CON
Δz
428
Σ
384
133

BLOCK #9

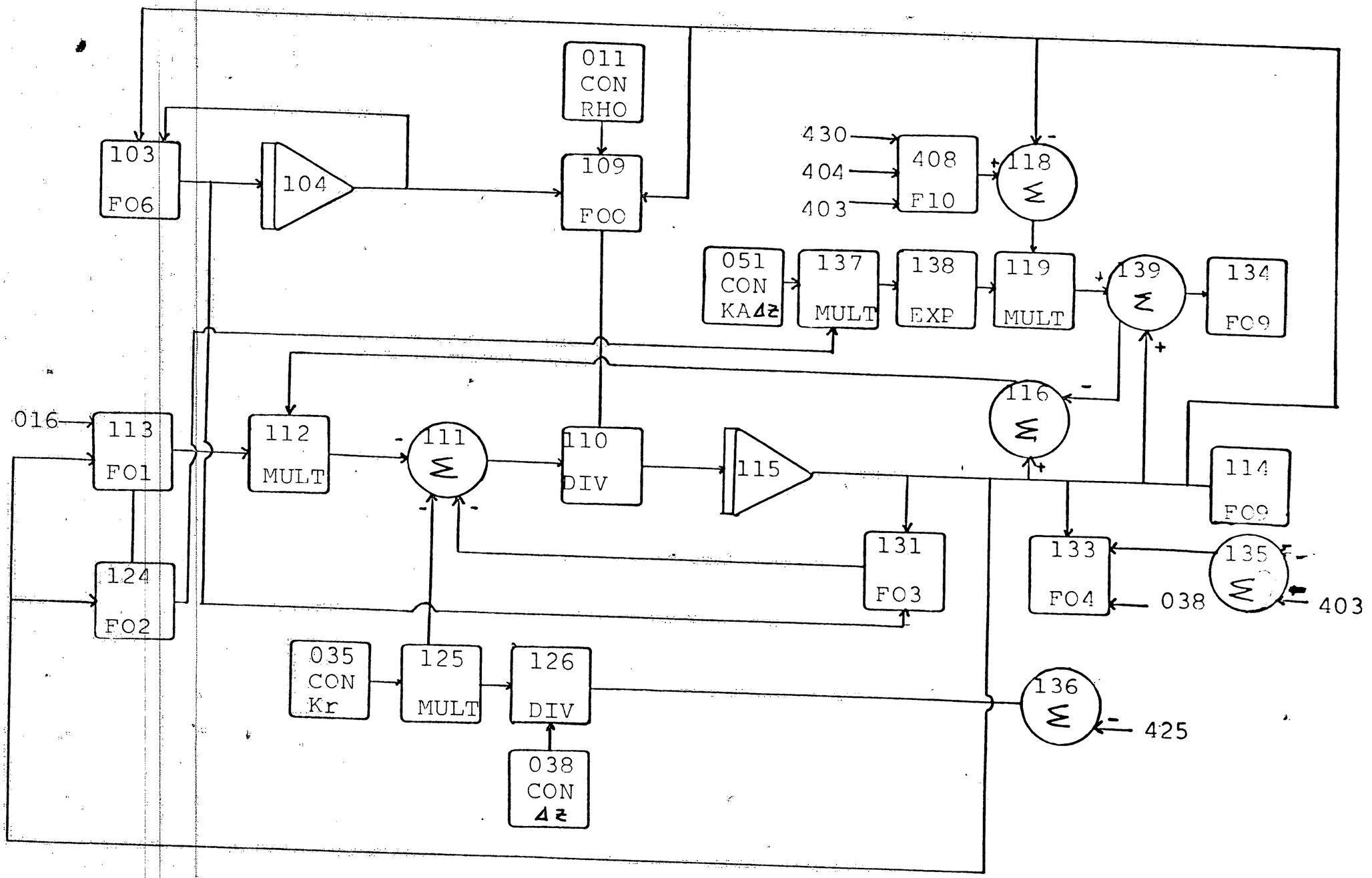
011
CON
RHO
103
FO6
104
109
FOO
430
404
403
408
F10
118
Σ
051
CON
KAΔz
137
MULT
138
EXP
119
MULT
139
Σ
134
FO9
016
113
FO1
112
MULT
111
Σ
110
DIV
115
116
Σ
114
FO8
124
FO2
131
FO3
133
FO4
135
Σ
038
403
035
CON
Kr
125
MULT
126
DIV
038
CON
Δz
136
Σ
425

BLOCK #10

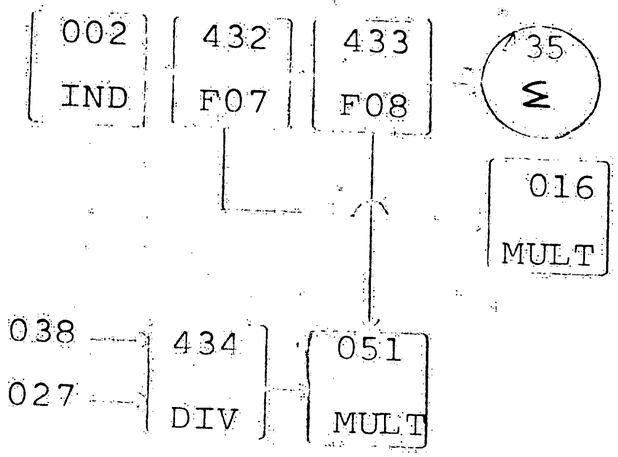

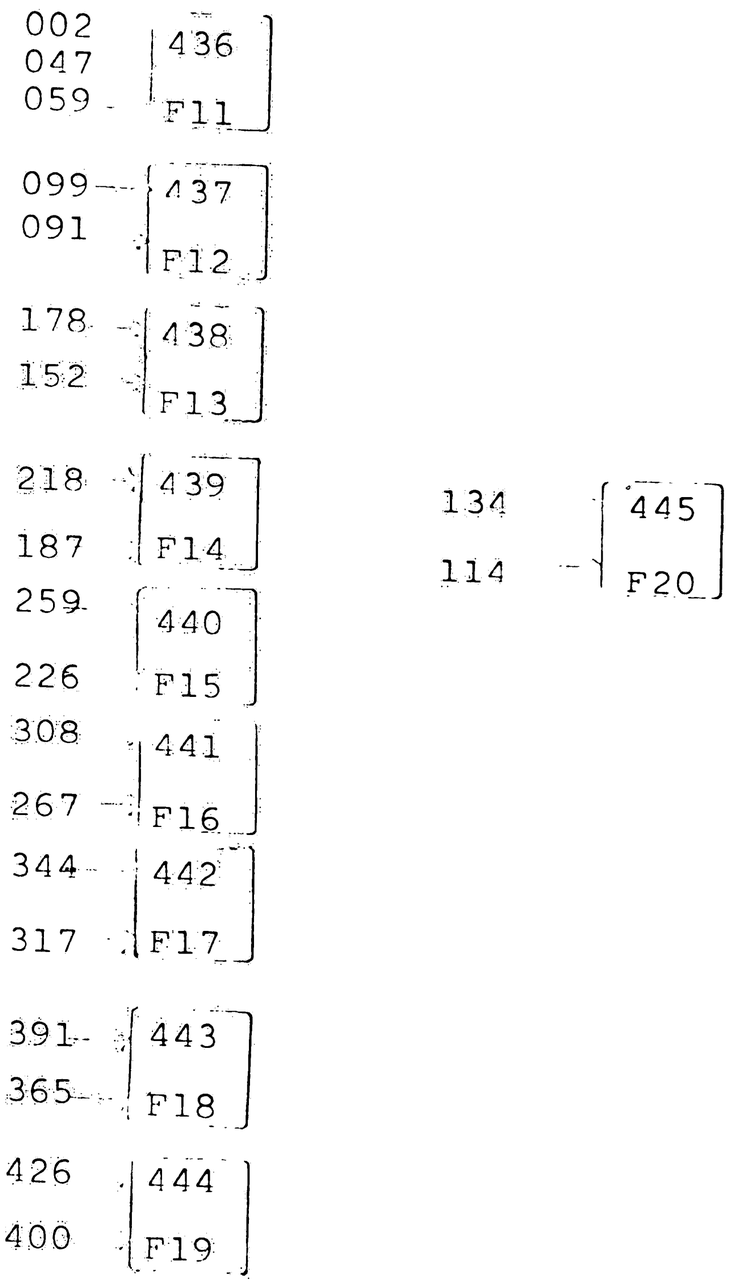

SUBROUTINES

APPENDIX D

COMPUTER PROGRAM USED

TO SOLVE THE DIFFERENTIAL EQUATIONS

The differential equations describing the temperature profiles developed in the packed bed of a traveling grate pelletizing machine during magnetite oxidation were solved using the computer program included in this appendix. The computer program is LEANS, the Lehigh Analog Simulator modified to allow the use of subroutines and to allow plotting with a Calcomp plotter. Information on LEANS is available from the Department of Chemical Engineering, Lehigh University. Both LEANS and the subroutines are written in Fortran IV and were run on a CDC 6400 Digital Computer.

The method used to solve the equations is explained in the section on method of solution. It is outlined more precisely in the block diagram included in this thesis as Appendix C. The program solves the differential equations using this block diagram. Because of the way in which LEANS is written, in order to use the program the input data must be entered into the various subroutines or into the LEANS data. The places at which data must be inserted in the subroutines are marked with a row of stars in the program listing. The subroutine or block number in which the value of the input variable must be entered is included in the list of required input data which follows:

A1 (J) = Values of A as determined by fitting the equation $ox = A\ B^{c^{2t}} + D$ to the experimental data obtained at different isothermal temperatures. The values obtained for the lowest temperature must be entered first (Subroutine SO 6).

ABAR = Pellet bed surface area per unit bed volume, cm^2/cm^3 (Subroutine SO 8).

B1 (J) = Values of B as determined by fitting the equation $ox = AB^{C^{2t}} + D$ to the experimental data obtained at different isothermal temperatures. The values obtained for the lowest temperature must be entered first (Subroutine SO 6).

C1 (J) = Values of C as determined by fitting the equation $ox = AB^{C^{2t}} + D$ to the experimental data obtained at different isothermal temperatures. The values obtained for the lowest temperature must be entered first.

COREK = Factor to convert ox% to $\frac{g\ Fe_2O_3}{cm^3\ pellet}$ (Subroutine SO 6).

D1 (J) = Temperature at a given second during the test run. The temperature for each second during the test run must be entered in this D1 array. D((L) is the temperature at a time of 0 seconds..... D (1201) is the temperature at a time of 1201 seconds (Subroutine SO 5).

D1 (J) = Values of D as determined by fitting the equation $ox = AB^{C^{2t}} + D$ to the experimental data obtained at different isothermal temperatures. The values to be used for 300°C must be entered as D1 (1),

for 400°C as D2 (2), ..., for 1000°C as D8 (8). (Subroutine SO 6).

D1 (J) = Flow rate at a given second during the test run. The temperature for each second during the test run must be entered in this D1 array. D1 (J) is the flow rate of 0 seconds..... D (1201) is the temperature at a time of 1201 seconds (Subroutine SO 7).

FRACT = Fraction solids in the pellet bed, dimensionless (Subroutine SO 0, SO 6).

JDUM = Number of Pot Test Temperatures to be plotted for each plot, dimensionless (Subroutine SPL).

$K_A \Delta z = \frac{(0.0407)\ a^{1.41}}{G_o^{0.41}} \Delta z$

where a = solid particle surface area per unit bed volume, cm^2/cm^3

G_o = gas mass velocity, g/min cm^2

Δz = distance between nodes, cm (Block 051)

$Kr = \frac{4\varepsilon}{4-\varepsilon} D_p \sigma$

where ε = emissivity of pellets, dimensionless

D_p = average particle diameter, cm.

σ = Stefan-Boltzmann constant

(Block 035)

RHO = Density of a dry pellet, gm/cm^3 (Block 011)

T1 = Temperature of a given node when the simulator time is zero.
(Node 1 - Block 057, Node 2 - Block 093,
Node 3 - Block 153, Node 4 - Block 190,
Node 5 - Block 230, Node 6 - Block 271,
Node 7 - Block 321, Node 8 - Block 366,
Node 9 - Block 403, Node 10 - Block 115)

THETA (J) = Value of time for which a pot test temperature value is to be plotted (Subroutine SPL).

TIMEO = The pot test time corresponding to zero simulator time (Subroutine S11).

TR1 (J) = One of the first group of pot test temperatures to be plotted. The value must correspond to a value in the THETA array. (Subroutine SPL).

TR2 (J) = One of the second group of pot test temperatures to be plotted. The value in the THETA array (Subroutine SPL).

TR3 (J) = One of the third group of pot test temperatures to be plotted. The value must correspond to a value in the THETA array (Subroutine SPL).

XHEM = Weight fraction of hematite in the ore prior to oxidation (Subroutine S00).

XMAG = Weight fraction of magnetite in the ore prior to oxidation (Subroutine S00).

Δz = Distance between nodes, cm (Block 038).

$\Delta z/2$ = One half of the distance between nodes, cm (Block 083). Note that this value is used only for radiation calculations.

The program listing follows:

Pages 93 through 132 are on file in the Office of the Department of Metallurgy and Materials Science.

PAGINATION IS OFF FROM HERE

ON JUMPS FROM PAGE 92 TO PAGE 123.

APPENDIX E

DATA USED FOR POT TEST SIMULATION AND COMPARISON OF PREDICTED AND OBSERVED RESULTS

The data used for the simulation of the pot test temperature versus time profiles during magnetite oxidation were made using the data tabulated in this appendix. This data follows:

Data For Simulation Of Test 1-1

Δz = 1.73" = 4.39 cm

ABAR = $\frac{6\ (1-\epsilon)}{D_p} = \frac{3.60}{(0.312)(2.54)} = 4.54$

Kr = 0.0

RHO = 3.90

FRACT = 0.60

TIMEO = 8 min., 42 sec.

THETA(J)	Program Time	Flow Rate	D1(J) (SO7)	TR1(J)	TR2(J)	TR3(J)
522 sec.	0	560	20.83	—	—	—
9 min	18 sec	470	17.48	850	210	180
10	78	425	15.81	1500	360	210
11	138	395	14.69	1630	630	330
12	198	360	13.39	1650	1020	500
13	258	355	13.21	1650	1340	750
14	318	305	11.35	2030	1700	1100
15	378	295	10.97	2420	1840	1320
16	438	265	9.86	2440	1970	1570
17	498	260	9.67	2450	2090	1820
18	558	260	9.67	2460	2180	1970
19	618	260	9.67	2460	2250	2060
20	678	280	10.42	2450	2315	2130
21	738	295	10.97	1770	2360	2210
22	798	295	10.97	1430	2400	2260
23	858	465	17.30	—	—	—

Data For Simulation Of Test 1-1

D1(J) SO5 Data

Test Time	Program Time	Hood Temperature ^{o}F	Hood Temperature ^{o}K
8:42	0	1500	1088.56
9:56	74	1600	1144.11
13:40	298	2450	1616.3
19:53	671	1300	977.44
22:22	820	60	288.56

Kinetic Data

Temperature ^{o}K	A1(J)	B1(J)	C1(J)	D1(J) SO6
573	0.22889	0.467866313	0.792681	-0.1000
673	0.56766	0.450653640	0.550524	-0.2000
773	0.41748	0.572731312	0.474257	-0.2000
873	2.46975	0.782768734	0.612815	-1.9000
973	50.84186	0.984716929	0.571198	-50.0000
1073	50.95296	0.982586149	0.565025	-50.0000
1173	51.02125	0.980448206	0.491935	-50.0000
1273	41.05629	0.974990911	0.483693	-40.0000

Data For Simulation Of Test 1-1

T (Temperature At Test Time = 0 Data)

Node Number	Depth	Temperature ^{o}F	Temperature ^{o}K
1	0.432	530	550
2	2.16	507	536.9
3	3.89	452	506.1
4	5.62	362	456.1
5	7.35	262	401.1
6	9.08	195	363.8
7	10.81	160	344.0
8	12.54	150	339.0
9	14.27	150	339.0
10	16.00	150	339.0

Data For Simulation Of Test 1-2

Δz = 3.99 cm

ABAR = $\frac{6\ (1-\epsilon)}{D_p} = \frac{3.60}{(0.794)} = 4.54$

Kr = 0.0

RHO = 3.90

FRACT = 0.60

TIMEO = 8 min., 56 sec.

THETA(J)	Program Time	Flow Rate	D1(J) (SO7)	TR1(J)	TR2(J)	TR3(J)
536 sec.	0	540	20.09	—	—	—
9 min	4 sec	450	16.74	750	250	190
10	64	415	15.44	1280	550	250
11	124	365	13.58	1730	1030	410
12	184	335	12.46	1870	1500	650
13	244	305	11.35	1910	1800	950
14	304	290	10.79	1960	1960	1350
15	364	265	9.86	2180	2070	1680
16	424	255	9.49	2300	2150	1920
17	484	250	9.30	2350	2220	2080
18	544	245	9.11	2390	2290	2180
19	604	250	9.30	2370	2340	2250
20	664	265	9.86	2310	2360	2310
21	724	330	12.28	—	—	—

Data For Simulation Of Test 1-2

D1(J) SO5 Data

Test Time	Program Time	Hood Temperature ^{o}F	Hood Temperature ^{o}K
8:56	0	1500	1089
10:12	76	1800	1255
14:02	306	2400	1589
17:52	536	2400	1589
18:02	546	2337	1553.8
18:12	556	2265	1513.8
18:22	566	2194	1474.2
18:32	576	2122	1434.1
18:42	586	2051	1394.6
18:52	596	1979	1355.0
19:02	606	1908	1315.4
19:12	616	1836	1275.3
19:22	626	1765	1235.8
19:32	636	1693	1195.7
19:42	646	1622	1156.1
19:52	656	1550	1116.0
20;02	666	1479	1077.0
20:12	676	1407	1036.9
20:22	686	1336	997.3
20:24	688	1300	977.0
20:25	689	60	288.6

Data For Simulation Of Test 1-2

Kinetic Data

Temperature ^{o}K	A1(J)	B1(J)	C1(J)	D1(J) SO6
573	0.22889	0.467866313	0.792681	-0.1000
673	0.56766	0.450653640	0.550524	-0.2000
773	0.41748	0.572731312	0.474257	-0.2000
873	2.46975	0.782768734	0.612815	-1.9000
973	50.84186	0.984716929	0.571198	-50.0000
1073	50.95296	0.982586149	0.565025	-50.0000
1173	51.02125	0.980448206	0.491935	-50.0000
1273	41.05629	0.974990911	0.483693	-40.0000

T (Temperature At Test Time = 0 Data)

Node Number	Depth	Temperature ^{o}F	Temperature ^{o}K
1	0.38	530	550
2	1.89	530	550
3	3.40	510	539
4	4.91	462	512.1
5	6.42	382	467.1
6	7.93	242	390.1
7	9.44	190	361.0
8	10.95	180	355.0
9	12.46	180	355.0
10	13.97	180	355.0

Data For Simulation Of Test 1-3

ΔZ = 3.99

ABAR = $\frac{6\ (1-\epsilon)}{D_p} = \frac{3.60}{0.794} = 4.54$

Kr = 0.0

RHO = 3.90

FRACT = 0.60

TIMEO = 8 min., 56 sec.

THETA(J)	Program Time	Flow Rate	D1(J) (SO7)	TR1(J)	TR2(J)	TR3(J)
536 sec.	0	555	20.65	—	—	—
9 min.	4	435	16.18	570	330	190
10	64	420	15.62	1660	670	340
11	124	400	14.88	1810	1110	550
12	184	365	13.58	1890	1580	820
13	244	325	12.09	2050	1870	1130
14	304	290	10.79	2410	2020	1500
15	364	285	10.60	2470	2150	1820
16	424	285	10.60	2480	2280	2040
17	484	300	11.16	2180	2350	2200
18	544	330	12.28	—	—	—

Data For Simulation Of Test 1-3

D1(J) SO5 Data

Test Time	Program Time	Hood Temperature ^{o}F	Hood Temperature ^{o}K
8:56	0	1700	1246
11:28	152	1800	1255
12:44	228	2450	1616
15:16	380	2387	1580.9
15:26	390	2315	1541.8
15:36	400	2243	1501.7
15:46	410	2171	1461.6
15:56	420	2099	1421.0
16:06	430	2027	1380.9
16:16	440	1955	1341.8
16:26	450	1883	1301.7
16:36	460	1811	1261.6
16:46	470	1739	1221.0
16:56	480	1667	1180.9
17:06	490	1595	1141.8
17:16	500	1523	1101.7
17:26	510	1451	1061.6
17:36	520	1379	1021.0
17:46	530	1307	980.9
17:47	531	1300	977.0
17:48	532	60	288.6

Data For Simulation Of Test 1-3

Kinetic Data

Temperature ^{o}K	A1(J)	B1(J)	C1(J)	D1(J) SO6
573	0.22889	0.467866313	0.792681	-0.1000
673	0.56766	0.450653640	0.550524	-0.2000
773	0.41748	0.572731312	0.474257	-0.2000
873	2.46975	0.782768734	0.612815	-1.9000
973	50.84186	0.984716929	0.571198	-50.0000
1073	50.95296	0.982586149	0.565025	-50.0000
1173	51.02125	0.980448206	0.491935	-50.0000
1273	41.05629	0.974990911	0.483693	-40.0000

T (Temperature At Test Time = 0 Data)

Node Number	Depth	Temperature ^{o}F	Temperature ^{o}K
1	0.38	540	555
2	1.89	540	555
3	3.40	490	527
4	4.91	430	494
5	6.42	365	457.8
6	7.93	320	433
7	9.44	282	412.1
8	10.95	260	400
9	12.46	240	389
10	13.97	230	383

Data For Simulation Of Test 2-1

Δz = 3.99 cm

ABAR = $\frac{6\ (1-\epsilon)}{D_p} = \frac{3.60}{0.794} = 4.54$

Kr = 0.0

RHO = 3.90

FRACT = 0.60

TIMEO = 8 min., 23 sec.

THETA(J)	Program Time	Flow Rate	D1(J) (SO7)	TR1(J)	TR2(J)	TR3(J)
503 sec.	0	570	21.20	—	—	—
9 min.	37	505	18.79	600	270	170
10	97	420	15.62	1240	460	200
11	157	345	12.83	1790	950	370
12	217	315	11.72	2190	1450	620
13	277	295	10.97	2370	1960	970
14	337	285	10.60	2430	2200	1410
15	397	265	9.86	2350	2380	1960
16	457	272	10.12	2160	2420	2180
17	517	272	10.12	1900	2410	2290
18	577	275	10.23	1640	2390	2400
19	637	282	10.49	1460	2250	2430
20	697	445	16.55	—	—	—

Data For Simulation Of Test 2-1

D1(J) SO5 Data

Test Time	Program Time	Hood Temperature ^{o}F	Hood Temperature ^{o}K
8:23	0	1200	922.0
9:31	68	1800	1255.0
10:39	136	2500	1644.0
14:02	339	1200	922.0
19:07	644	60	288.6

Kinetic Data

Temperature ^{o}K	A1(J)	B1(J)	C1(J)	D1(J) SO6
573	0.16435	0.606131610	0.808889	-0.1000
673	0.29608	0.452912160	0.452583	-0.1000
773	0.46437	0.296582763	0.540299	-0.1000
873	0.61703	0.228535831	0.486170	-0.1000
973	0.73698	0.192385976	0.491075	-0.1000
1073	0.94572	0.152951022	0.540247	-0.1000
1173	7.05184	0.850740955	0.469176	-6.0000
1273	51.08035	0.979168478	0.436195	-50.0000

Data For Simulation Of Test 2-1

T (Temperature At Test Time = 0 Data)

Node Number	Depth	Temperature ^{o}F	Temperature ^{o}K
1	0.38	400	477
2	1.89	400	477
3	3.40	358	454.4
4	4.91	290	416
5	6.42	220	377
6	7.93	182	356.1
7	9.44	159	344
8	10.95	150	339
9	12.46	150	339
10	13.97	150	339

Data For Simulation Of Test 2-2

Δz = 1.62" = 4.12 cm

ABAR = $\frac{6\ (1-\epsilon)}{D_p} = \frac{3.60}{0.794} = 4.54$

Kr = 0.0

RHO = 3.90

FRACT = 0.60

TIMEO = 8 min., 33 sec.

THETA(J)	Program Time	Flow Rate	D1(J) (SO7)	TR1(J)	TR2(J)	TR3(J)
513 sec.	0	605	22.51	—	—	—
9 min.	27	520	19.34	540	230	200
10	87	480	17.86	1000	410	250
11	147	420	15.62	1350	660	350
12	207	375	13.95	1750	960	500
13	267	282	10.49	2020	1360	680
14	327	275	10.23	2270	1750	870
15	387	252	9.37	2380	2050	1150
16	447	245	9.11	2420	2240	1600
17	507	244	9.08	2420	2350	1940
18	567	275	10.23	2370	2420	2200
19	627	282	10.49	2130	2440	2350
20	687	290	10.79	1850	2440	2420
21	747	305	11.35	1600	2400	2440
22	807	315	11.72	1470	2310	2450
23	867	420	15.62	—	—	—

Data For Simulation Of Test 2-2

D1(J) SO5 Data

Test Time	Program Time	Hood Temperature ^{o}F	Hood Temperature ^{o}K
8:33	0	1300	977.0
10:27	114	1750	1227
11:24	171	2000	1366
12:21	228	2450	1616
17:06	513	1300	977.0
22:48	855	60	288.6

Kinetic Data

Temperature ^{o}K	A1(J)	B1(J)	C1(J)	D1(J) SO6
573	0.16435	0.606131610	0.808889	-0.1000
673	0.29608	0.452912160	0.452583	-0.1000
773	0.46437	0.296582763	0.540299	-0.1000
873	0.61703	0.228535831	0.486170	-0.1000
973	0.73698	0.192385976	0.491075	-0.1000
1073	0.94572	0.152951022	0.540247	-0.1000
1173	7.05184	0.850740955	0.469176	-6.0000
1273	51.08035	0.979168478	0.436195	-50.0000

Data For Simulation Of Test 2-2

T (Temperature At Test Time = 0 Data)

Node Number	Depth	Temperature ^{o}F	Temperature ^{o}K
1	0.41	500	533
2	2.03	430	494
3	3.65	340	444
4	5.27	230	383
5	6.89	200	366
6	8.51	200	366
7	10.13	200	366
8	11.75	200	366
9	13.37	200	366
10	14.99	200	366

Data For Simulation Of Test 2-3

Δz = 1.62" = 4.12 cm

ABAR = $\frac{6\ (1-\epsilon)}{D_p} = \frac{3.60}{1.27} = 2.84$

Kr = 0.0

RHO = 3.90

FRACT = 0.60

TIMEO = 8 min., 6 sec.

THETA(J)	Program Time	Flow Rate	D1(J) (S07)	TR1(J)	TR2(J)	TR3(J)
486 sec.	0	525	19.53	—	—	—
9 min.	54	424	15.77	440	160	140
10	114	380	14.14	830	190	150
11	174	340	12.65	1260	250	170
12	234	255	9.49	1750	440	200
13	294	240	8.93	2120	710	260
14	354	225	8.37	2300	1080	350
15	414	215	8.00	2400	1520	490
16	474	215	8.00	2420	1920	700
17	534	235	8.74	2400	2160	1000
18	594	245	9.11	2350	2410	1360
19	654	250	9.30	2200	2430	1850
20	714	282	10.49	2020	2390	2100
21	774	265	9.86	1800	2360	2280
22	834	272	10.12	1610	2330	2360
23	894	360	13.39	—	—	—

Data For Simulation Of Test 2-3

D1(J) SO5 Data

Test Time	Program Time	Hood Temperature ^{o}F	Hood Temperature ^{o}K
8:06	0	1300	977
9:54	108	1750	1227
10:48	162	2000	1366
11:42	216	2450	1616
16:12	486	1300	977
22:30	864	60	288.6

Kinetic Data

Temperature ^{o}K	A1(J)	B1(J)	C1(J)	D1(J) SO6
573	0.16435	0.606131610	0.808889	-0.1000
673	0.29608	0.452912160	0.452583	-0.1000
773	0.46437	0.296582763	0.540299	-0.1000
873	0.61703	0.228535831	0.486170	-0.1000
973	0.73698	0.192385976	0.491075	-0.1000
1073	0.94572	0.152951022	0.540247	-0.1000
1173	7.05184	0.850740955	0.469176	-6.0000
1273	51.08035	0.979168478	0.436195	-50.0000

Data For Simulation Of Test 2-3

T (Temperature At Test Time = 0 Data)

Node Number	Depth	Temperature ^{o}F	Temperature ^{o}K
1	0.41	300	422
2	2.03	240	389
3	3.65	200	366
4	5.27	200	366
5	6.89	200	366
6	8.51	200	366
7	10.13	200	366
8	11.75	200	366
9	13.37	200	366
10	14.99	200	366

TABLE I

Properties of Ore Balls Made From Ore 1 And Ore 2

Screen Analyses of Concentrate Before Balling

	Ore 1 (% ind.)	Ore 2 (% ind.)
+20	0.05	—
+28	0.05	—
+35	0.05	0.1
+48	0.05	0.1
+65	0.05	0.3
+100	0.10	0.5
+150	0.15	0.9
+200	0.50	2.2
+325	3.7	7.9
-325	95.4	88.0

Properties of Ore Concentrate Balls

	Ore 1		Ore 2	
	Commercial Practice	This Investigation	Commercial Practice	This Investigation
Bentonite (lb/wet LT)	14 - 15	11.3	14 - 15	11.3
Free Moisture (wt %)	9.5-10	9.7	9.5 - 10	9.9
Fe^{++} (wt %)	21.6	19.9	21.4	20.2
Fe Total (wt %)	66.6	—	68.5	—

TABLE II

Results of Test Runs CO-1, 2, and 3

RUN CO-1

(Sample Weight = 4.2880 g, Temperature = 800°C)
(Flowrate = 18 SCFH)

Time (Min)	Weight Gain (mg) (From Time = 0)	% Ox
0	0	0.0
2	63	51.5
4	85	69.5
6	99	81.0
8	108	88.2
10	112	91.6
12	114	93.2
14	116	94.8

RUN CO-2

(Sample Weight = 8.6200 g, Temperature = 800°C)
(Flowrate = 18 SCFH)

Time (min)	Weight Gain (mg) (From Time = 0)	% Ox
0	0	0.0
2	123	50.2
4	167	68.2
6	193	78.7
8	211	86.2
10	222	90.6
12	226	92.4
14	229	93.5

RUN CO-3

(Sample Weight = 12.540 g, Temperature = 800°C)
(Flowrate = 18 SCFH)

Time (Min)	Weight Gain (mg) (From Time = 0)	% Ox
0	0	0.0
2	179	50.5
4	241	67.9
6	279	78.7
8	304	85.7
10	315	88.8
12	322	90.7
14	326	92.0
	154	

TABLE III

Results of Test Runs CO-4, 5, 6, 7, 8, 9, And 10

Test #	Sample Weight (gm)	(SCFH)	Temp. (^oC)	Time (min)	Weight Gain (mg) (from time = 0)	% Ox by Wt.	% Ox by analyses	% Ox* by shell width
CO-4	8.7370	18	800	2	122	49.0	50.7	57.0
CO-5	8.6000	18	800	4	170	69.4	68.2	75.2
CO-6	7.9610	18	800	6	117	78.0	76.4	89.7
CO-7	8.8280	18	800	8	252	81.0	82.0	92.8
CO-8	9.3330	18	800	10	231	86.8	83.8	96.2
CO-9	9.0150	18	800	12	226	87.9	86.8	———
CO-10	8.6790	18	800	14	232	93.9	90.6	———

* Note: These are representative values picked from the many measurements made.

TABLE IV

Results of Test Runs CO-11, 12, 13, And 14

Run CO-11

(Sample Weight = 8.7660 g, Temperature = 800°C)
(Flowrate = 10 SCFH)

Time (min)	Weight Gain (mg) (From Time = 0)	% Ox
0	0	0.0
2	114	45.7
4	158	63.2
6	187	74.9
8	206	82.5
10	217	86.8
12	222	89.0
14	225	90.0

Run CO-12

(Sample Weight = 9.0710 g, Temperature = 800°C)
(Flowrate = 12 SCFH)

Time (min)	Weight Gain (mg) (From Time = 0)	% Ox
0	0	0.0
2	116	44.8
4	163	63.0
6	193	74.5
8	212	82.0
10	224	86.5
12	229	88.5
14	234	90.5

Run CO-13

(Sample Weight = 8.6920 g, Temperature = 800°C)
(Flowrate = 15 SCFH)

Time (min)	Weight Gain (mg) (From Time = 0)	% Ox
0	0	0.0
2	119	48.2
4	163	66.0
6	190	77.0
8	208	84.2
10	220	89.0
12	225	91.2
14	228	92.4

TABLE IV (CONTINUED)

Run CO-14

(Sample Weight = 9.1700 g, Temperature = 800°C)
(Flowrate = 21 SCFH)

Time (min)	Weight Gain (mg) (From Time = 0)	% Ox
0	0	0.0
2	122	46.8
4	171	65.5
6	205	78.5
8	223	85.5
10	236	90.5
12	242	92.8
14	245	94.0

TABLE V

Results of Tests Using Ore Concentrate Balls of Ore 1

Run 1-300

(Sample Weight = 8.6620 g, Temperature = 300°C)
(Flowrate = 18 SCFH)

Time (min)	Weight Gain (mg) (From Time = 0)	% Ox
0	0	0.0
2	7	2.83
4	12	4.86
6	15	6.07
8	17	6.87
10	19	7.70
12	22	8.91
14	23	9.32

Run 1-400

(Sample Weight = 8.7870 g, Temperature = 400°C)
(Flowrate = 18 SCFH)

Time (min)	Weight Gain (mg) (From Time = 0)	% Ox
0	0	0.0
2	40	16.0
4	48	19.2
6	50	20.0
8	51	20.35
10	52	20.75
12	53	21.15
14	54	21.55

Run 1-500

(Sample Weight = 8.8580 g, Temperature = 500°C)
(Flowrate = 18 SCFH)

Time	Weight Gain (mg) (From Time = 0)	% Ox
0	0	0.0
2	57	22.6
4	73	29.0
6	78	31.0
8	81	32.2
10	85	33.7
12	88	34.9
14	91	36.1

TABLE V (CONTINUED)

Run 1-600

(Sample Weight = 9.2300 g, Temperature = 600°C)
(Flowrate = 18 SCFH)

Time (min)	Weight Gain (mg) (From Time = 0)	% Ox
0	0	0.0
2	66	25.1
4	96	36.5
6	117	44.5
8	127	48.3
10	134	51.0
12	139	52.8
14	144	54.7

Run 1-700

(Sample Weight = 8.8020 g, Temperature = 700°C)
(Flowrate = 18 SCFH)

Time (min)	Weight Gain (mg) (From Time = 0)	% Ox
0	0	0.0
2	112	44.6
4	151	60.3
6	175	69.7
8	190	75.8
10	199	79.4
12	204	81.4
14	207	82.5

Run 1-800

The Results Of CO-2 Were Used For The 800°C

Run 1-900

(Sample Weight = 8.5180 g, Temperature = 900°C)
(Flowrate = 18 SCFH)

Time (min)	Weight Gain (mg) (From Time = 0)	% Ox
0	0	0.0
2	136	56.0
4	187	77.0
6	216	89.0
8	235	96.7
10	243	99.9
12	245	100.8
14	247	101.5

TABLE V (CONTINUED)

Run 1-1000

(Sample Weight = 9.1940 g, Temperature = 1000°C)
(Flowrate = 21 SCFH)

Time (min)	Weight Gain (mg) (From Time = 0)	% Ox
0	0	0.0
2	156	59.5
4	211	80.5
6	242	92.4
8	263	100.5
10	272	103.8
12	274	104.5
14	275	105.0

TABLE VI

Results of Tests Using Ore Concentrate Balls of Ore 2

Run 2-300

(Sample Weight = 7.5050 g, Temperature = 300°C)
(Flowrate = 18 SCFH)

Time (min)	Weight Gain (mg) (From Time = 0)	% Ox
0	0	0.0
2	2	0.923
4	4	1.84
6	6	2.76
8	7	3.23
10	8	3.69
12	9	4.15
14	10	4.61

Run 2-400

(Sample Weight = 7.8860 g, Temperature = 400°C)
(Flowrate = 18 SCFH)

Time (min)	Weight Gain (mg) (From Time = 0)	% Ox
0	0	0.0
2	35	15.35
4	40	17.55
6	41	18.0
8	42	18.4
10	43	18.9
12	43.5	19.1
14	44	19.3

Run 2-500

(Sample Weight = 7.8690 g, Temperature = 500°C)
(Flowrate = 18 SCFH)

Time (min)	Weight Gain (mg) (From Time = 0)	% Ox
0	0	0.0
2	44	19.35
4	61	26.8
6	67	29.4
8	72	31.6
10	75	33.0
12	78	34.3
14	81	35.6
	161	

TABLE VI (CONTINUED)

Run 2-600

(Sample Weight = 7.9960 g, Temperature = 600°C)
(Flowrate = 18 SCFH)

Time (min)	Weight Gain (mg) (From Time = 0)	% Ox
0	0	0.0
2	66	28.5
4	88	38.0
6	102	44.0
8	107	46.1
10	111	47.9
12	115	49.6
14	117	50.5

Run 2-700

(Sample Weight = 8.3040 g, Temperature = 700°C)
(Flowrate = 18 SCFH)

Time (min)	Weight Gain (mg) (From Time = 0)	% Ox
0	0	0.0
2	78	32.5
4	106	44.2
6	123	51.3
8	137	57.0
10	143	59.5
12	147	61.2
14	150	62.5

Run 2-800

(Sample Weight = 7.8660 g, Temperature = 800°C)
(Flowrate = 18 SCFH)

Time (min)	Weight Gain (mg) (From Time = 0)	% Ox
0	0	0.0
2	80	35.2
4	114	50.0
6	139	61.0
8	162	71.0
10	172	75.5
12	181	79.4
14	188	82.4
	162	

TABLE VI (CONTINUED)

Run 2-900

(Sample Weight = 7.7850 g, Temperature = 900°C)
(Flowrate = 18 SCFH)

Time (min)	Weight Gain (mg) (From Time = 0)	% Ox
0	0	0.0
2	123	54.5
4	180	79.6
6	209	92.5
8	227	100.5
10	232	102.8
12	235	104.0
14	236	104.5

Run 2-1000

(Sample Weight = 7.9130 g, Temperature = 1000°C)
(Flowrate = 18 SCFH)

Time (min)	Weight Gain (mg) (From Time = 0)	% Ox
0	0	0.0
2	148	64.6
4	197	86.0
6	225	98.2
8	240	104.9
10	244	106.5
12	245	107.0
14	247	107.9

TABLE VII

Coefficients for % Ox Versus Time Curves

For Ore 1 And Cre 2

Ore 1

Test	Temperature (oC)	A	B	C	D
1-300	300	0.22889	0.467866313	0.792681	-0.1000
1-400	400	0.56766	0.450653640	0.550524	-0.2000
1-500	500	0.41748	0.572731312	0.474257	-0.2000
1-600	600	2.46975	0.782768734	0.612815	-1.9000
1-700	700	50.84186	0.984716929	0.571198	-50.0000
1-800	800	50.95296	0.982586149	0.565025	-50.0000
1-900	900	51.02125	0.980448206	0.491935	-50.0000
1-1000	1000	41.05629	0.974990911	0.483693	-40.0000

Ore 2

1-300	300	0.16435	0.606131610	0.808889	-0.1000
1-400	400	0.29608	0.452912160	0.452583	-0.1000
1-500	500	0.46437	0.296582763	0.540299	-0.1000
1-600	600	0.61703	0.228535831	0.486170	-0.1000
1-700	700	0.73698	0.192385976	0.491075	-0.1000
1-800	800	0.94572	0.152951022	0.540247	-0.1000
1-900	900	7.05184	0.850740955	0.469176	-6.0000
1-1000	1000	51.08035	0.979168478	0.436195	-50.0000

TABLE VIII

Variation of $\frac{T_f + 110.4}{T_f^{3/2}}$ With Temperature

T_f, °K	$T_f + 110.4$	$T_f^{3/2}$	$\frac{T_f + 110.4}{T_f^{3/2}}$	$\left(\frac{T_f + 110.4}{T_f^{3/2}}\right)^{-0.41}$
1000	1110.4	31,600	0.0352	0.254
1100	1210.4	36,400	0.0333	0.248
1200	1310.4	41,500	0.0316	0.242
1300	1410.4	47,000	0.0300	0.238
1400	1510.4	52,400	0.0288	0.234
1500	1610.4	58,100	0.02765	0.229
1600	1710.4	64,700	0.0264	0.226
1700	1810.4	70,000	0.0258	0.222

TABLE IX

Partial Pressure Of Oxygen In The Bed

As Determined For Test 1-1

Minute	SCFM O_2 Used per Ft^2	SCFM total per Ft^2	SCFM O_2 Orig.	SCFM O_2 at bottom	SCFM total at bottom	%	P_{O_2}
1	1.92	470	98.7	96.7	468	99.6	0.207
2	7.63	425	89.3	81.7	417	98.1	0.196
3	14.57	395	83.0	68.4	380	96.2	0.180
4	19.43	360	75.6	56.2	340	94.4	0.165
5	20.65	355	74.6	54.0	334	94.1	0.162
6	18.57	305	64.0	45.4	286	93.8	0.159
7	13.63	295	62.0	48.4	281	95.3	0.172
8	9.50	265	55.6	46.1	256	96.6	0.180
9	6.61	260	54.6	48.0	253	97.3	0.190
10	4.62	260	54.6	50.0	255	98.1	0.196
11	3.22	260	54.6	51.4	257	98.8	0.200
12	2.22	280	58.8	56.6	278	99.3	0.204
13	1.52	295	62.0	60.5	293	99.3	0.206
14	0.99	295	62.0	61.0	294	99.7	0.207

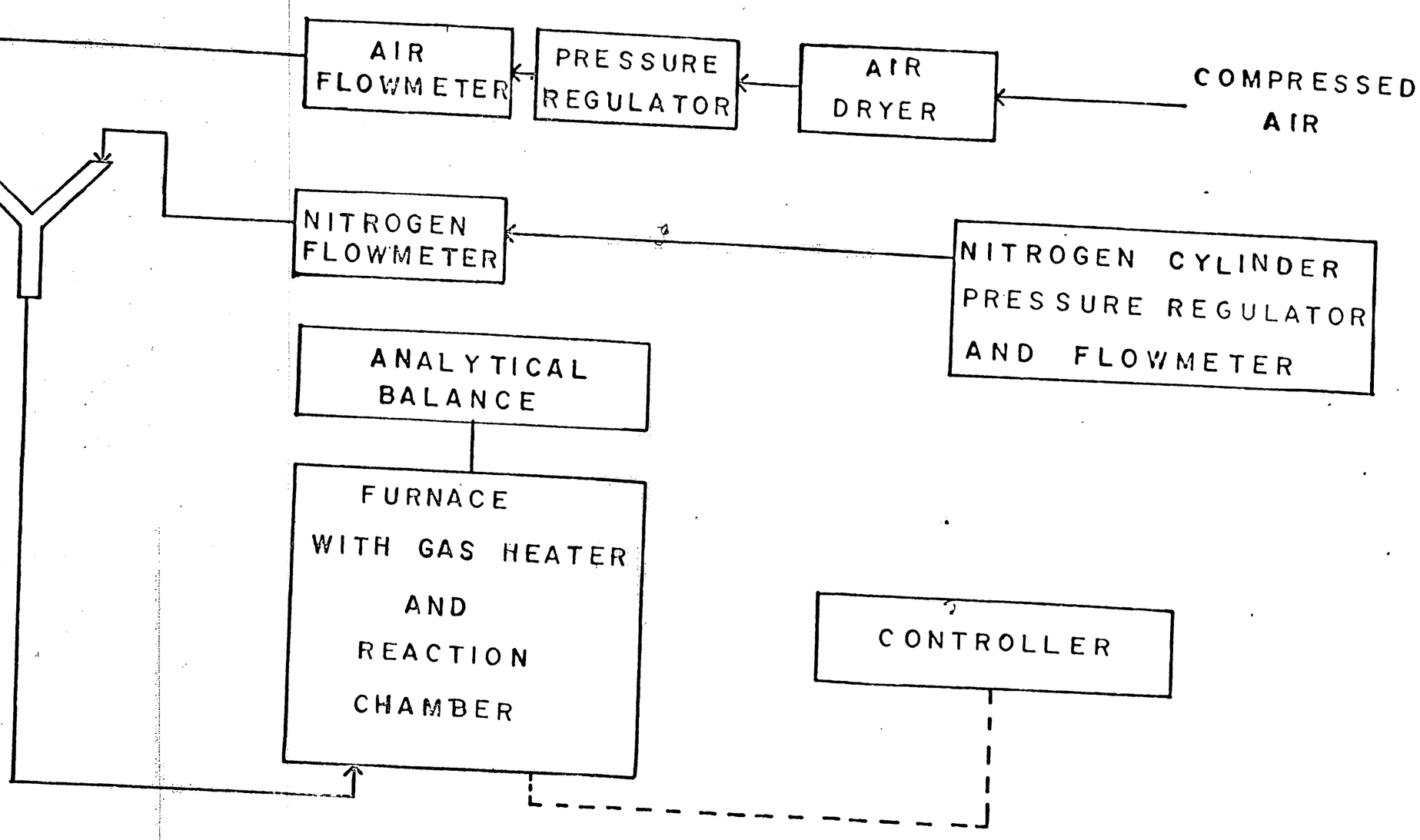

FIGURE 1

BLOCK DIAGRAM OF EXPERIMENTAL SETUP

168

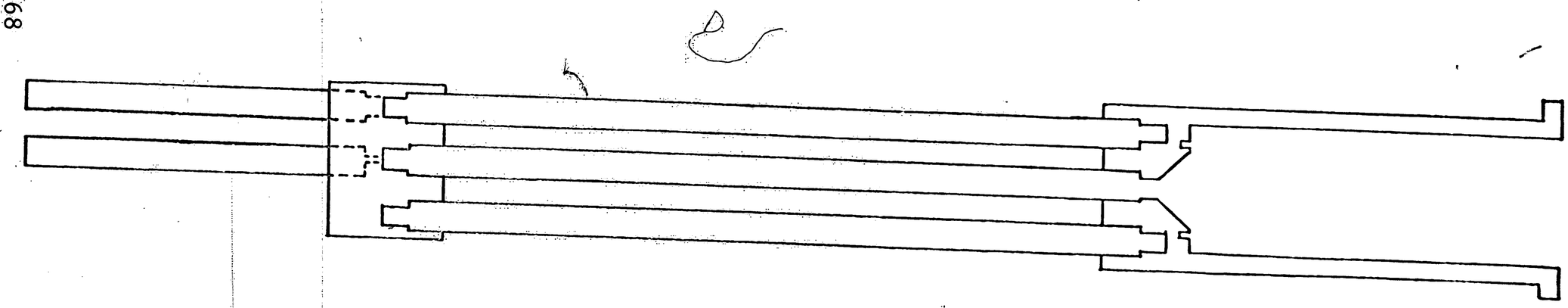

FIGURE 2

CROSSECTION OF GAS HEATER AND REACTION CHAMBER

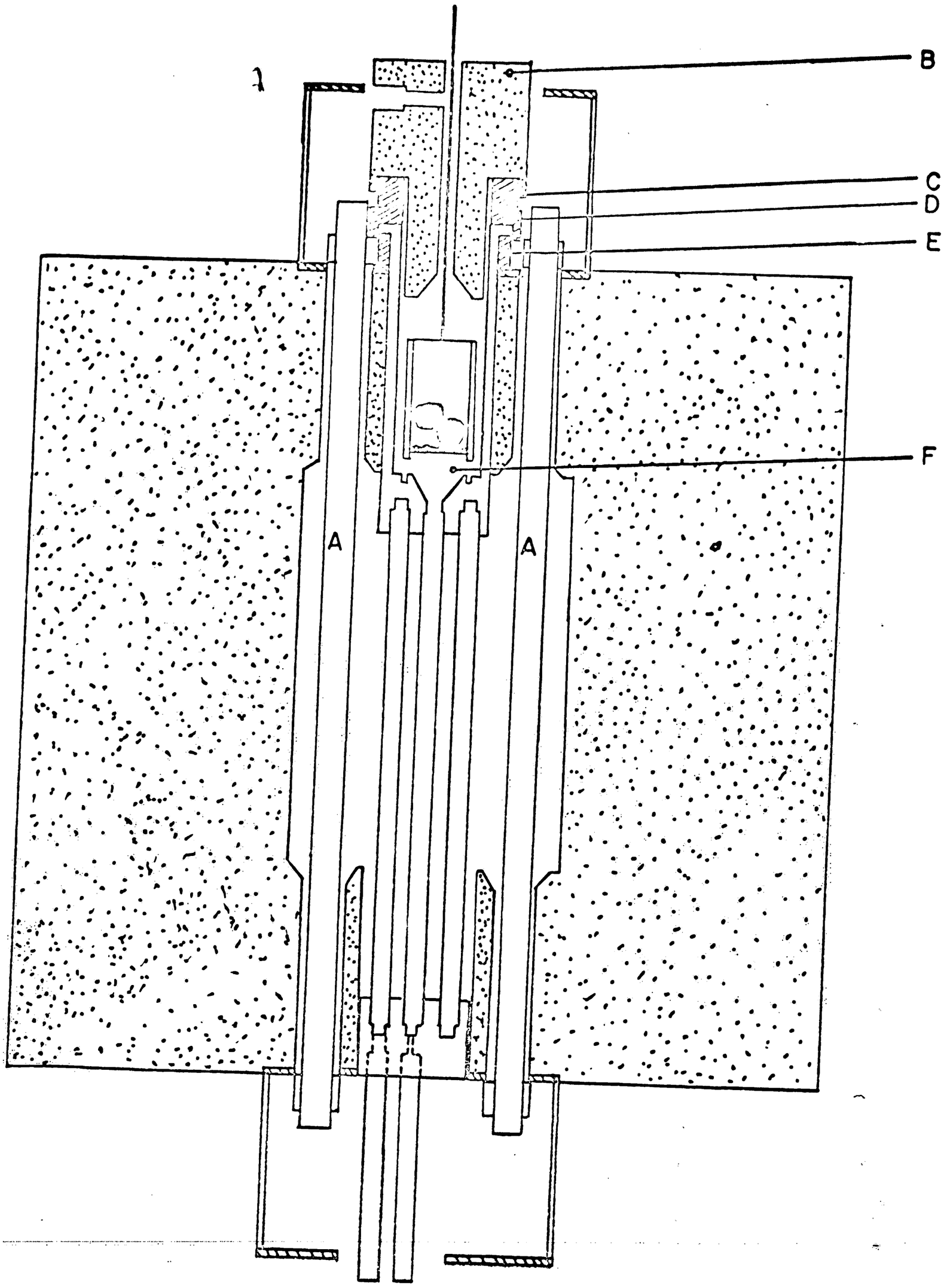

FIGURE 3
CROSSECTION OF FURNACE WITH GAS HEATER, REACTION CHAMBER AND SAMPLE HOLDER

A-SILICON CARBIDE HEATING ELEMENTS
B-LAVITE LID
C,D,E-TRANSITE WASHERS
F-GAS HEATER AND REACTION CHAMBER

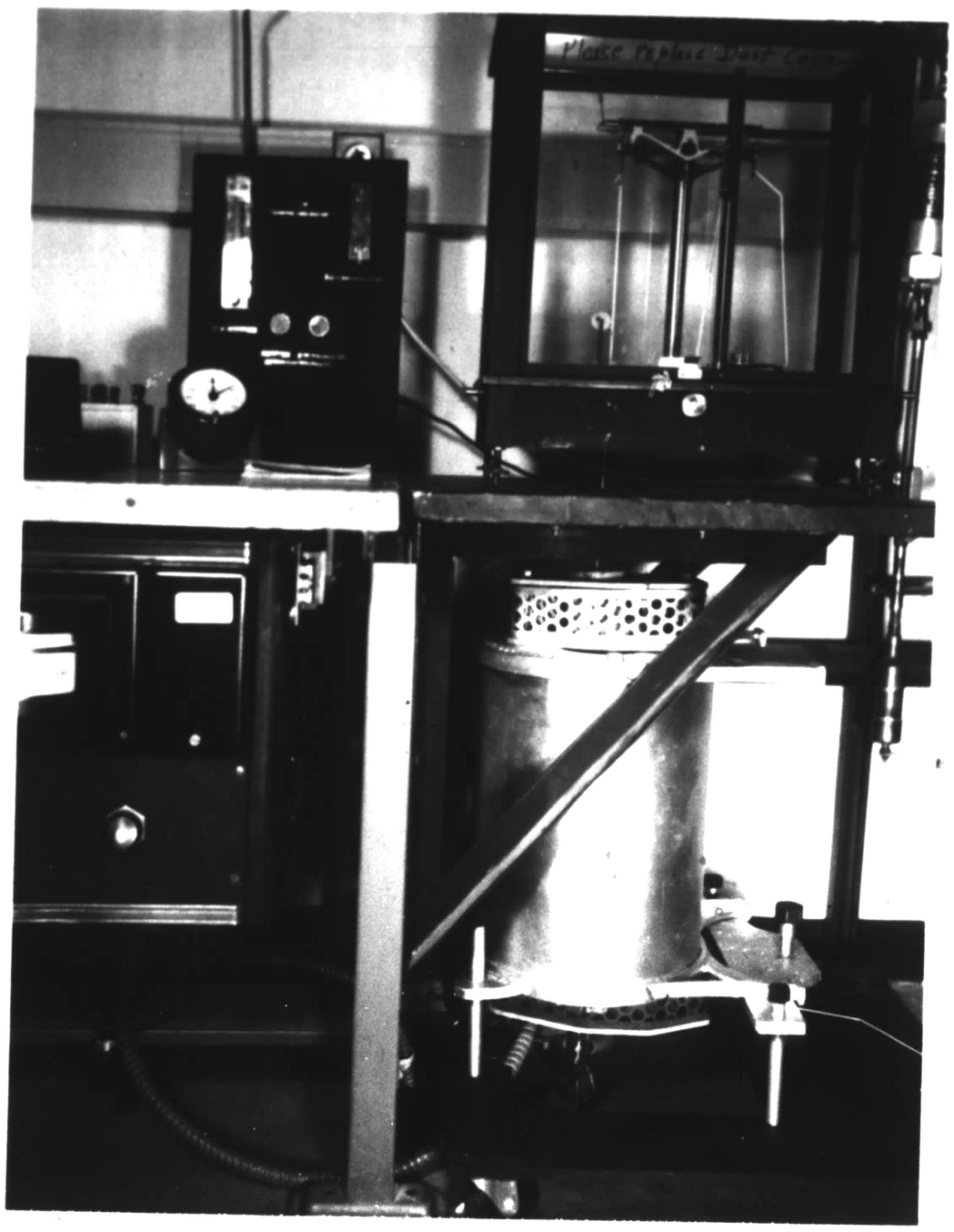

FIGURE 4

PHOTOGRAPH OF EXPERIMENTAL SETUP

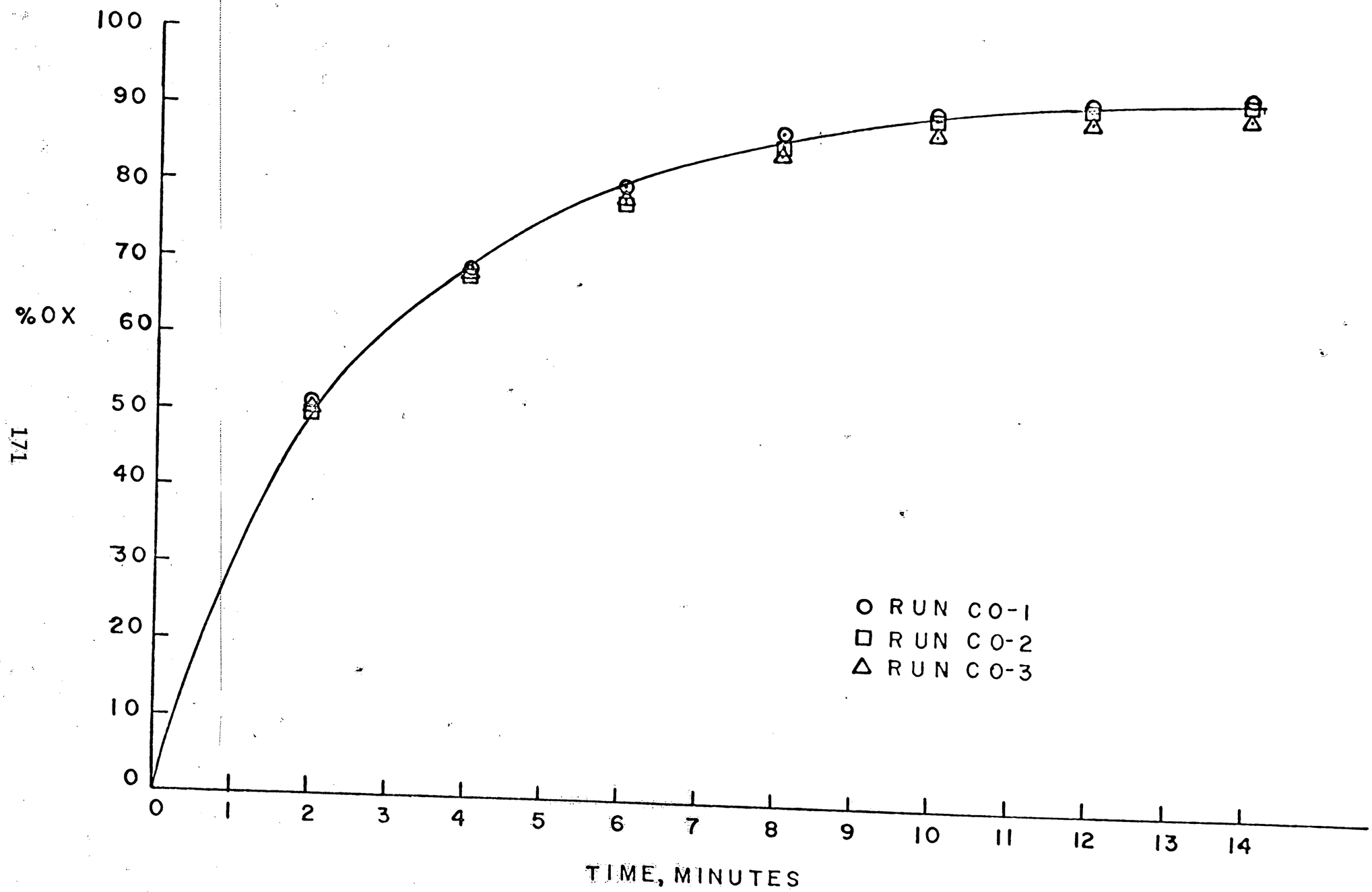

FIGURE 5-RUNS MADE TO ILLUSTRATE REPRODUCIBILITY

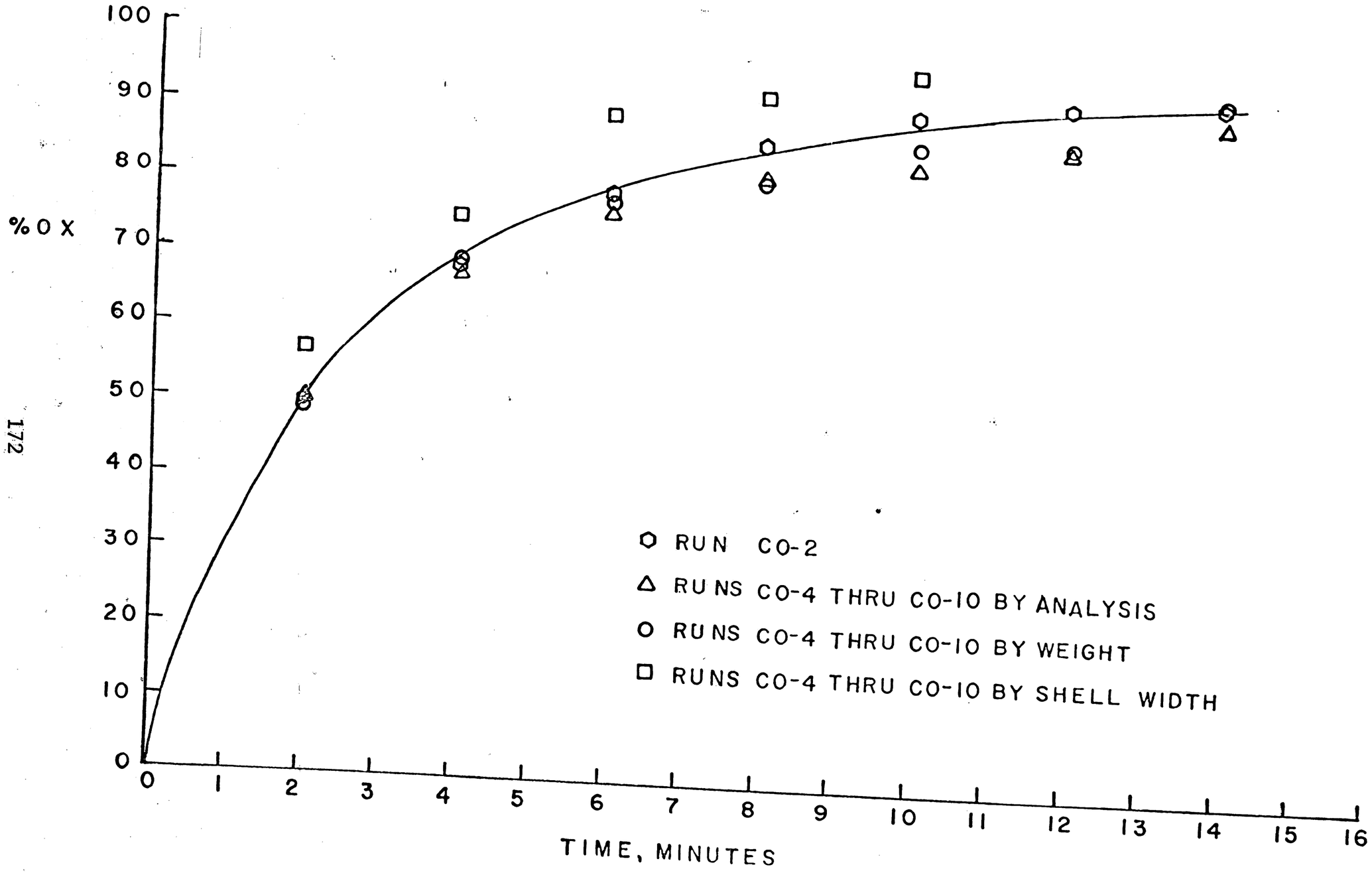

FIGURE 6-RUNS MADE TO CHECK ACCURACY OF WEIGHT MEASUREMENTS

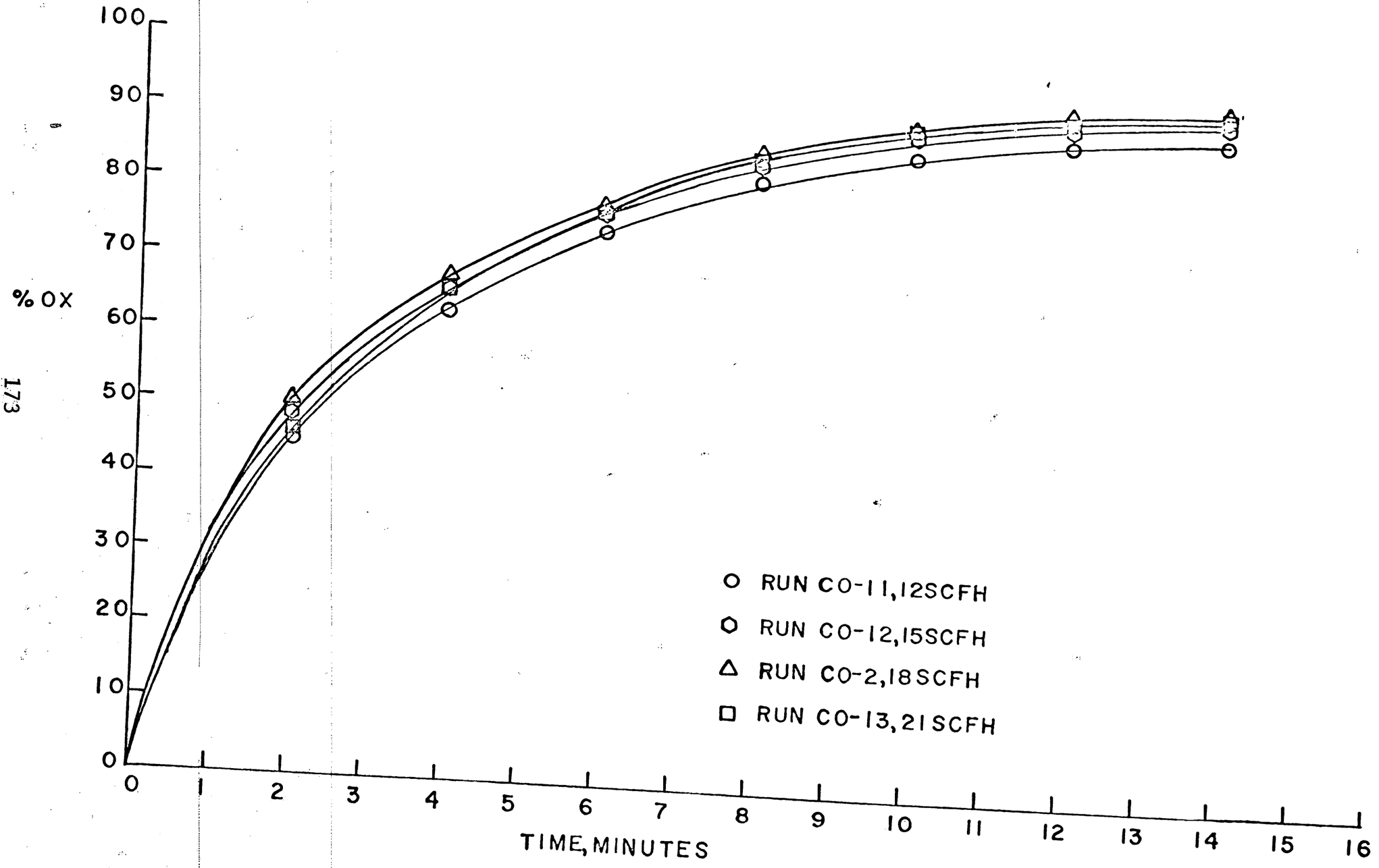

FIGURE 7-RUNS MADE AT DIFFERENT FLOWRATES

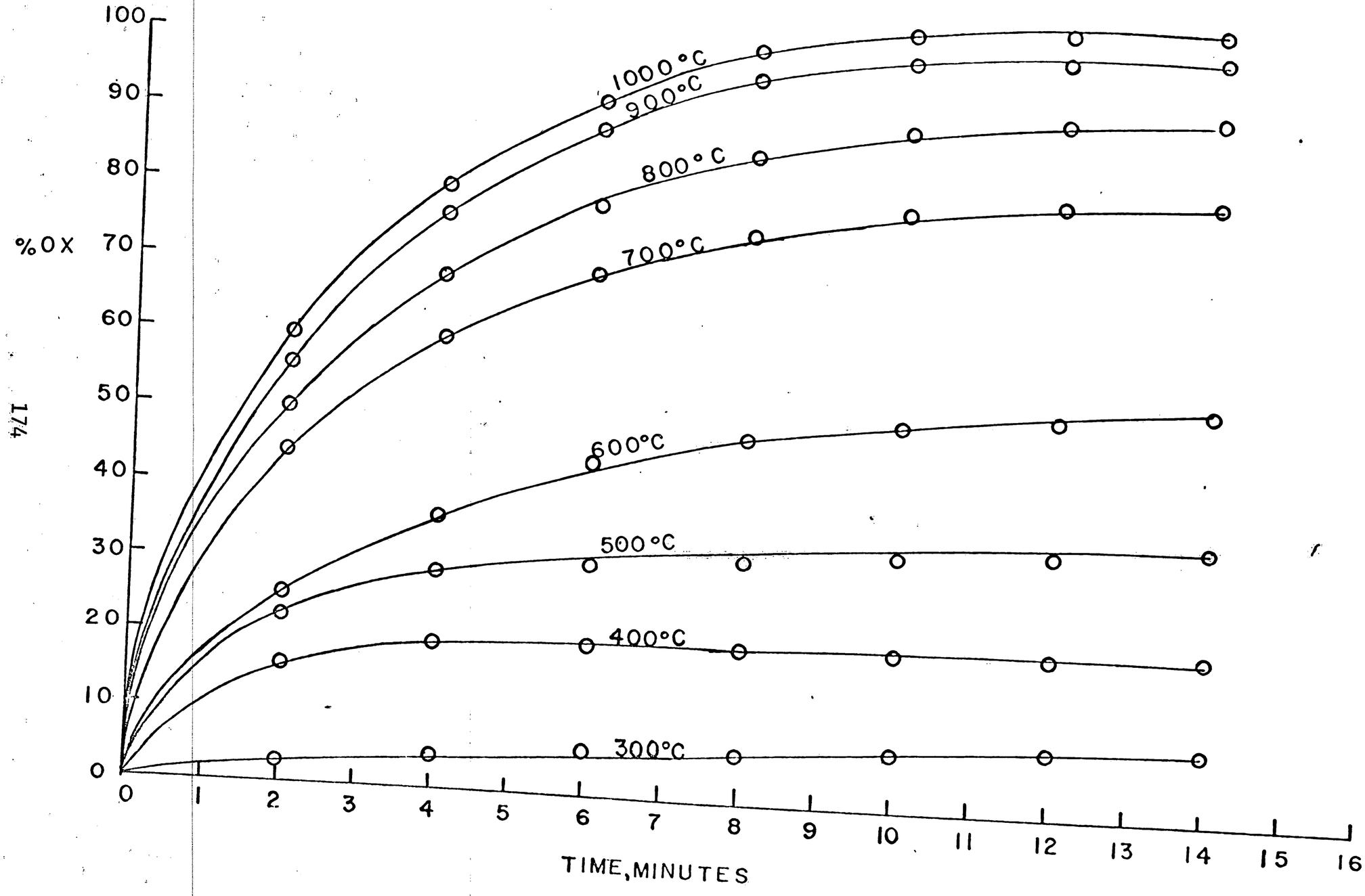

FIGURE 8- DATA TAKEN ON ORE BALLS OF ORE 1

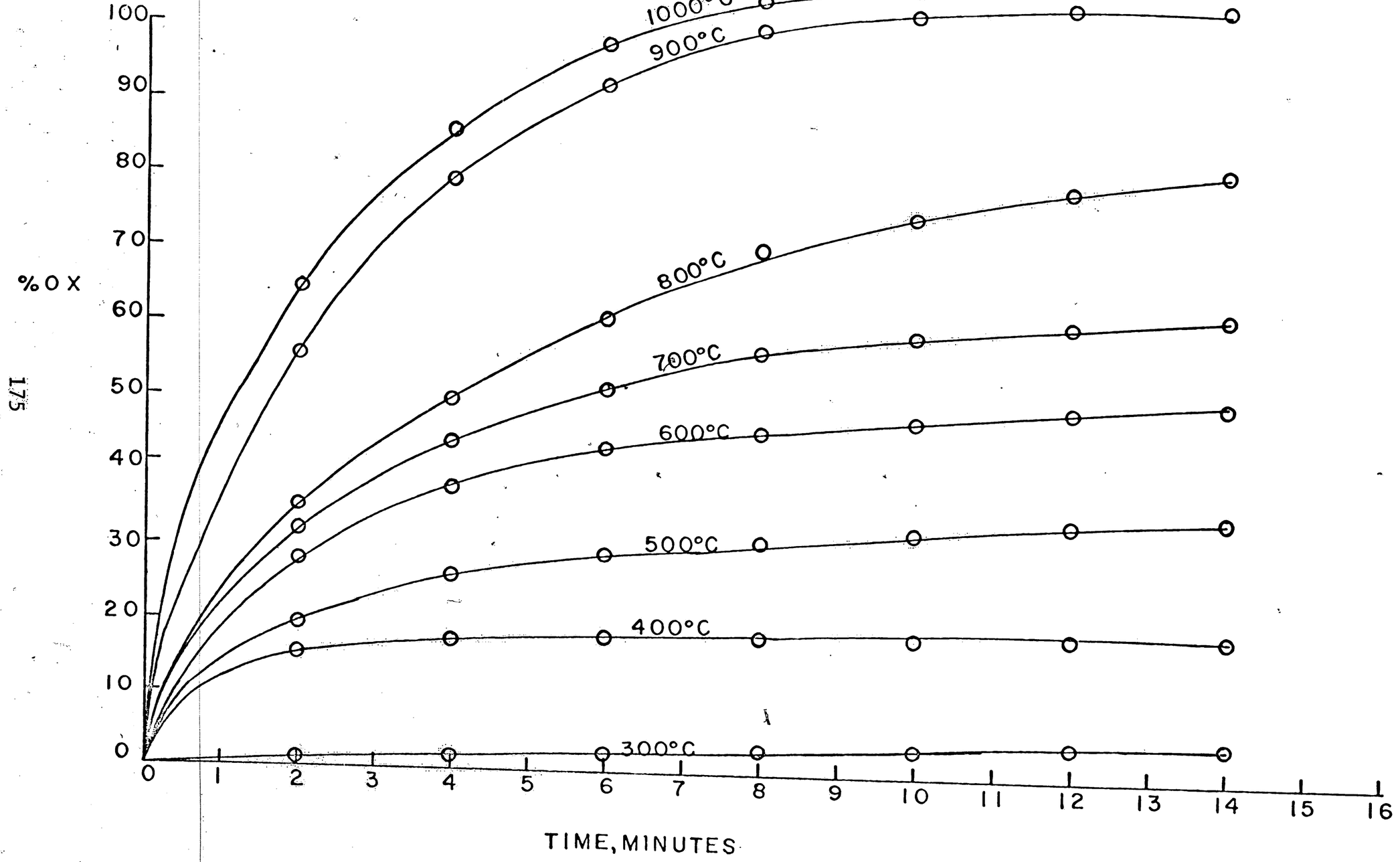

FIGURE 9-DATA ON ORE BALLS OF ORE 2

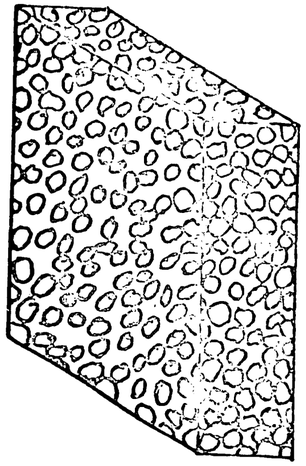

(A) SLICE USED FOR MODEL

AIR LUMP
(ALL AIR, NO PELLETS)

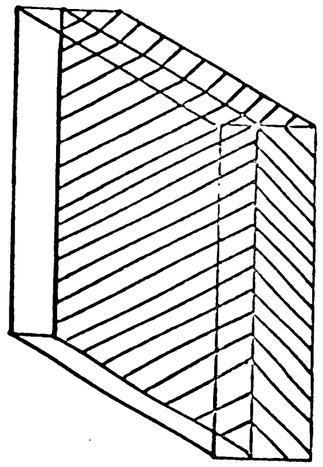

PELLET LUMP
(ALL PELLETS, NO AIR)

(B) AIR LUMP AND PELLET LUMP

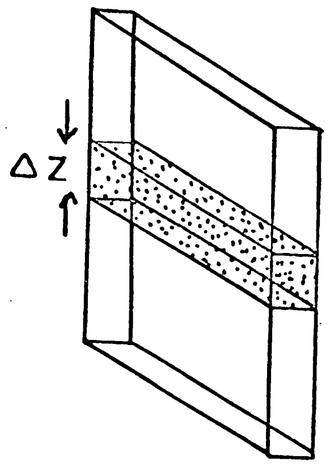

(C) AIR LUMP ELEMENT

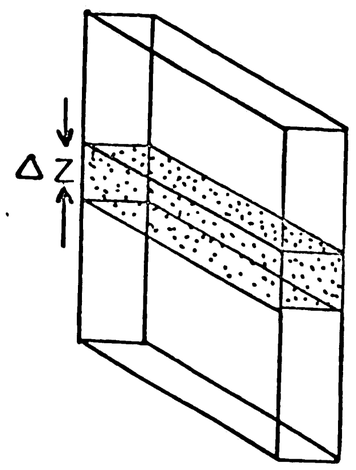

(D) PELLET LUMP ELEMENT

FIGURE 10

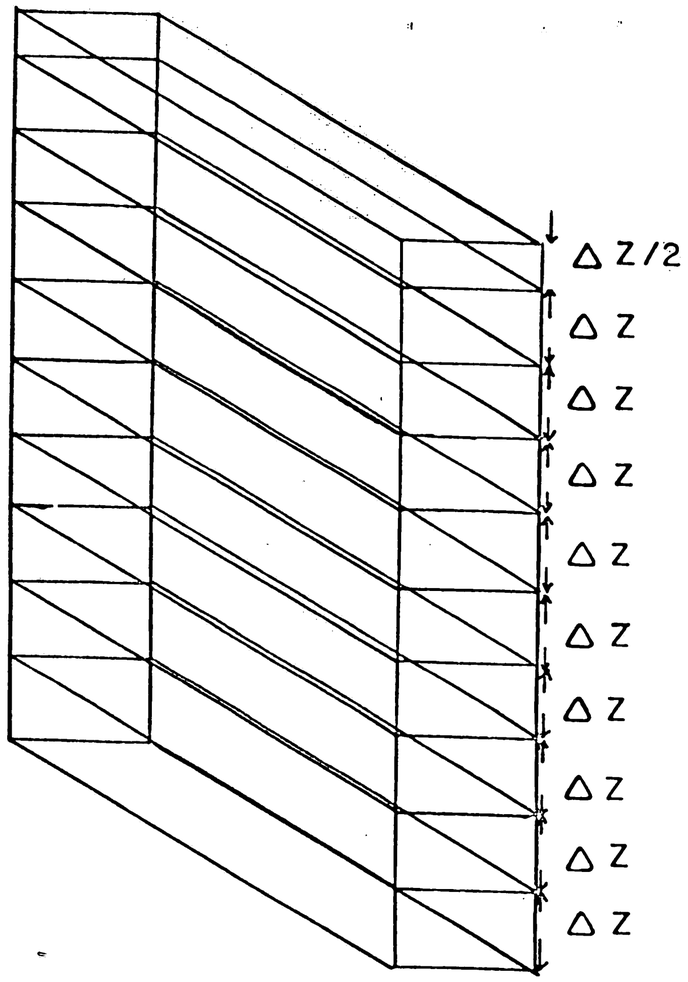

FIGURE 11

DIVISION OF THE THIN SLICE INTO CELLS

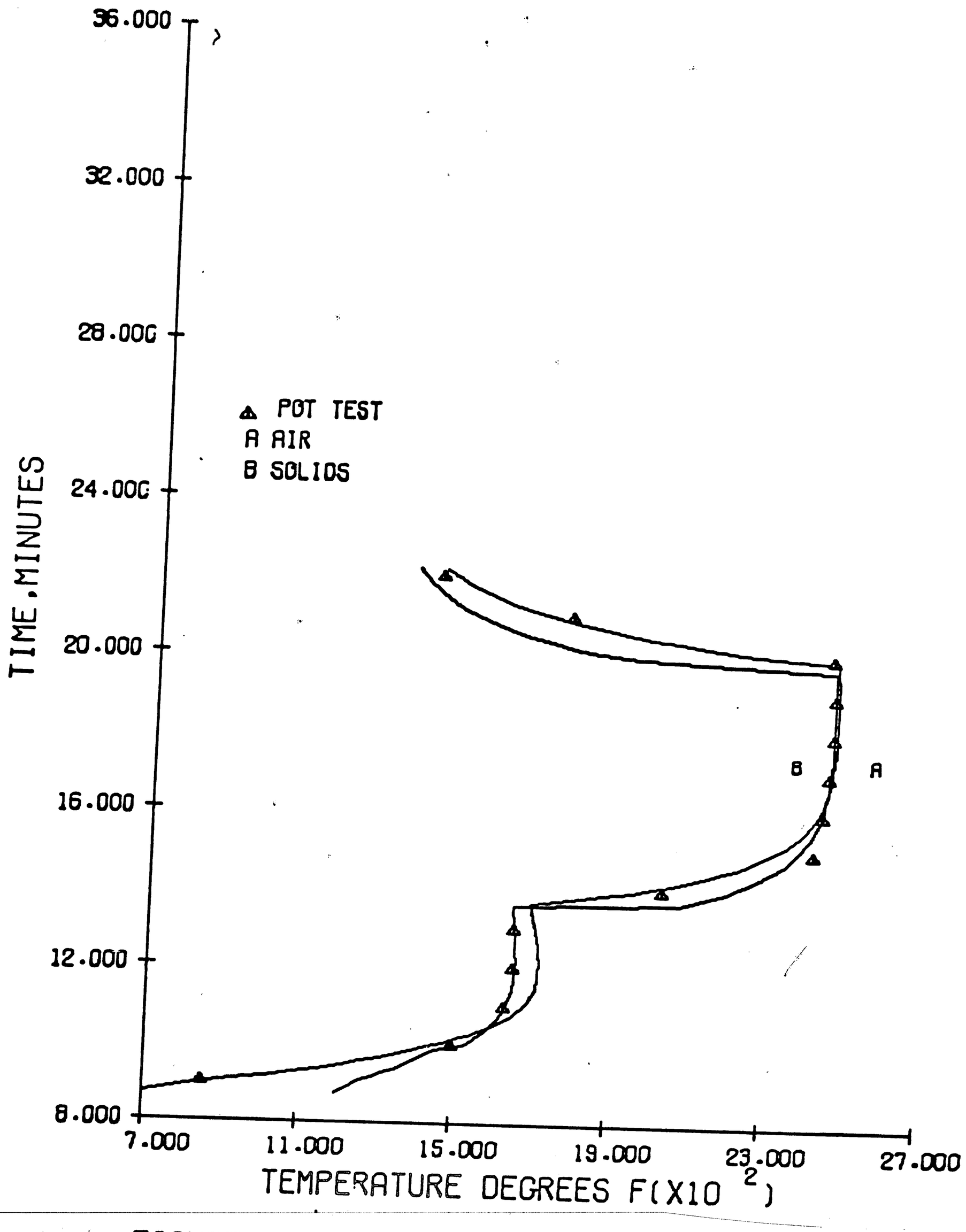

FIGURE 12-COMPUTER SIMULATION TEST1-1
POT TEST TEMPERATURES TAKEN 1.0INCHES
BELOW THE TOP OF THE BED.SIMULATION
DONE FOR .43 INCHES BELOW THE TOP

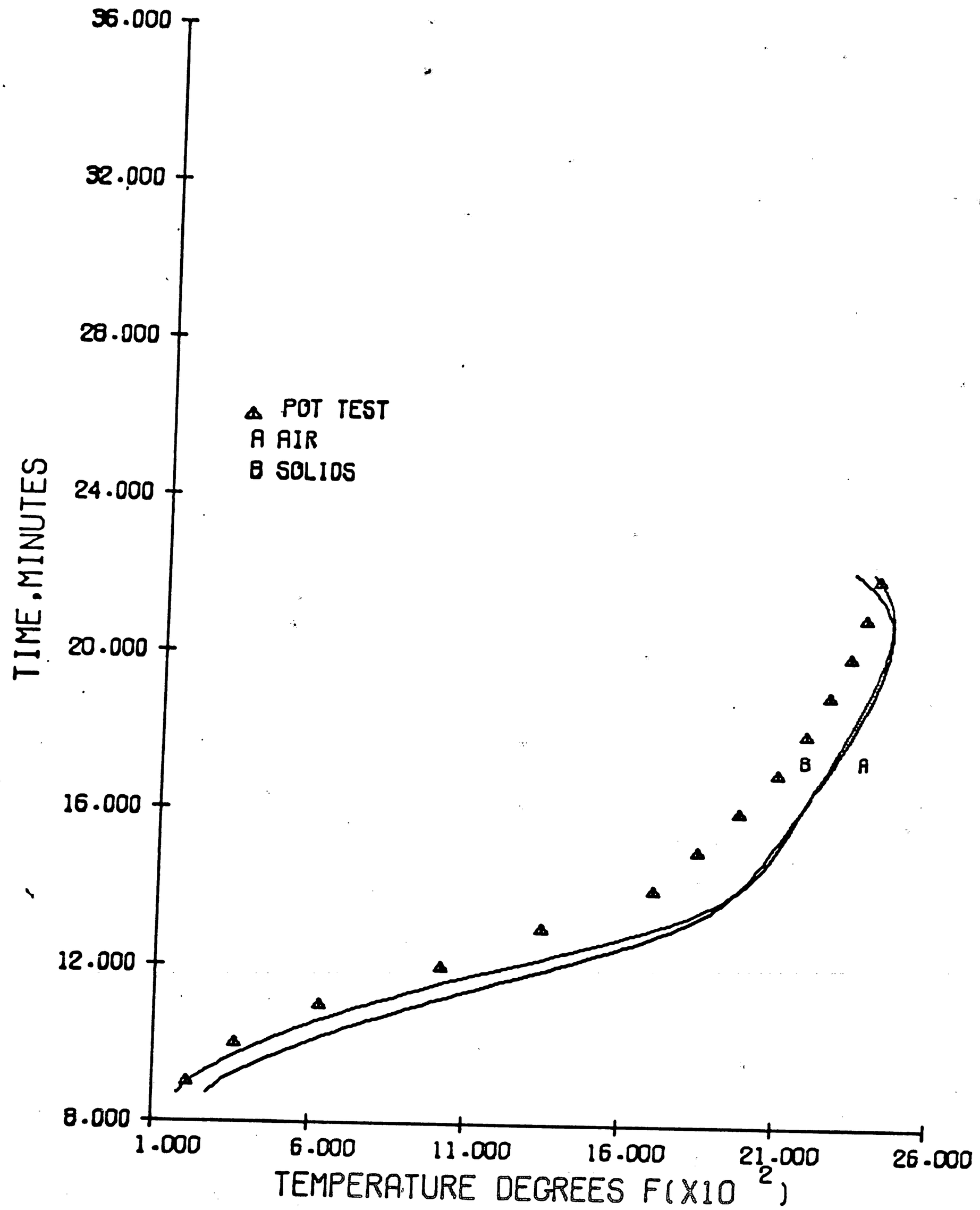

FIGURE 13-COMPUTER SIMULATION TEST1-1
POT TEST TEMPERATURES TAKEN10.0INCHES
BELOW THE TOP OF THE BED.SIMULATION
DONE FOR10.81 INCHES BELOW THE TOP

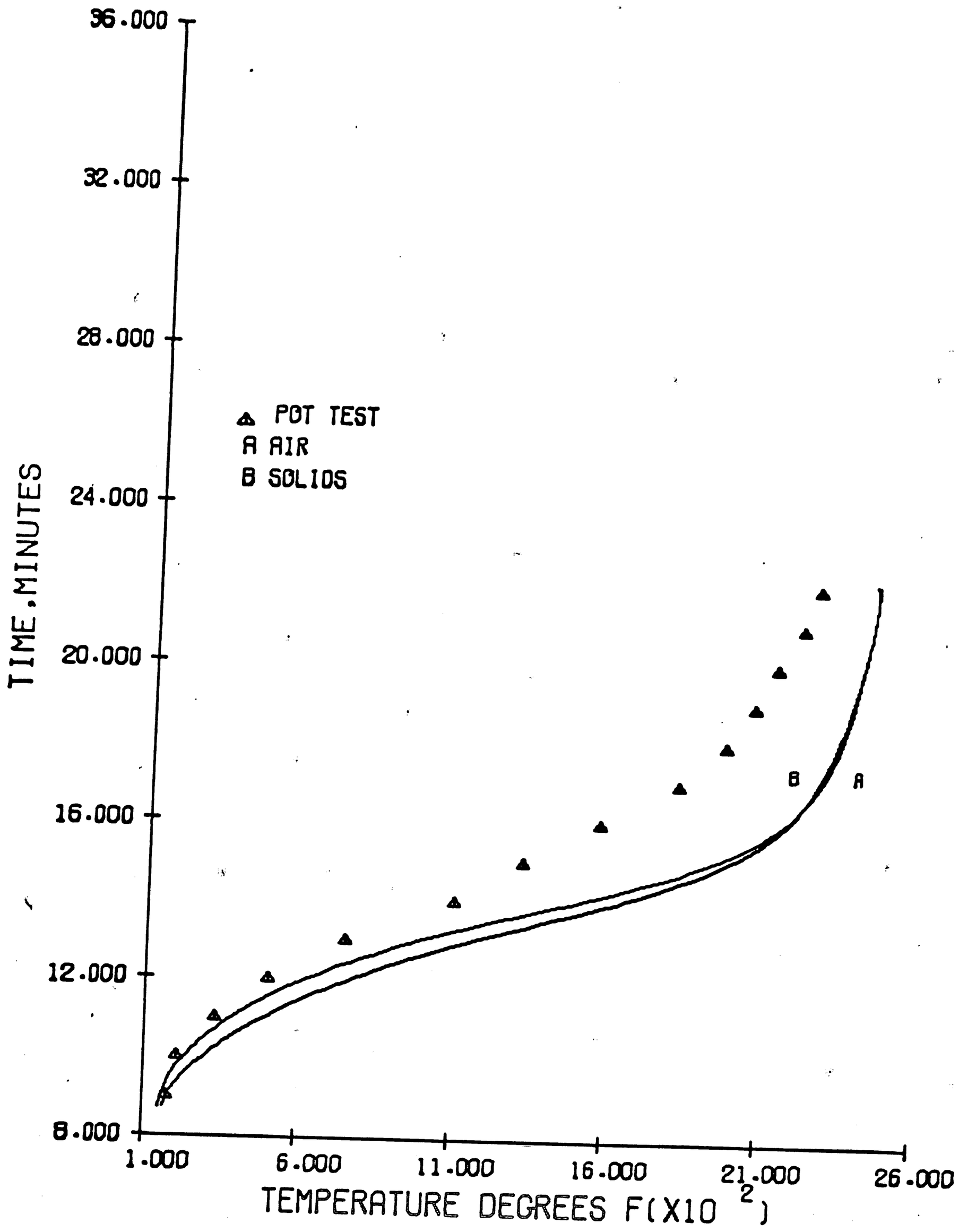

FIGURE 14-COMPUTER SIMULATION TEST1-1
POT TEST TEMPERATURES TAKEN16.0INCHES
BELOW THE TOP OF THE BED.SIMULATION
DONE FOR16.00 INCHES BELOW THE TOP

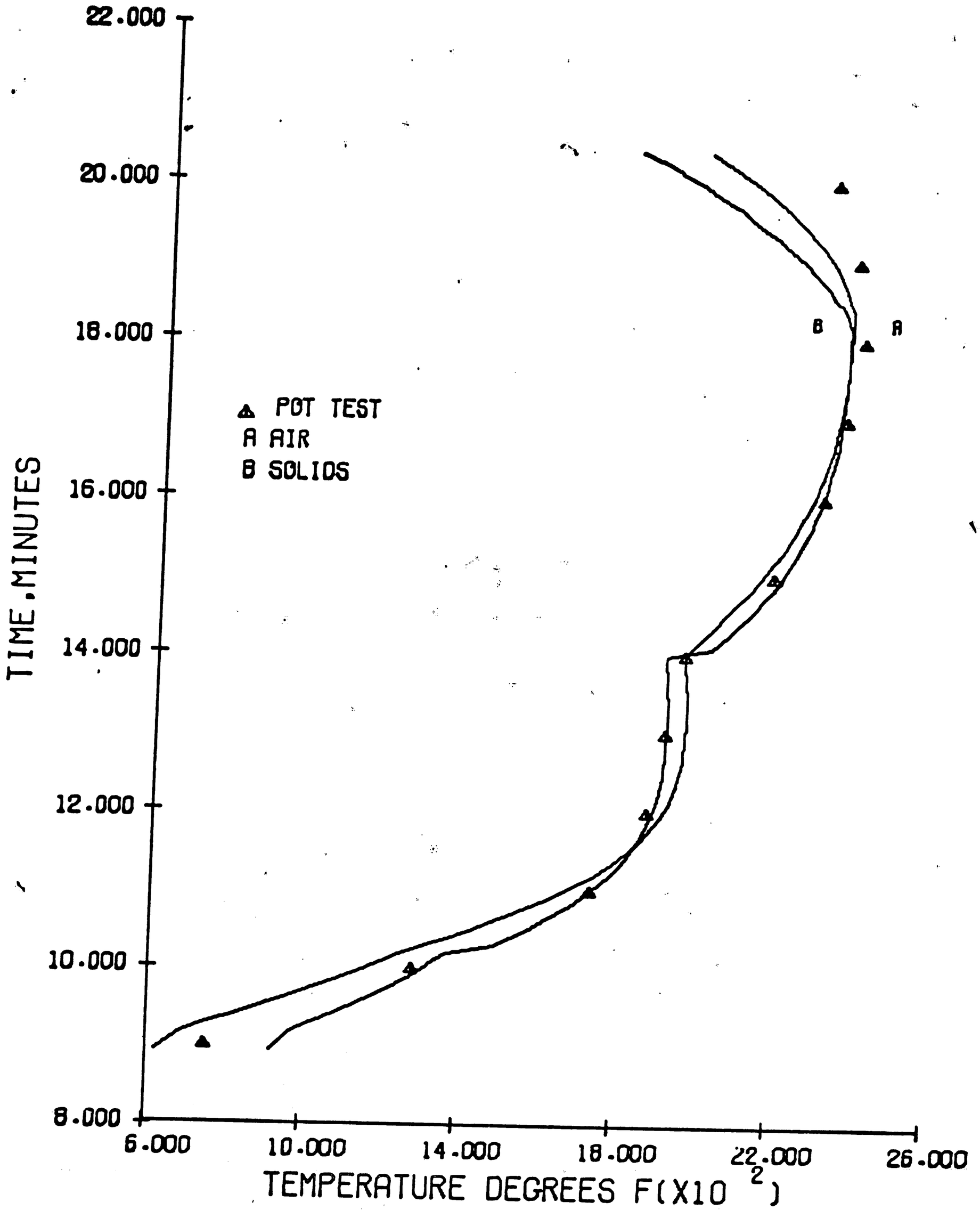

FIGURE 15-COMPUTER SIMULATION TEST1-2
POT TEST TEMPERATURES TAKEN 2.0INCHES
BELOW THE TOP OF THE BED.SIMULATION
DONE FOR 1.89 INCHES BELOW THE TOP

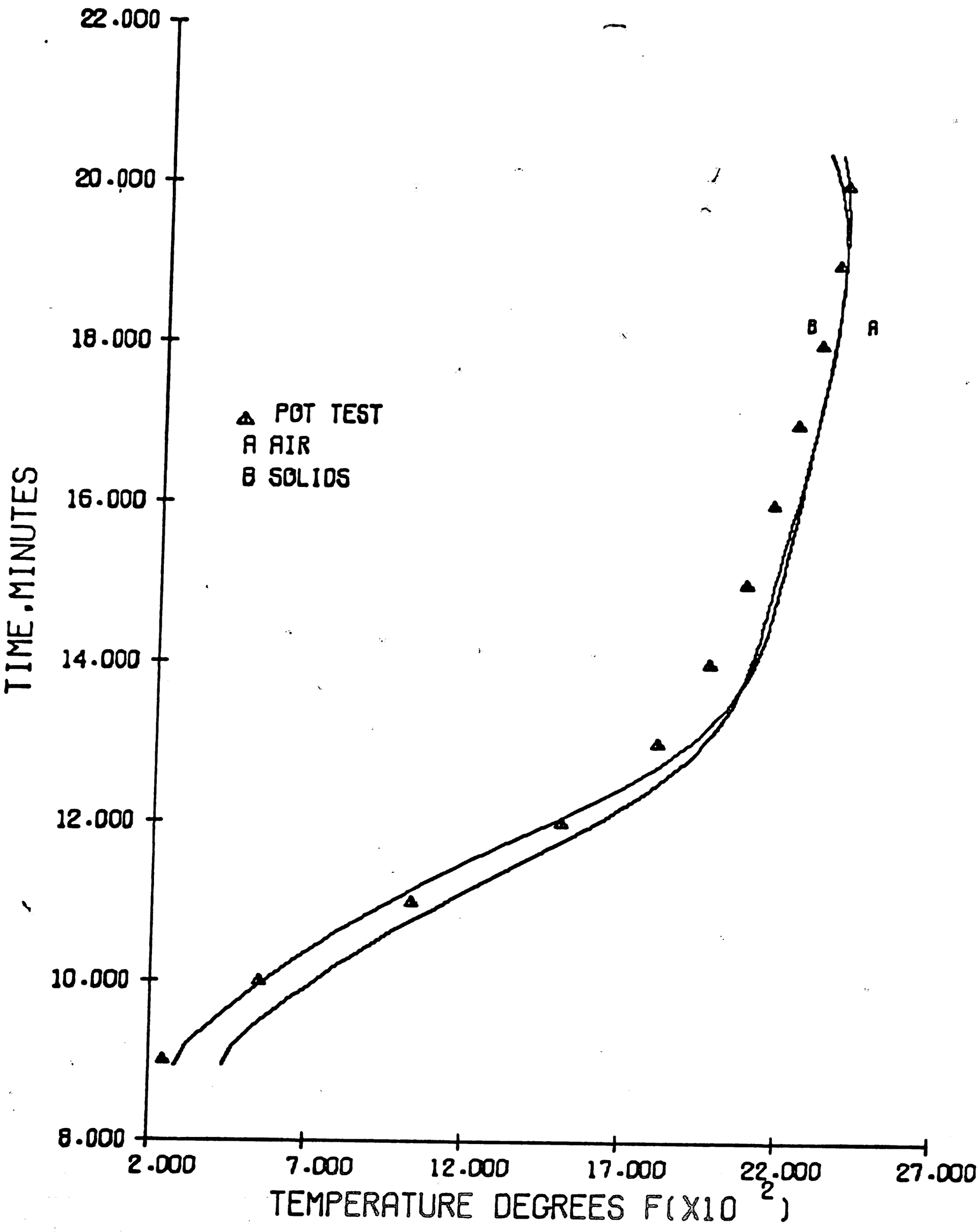

FIGURE 16-COMPUTER SIMULATION TEST1-2
POT TEST TEMPERATURES TAKEN 8.0INCHES
BELOW THE TOP OF THE BED.SIMULATION
DONE FOR 7.93 INCHES BELOW THE TOP

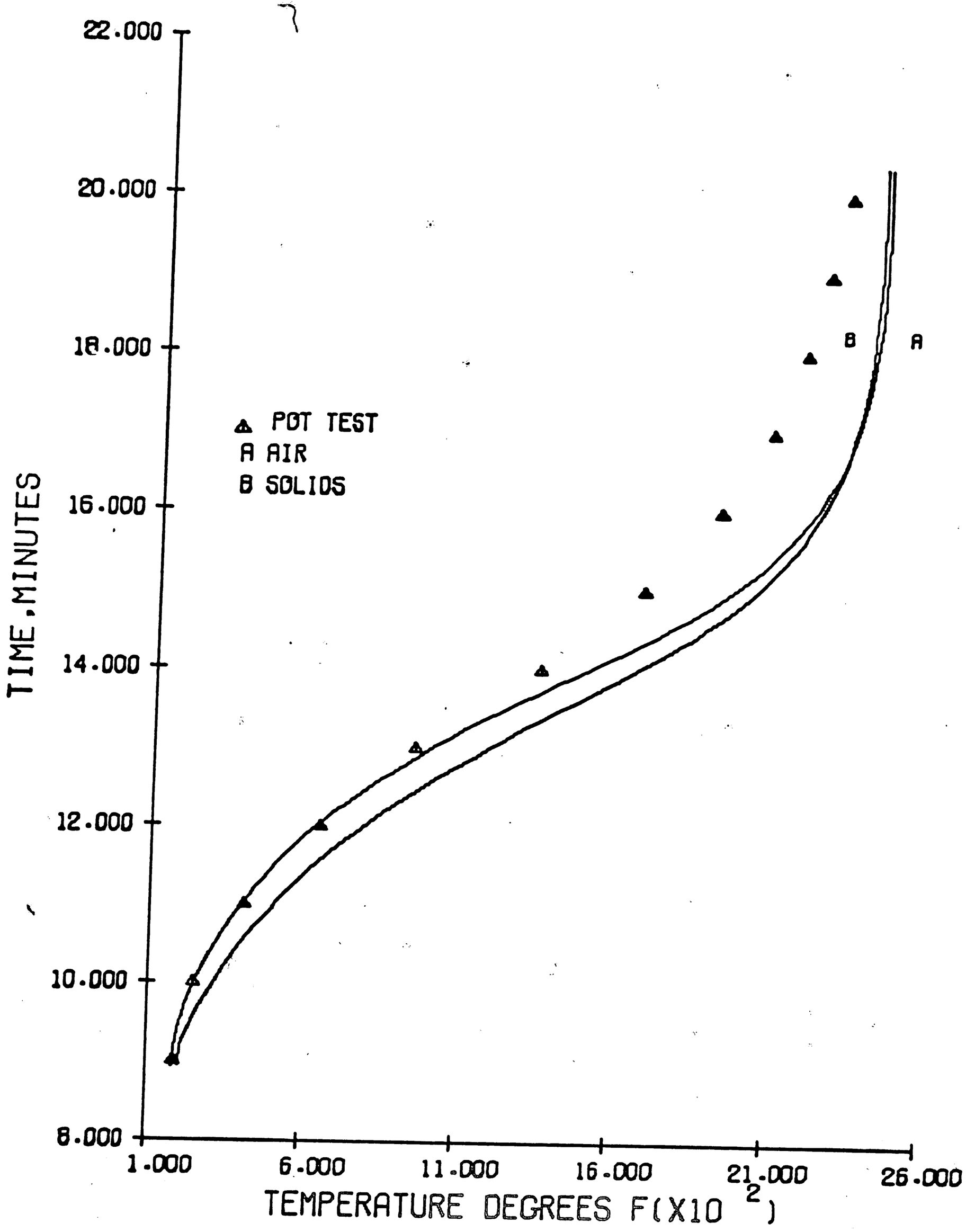

FIGURE 17-COMPUTER SIMULATION TEST1-2
POT TEST TEMPERATURES TAKEN14.0INCHES
BELOW THE TOP OF THE BED.SIMULATION
DONE FOR13.97 INCHES BELOW THE TOP

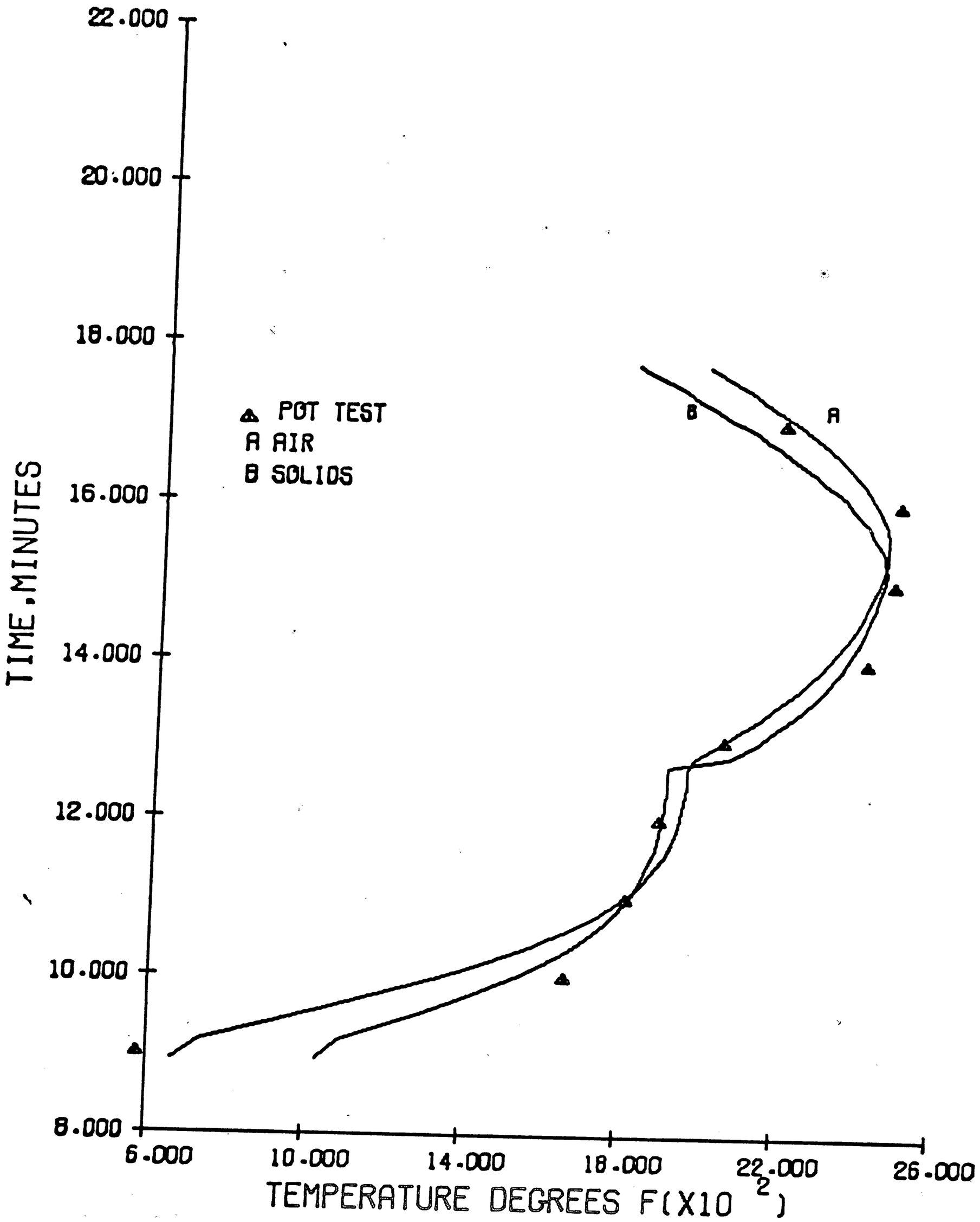

FIGURE 18-COMPUTER SIMULATION TEST1-3
POT TEST TEMPERATURES TAKEN 2.0INCHES
BELOW THE TOP OF THE BED.SIMULATION
DONE FOR 1.89 INCHES BELOW THE TOP

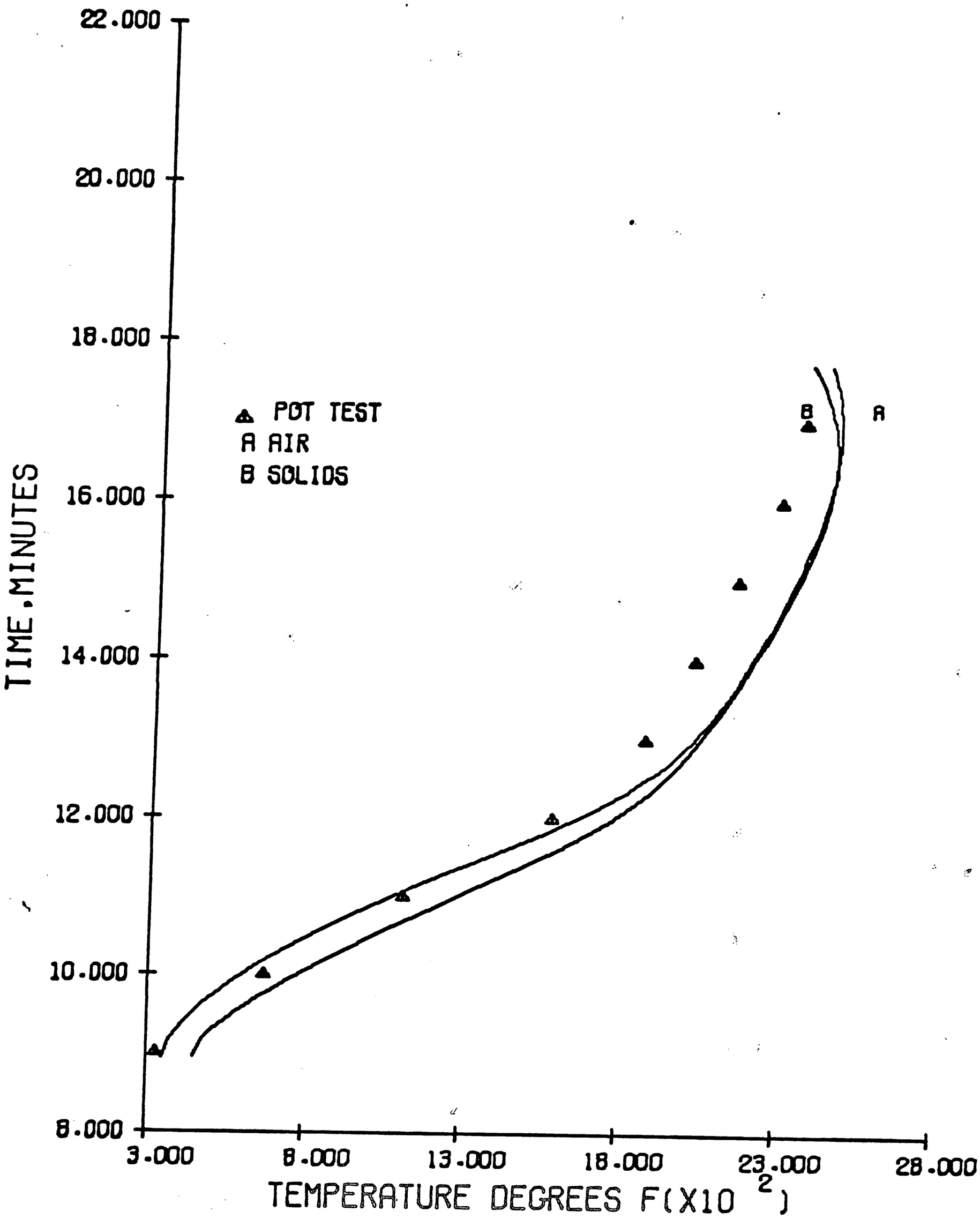

FIGURE 19-COMPUTER SIMULATION TEST1-3
PDT TEST TEMPERATURES TAKEN 8.0INCHES
BELOW THE TOP OF THE BED.SIMULATION
DONE FOR 7.93 INCHES BELOW THE TOP

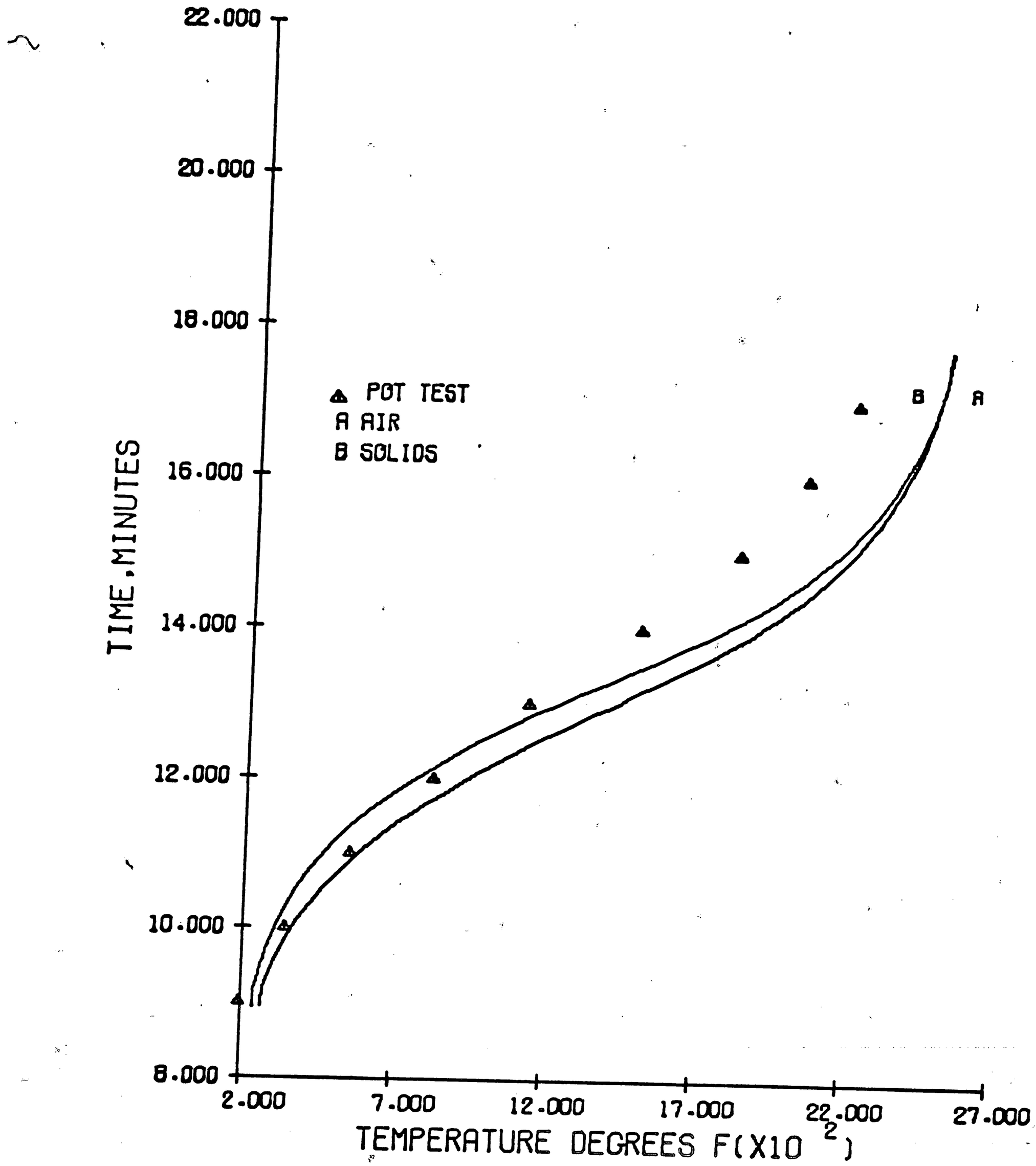

FIGURE 20-COMPUTER SIMULATION TEST1-3
POT TEST TEMPERATURES TAKEN14.0INCHES
BELOW THE TOP OF THE BED.SIMULATION
DONE FOR13.97 INCHES BELOW THE TOP

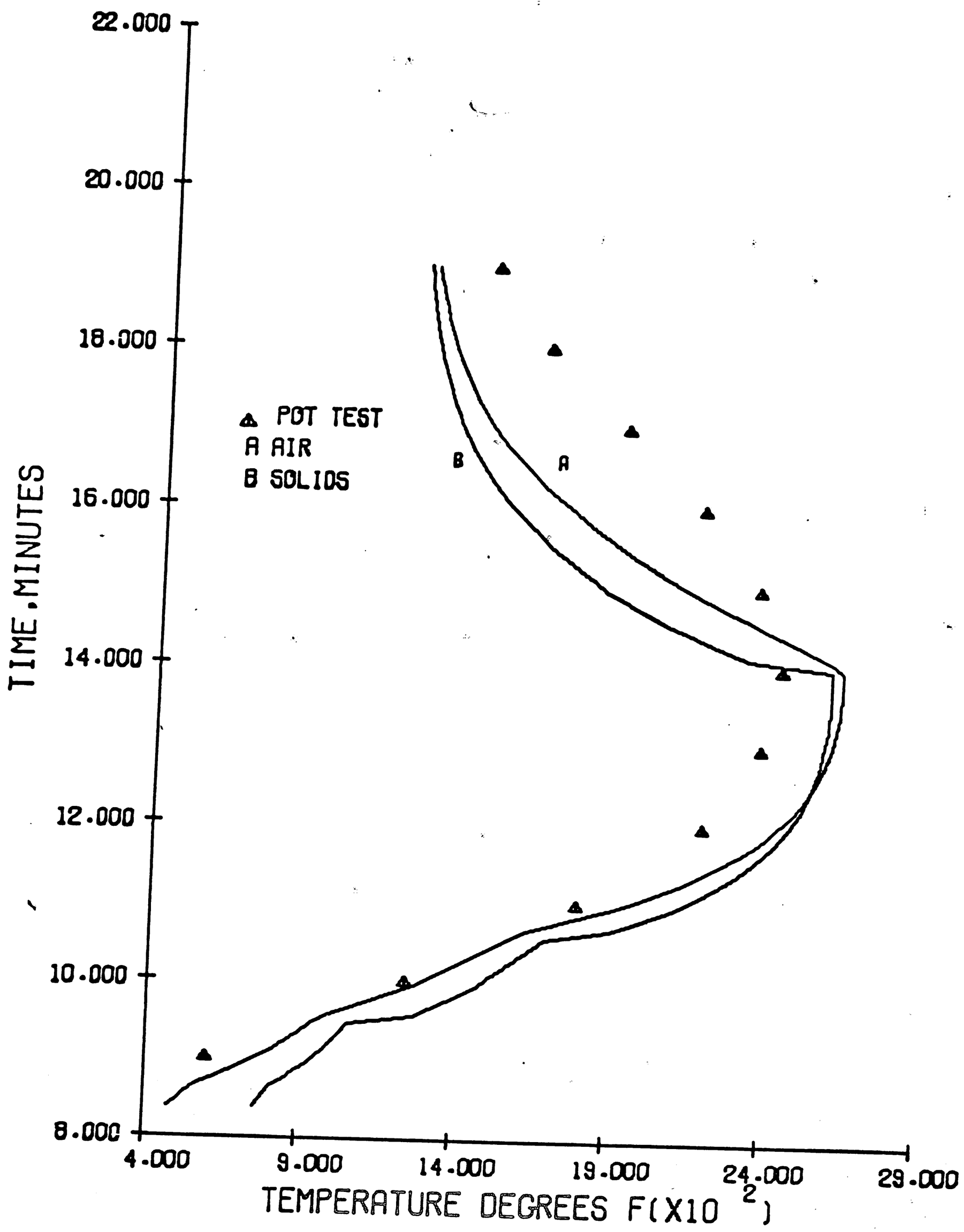

FIGURE 21-COMPUTER SIMULATION TEST2-1
POT TEST TEMPERATURES TAKEN 2.0INCHES
BELOW THE TOP OF THE BED.SIMULATION
DONE FOR 1.89 INCHES BELOW THE TOP

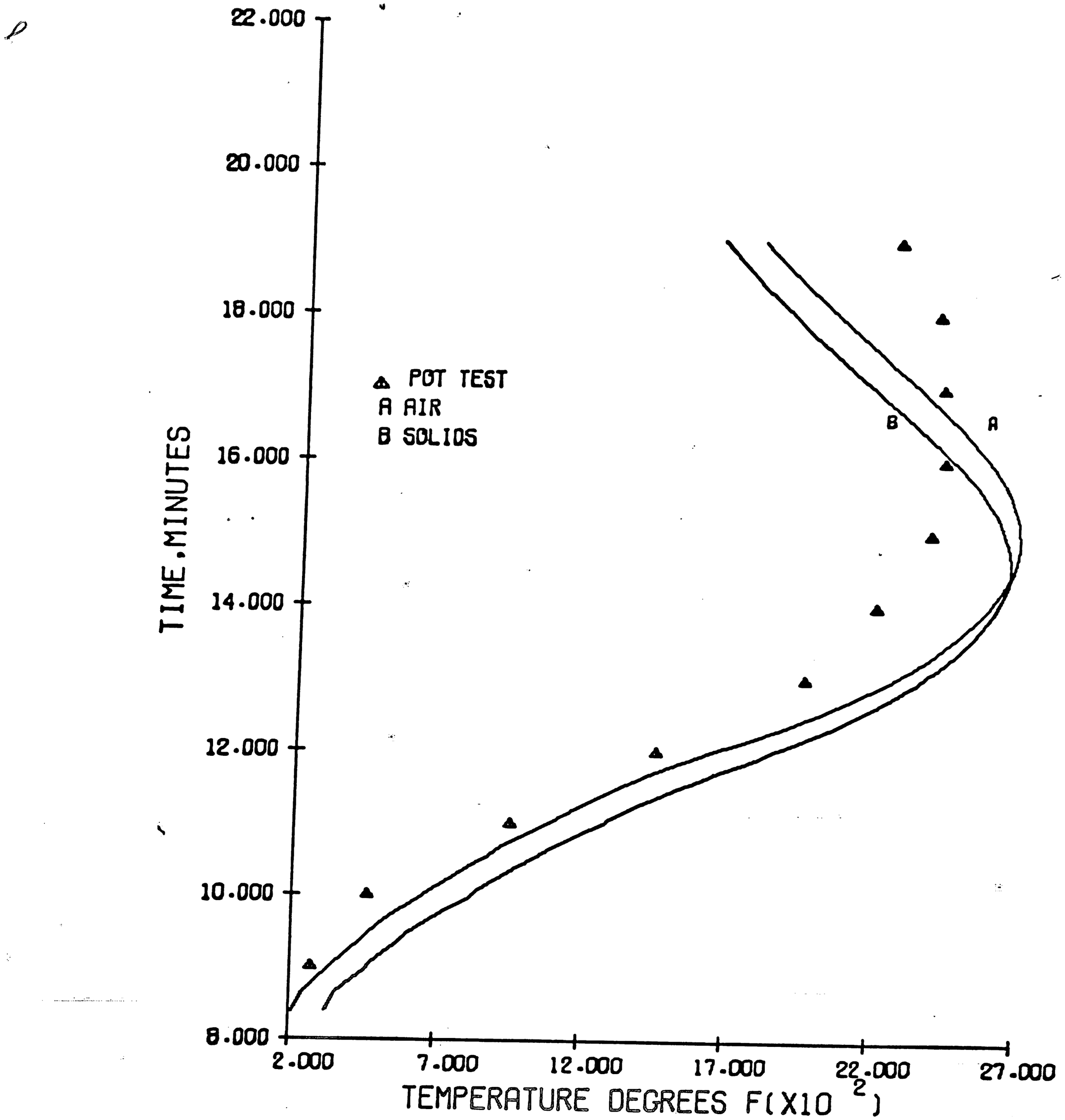

FIGURE 22-COMPUTER SIMULATION TEST2-1
POT TEST TEMPERATURES TAKEN 8.0INCHES
BELOW THE TOP OF THE BED.SIMULATION
DONE FOR 7.93 INCHES BELOW THE TOP

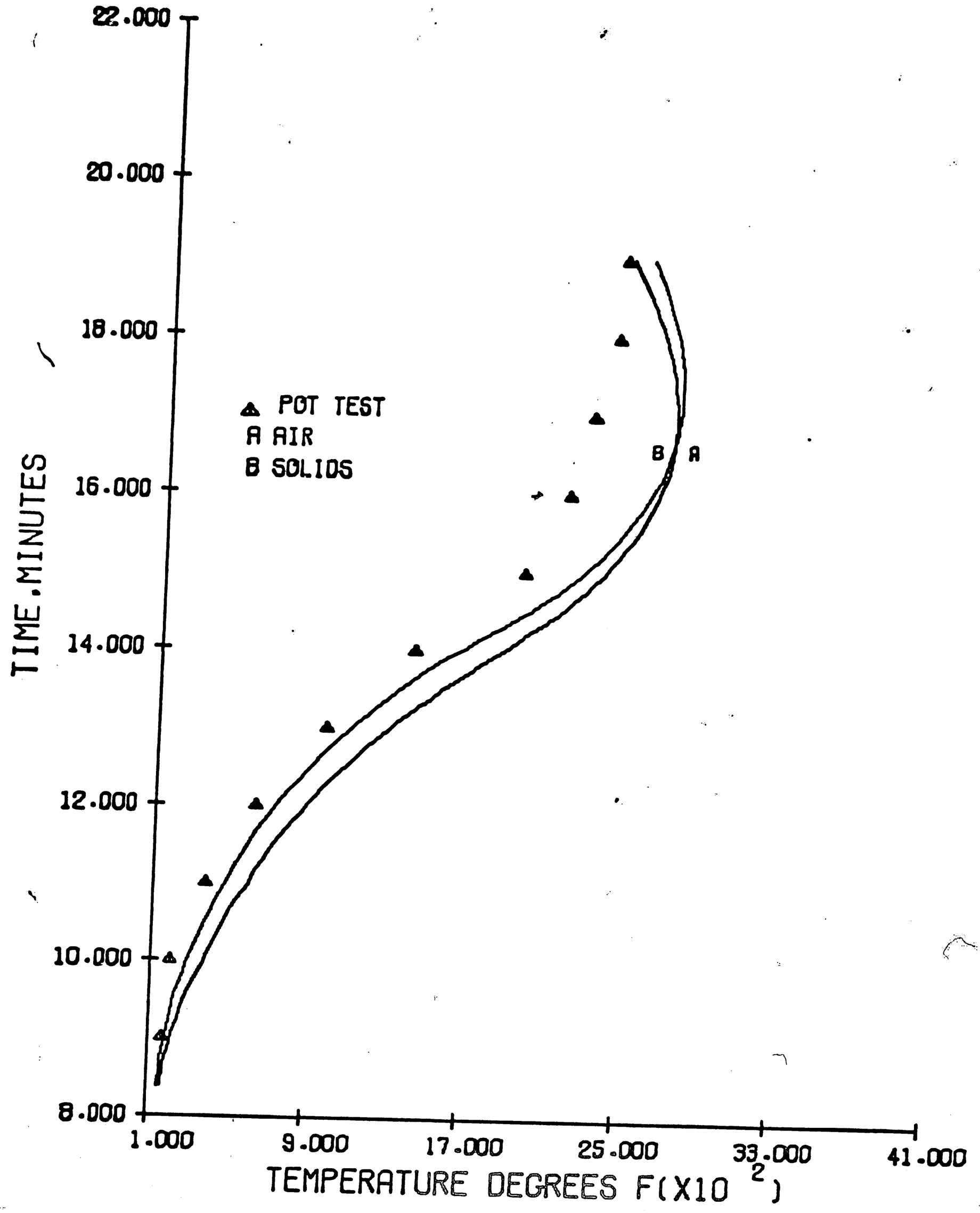

FIGURE 23-COMPUTER SIMULATION TEST2-1
POT TEST TEMPERATURES TAKEN14.0INCHES
BELOW THE TOP OF THE BED.SIMULATION
DONE FOR13.97 INCHES BELOW THE TOP

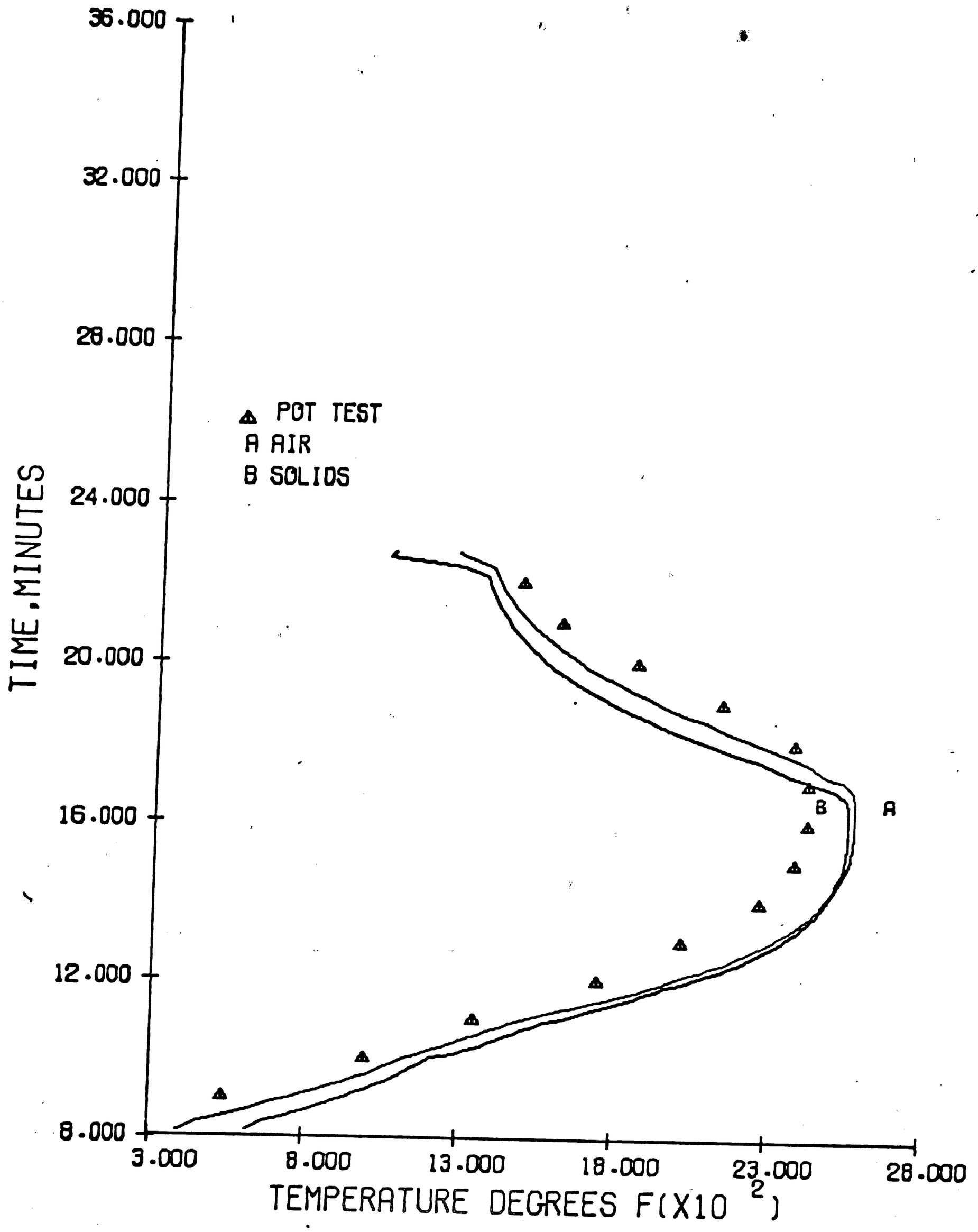

FIGURE 24-COMPUTER SIMULATION TEST2-2
POT TEST TEMPERATURES TAKEN 3.0INCHES
BELOW THE TOP OF THE BED,SIMULATION
DONE FOR 3.65 INCHES BELOW THE TOP

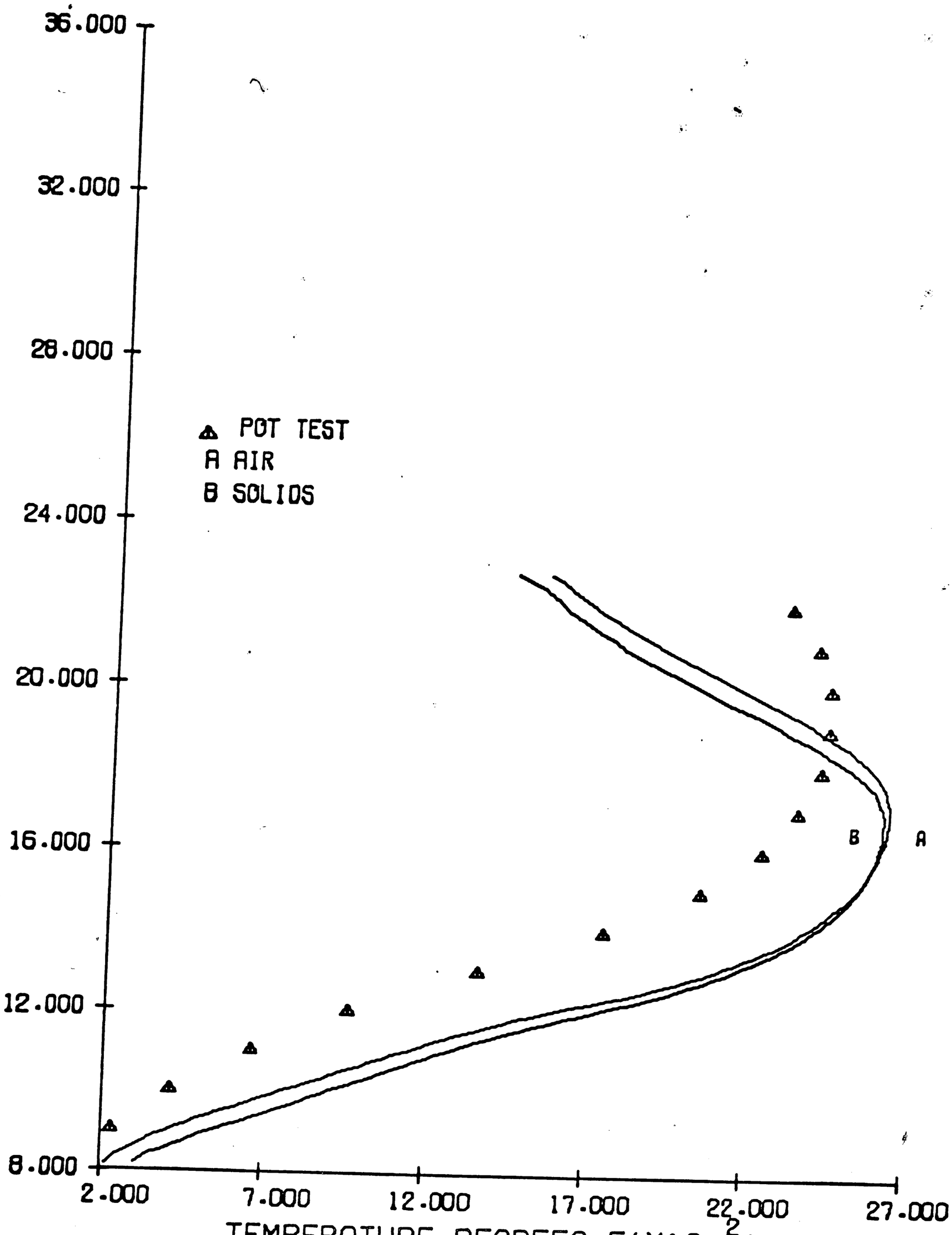

FIGURE 25-COMPUTER SIMULATION TEST2-2
POT TEST TEMPERATURES TAKEN 9.0INCHES
BELOW THE TOP OF THE BED.SIMULATION
DONE FOR 8.51 INCHES BELOW THE TOP

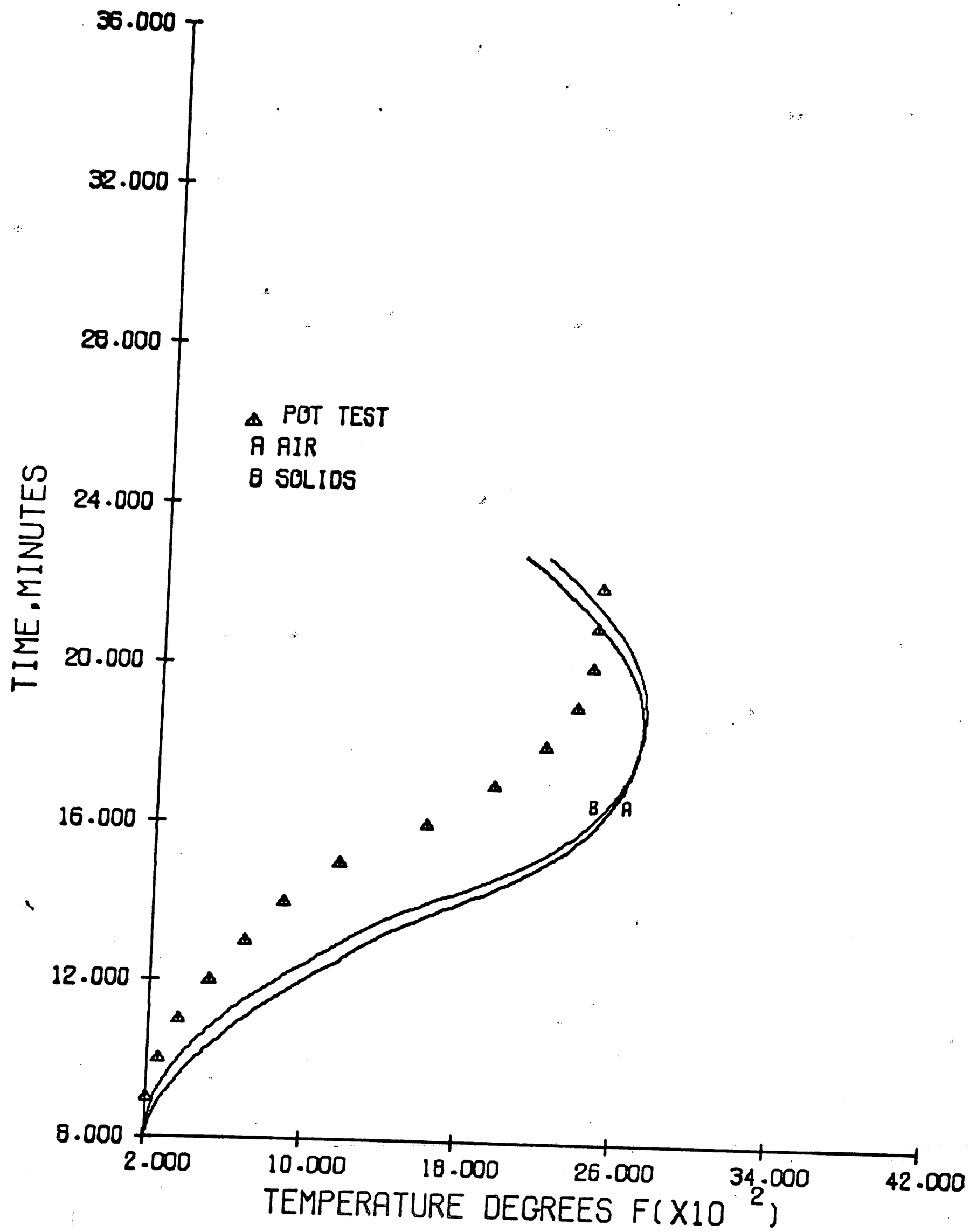

FIGURE 26-COMPUTER SIMULATION TEST2-2
POT TEST TEMPERATURES TAKEN15.0INCHES
BELOW THE TOP OF THE BED,SIMULATION
DONE FOR14.99 INCHES BELOW THE TOP

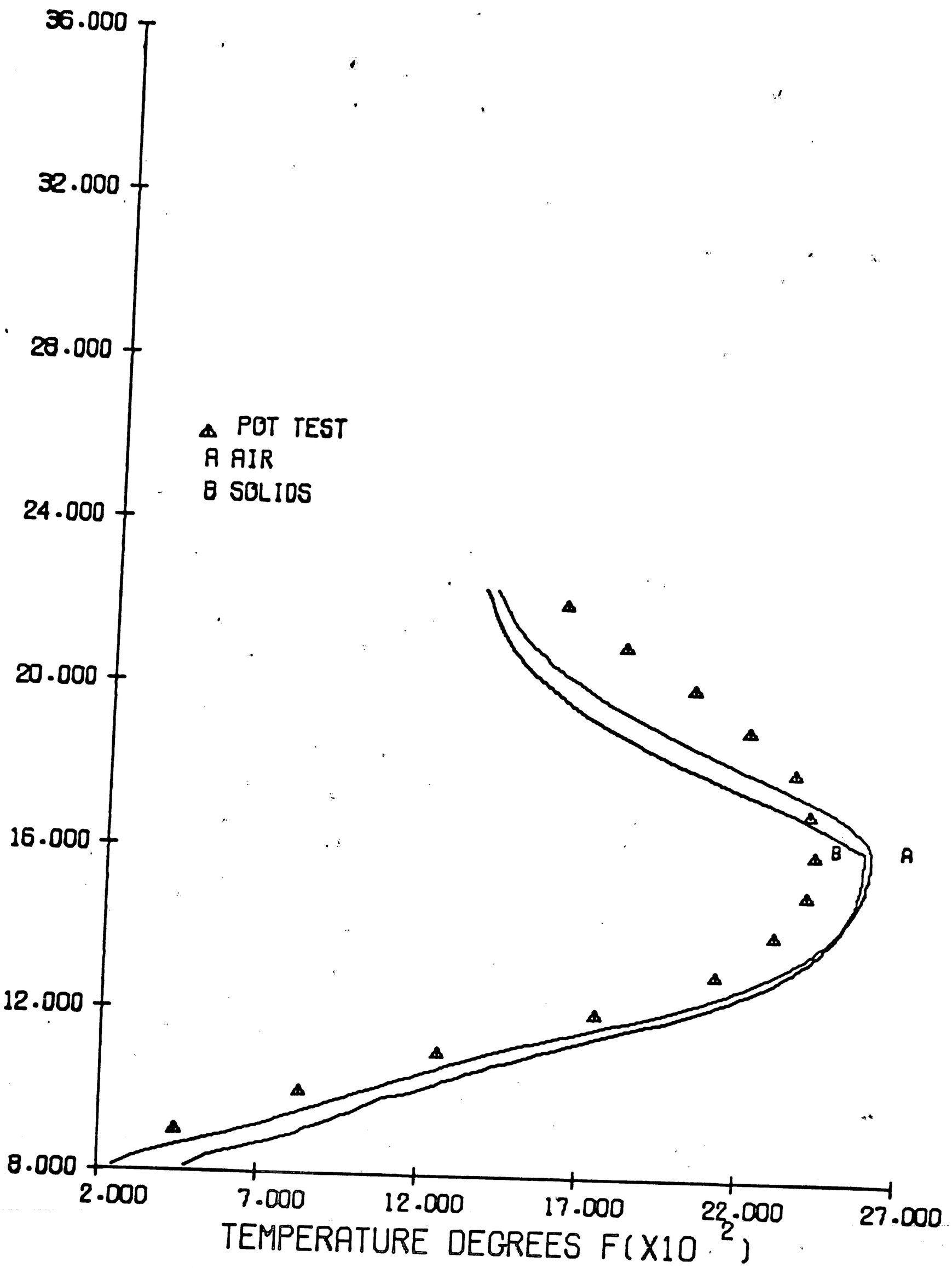

FIGURE 27-COMPUTER SIMULATION TEST2-3
POT TEST TEMPERATURES TAKEN 3.0INCHES
BELOW THE TOP OF THE BED.SIMULATION
DONE FOR 3.65 INCHES BELOW THE TOP

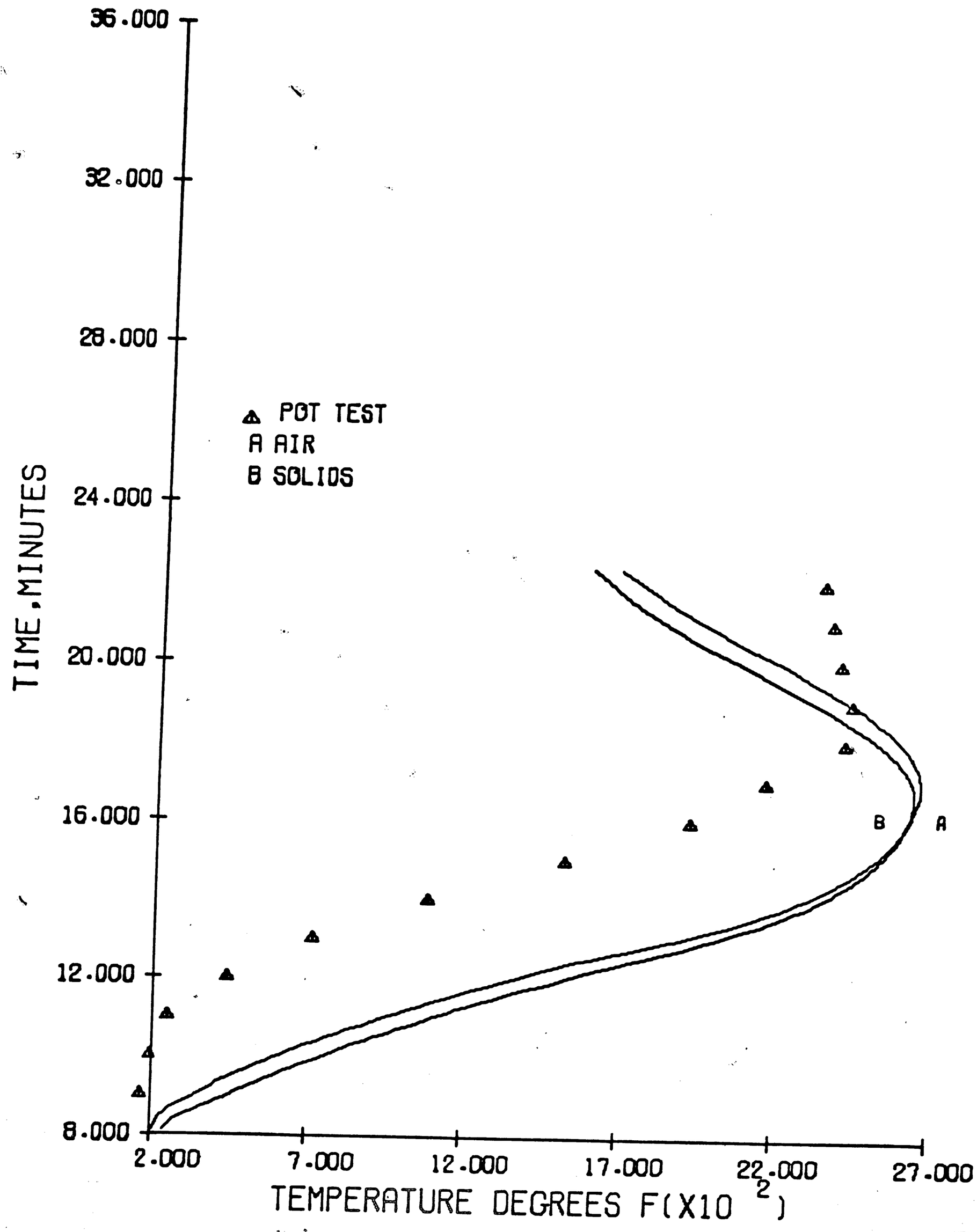

FIGURE 28-COMPUTER SIMULATION TEST2-3
POT TEST TEMPERATURES TAKEN 9.0INCHES
BELOW THE TOP OF THE BED,SIMULATION
DONE FOR 8.51 INCHES BELOW THE TOP

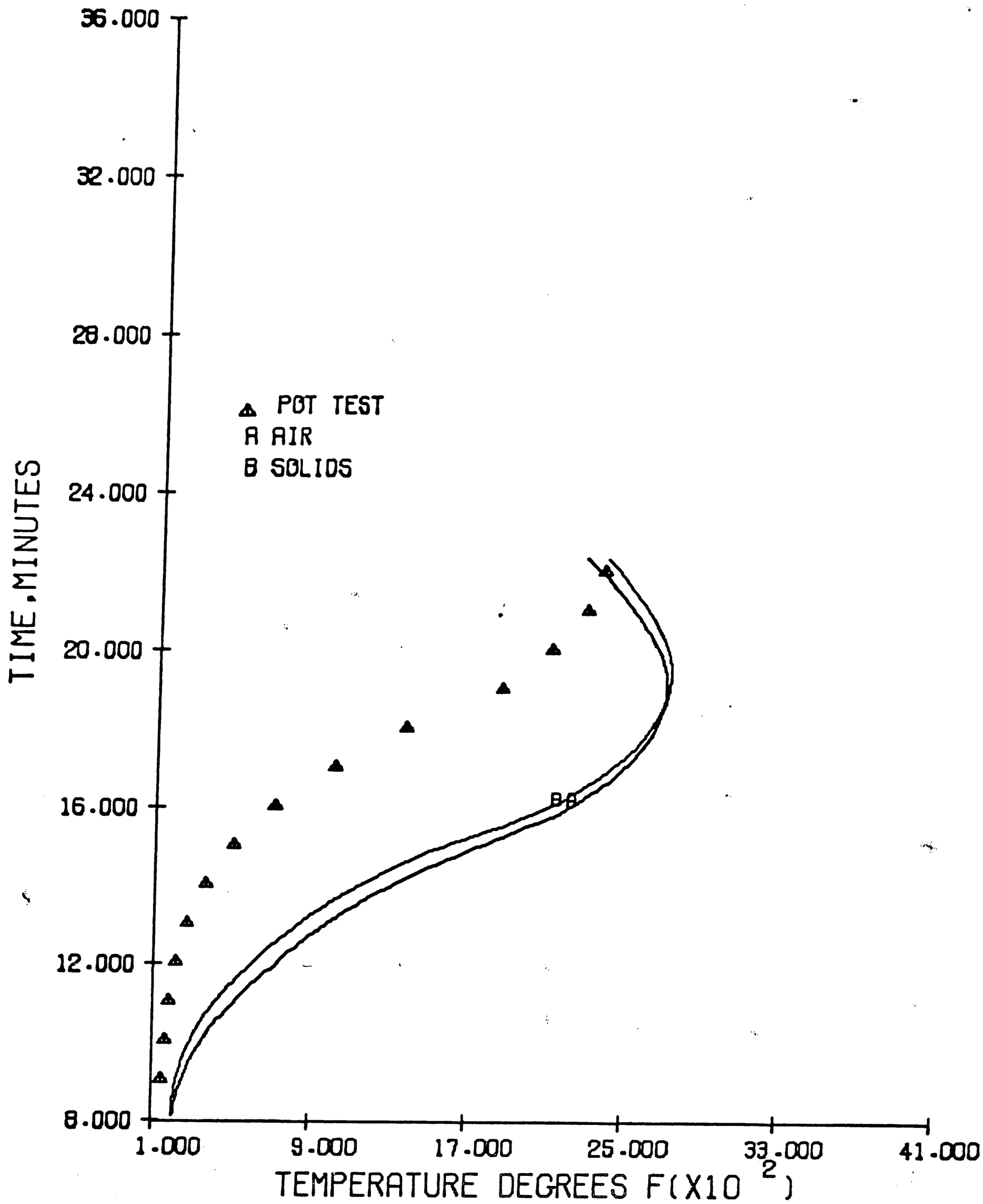

FIGURE 29-COMPUTER SIMULATION TEST2-3
POT TEST TEMPERATURES TAKEN15.0INCHES
BELOW THE TOP OF THE BED.SIMULATION
DONE FOR14.99 INCHES BELOW THE TOP

REFERENCES

(1) P. K. Strangway and H. U. Ross: "The Kinetics of Magnetite Reduction," Paper presented at the Annual A.I.M.E. Meeting, Los Angeles, February 20, 1967.

(2) O. Levenspiel: Chemical Reaction Engineering, John Wiley, New York, 1962.

(3) D. D. Phelps and J. A. Anthes: "Improvements in the Grate Pelletizing Process," Proceedings, vol. 21, 1962, p. 317-344.

(4) K. Smrcek: "Oxydace Magnetitu A Tepelny Rozpod Hematitu Pu Vytvrzovani Sbalku," Sbornik praci VUZDH, vol. 3, 1962, pp. 99-112.

(5) J. D. Zetterstrom: "Oxidation of Magnetite Concentrates," Report of Investigations #4728, U. S. Bureau of Mines, 1950.

(6) J. O. Edstrom: "Study of the Mechanism and Kinetics of Oxidation of Green Magnetite Pellets," Jernkontorets Annaler, vol. 141, 1957, (8), pp. 457-478 (In English).

(7) J. O. Edstrom: "Reactions in Pelletizing and Iron Ore Reduction," Jernkotorets Annaler, vol. 142, 1958, (7), pp. 401-428 or Brutcher Translation No. 4559.

(8) J. H. Heasley: "Transient Heat Flow Between Contacting Solids," Int. J. Heat Mass Transfer, vol. 8, 1965, pp. 147-154.

(9) J. F. Elliott: "Some Problems in Microscopic Transport," Trans. TMS-AIME, vol. 227, 1963, pp. 802-820.

(10) W. D. Munro and N. R. Amundson: "Solid-Fluid Heat Exchange in Moving Beds," Ind. and Eng. Chem., vol. 42, 1950, pp. 1481-1488.

(11) A. Eucken and M. Jakob: Der Chemie-Ingenieur, vol. III, Part 1, Akademische Verlagsgesellschaft M.B.H., Leipzig, 1937, pp. 445-447.

(12) W. B. Argo and J. M. Smith: "Heat Transfer in Packed Beds," Chemical Engineering Progress, vol. 49, 1953, pp. 443-451.

(13) J. C. Chen and S. W. Churchill: "Radiant Heat Transfer in Packed Beds," A.I.Ch.E. Journal, vol. 9, 1963, pp. 35-41.

(14) W. H. McAdams: Heat Transmission, pp. 290-295, McGraw-Hill Book Co., New York, 1954.

(15) R. B. Bird, W. E. Stewart and E. N. Lightfoot: Transport Phenomena, pp. 411-412, Wiley, New York, 1960.

(16) F. Yashida, D. Ramaswami and O. A. Hougen: "Temperatures and Partial Pressures at the Surfaces of Catalyst Particles," A.I.Ch.E. Journal, vol. 8, 1962, pp. 5-11.

(17) O. A. Hougen, K. M. Watson and R. A. Ragatz: C P P Charts, Wiley, New York, 1964.

(18) J. J. Barker: "Heat Transfer in Packed Beds," Ind. and Eng. Chem., vol. 48, 1956, pp. 26-50.

(19) R. R. Smith, G. Kotonias and D. R. Rathburn: "Preparation and Startup of the Groveland Pelletizing Plant," Ironmaking Proceedings, vol. 23, 1964, pp. 325-340.

(20) N. R. Amundson: "Solid-Fluid Interactions in Fixed and Moving Beds," Ind. and Eng. Chem., vol. 48, 1956, pp. 26-50.

(21) J. F. Elliott and J. C. Humbert: "Heat Transfer from Gas Streams to Granular Solids-An Idealized Analysis," Blast Furnace, Coke Oven, and Raw Materials Proceedings, vol. 20, 1961, pp. 130-157.

(22) L. E. Daws and H. Herne: "Heat Transfer Conditions in Pellet Firing," (Appendix II to Paper by Ridgion, Cohen, and Lang), J.I.S.I., vol. 177, 1954, pp. 60-63.

(23) C. O. Beale, J. E. Appleby, P. Butterfield and P. A. Young: "Pelletizing," Special Report of the Iron and Steel Institute, vol. 78, 1963, pp. 50-62.

(24) W. Callender: "Heat Hardening of Artificial Magnetite Pellets," International Symposium on Agglomeration, April 12-14, 1961, Philadelphia, Pennsylvania, A.I.M.E.

(25) W. F. Hildebrand and G. E. F. Lundell: Applied Inorganic Analysis, p. 907, John Wiley, New York, 1953.

(26) S. R. B. Cooke and W. F. Stowasser, Jr.: "The Effect of Heat Treatment and Certain Additives on the Strength of Fired Magnetite Pellets," Trans. A.I.M.E. Mining Eng., vol. 193, 1952, pp. 1224-1231.

(27) G. E. Wicks and F. E. Black: "Thermodynamic Properties of 65 Elements--Their Oxides, Halides, Carbides, and Nitrides," U.S.B.M. Bulletin #605, United States Government Printing Office, Washington, D.C., 1963.

(28) L. S. Darken and R. W. Gurry: Physical Chemistry of Metals, McGraw-Hill, New York, 1953.

(29) Tables of Thermal Properties of Gases, National Bureau of Standards, Circular 564, 1955.

(30) O. Kubaschewski and E. LL. Evans: Metallurgical Thermochemistry, Pergamon Press, New York, 1958.

(31) Stanley M. Morris: The Lehigh Analog Simulator, M.S. Thesis, Lehigh University, Bethlehem, Pa., 1965.

VITA

Karl David Libsch, the son of Dr. and Mrs. Joseph F. Libsch of Bethlehem, Pennsylvania, was born in Springfield, Massachusetts, on January 14, 1944. He attended elementary schools in the Bethlehem Area School District and graduated from Liberty High School in Bethlehem in 1961. The author entered Lehigh University in the fall of 1961 and graduated in 1965 with a Bachelor of Science degree in Metallurgical Engineering. Upon receipt of this degree the author was employed as Assistant Engineer, Development, by the Dravo Corporation in Pittsburgh, Pennsylvania. His two years with the Dravo Corporation included extensive experience in the design and start-up of pelletizing plants. In September, of 1967, Karl began his studies for a Master of Science degree in the Chemical Metallurgy Program in the Department of Metallurgy and Material Science at Lehigh. He is married and the father of a daughter.